DESIGN, TESTING AND IMPLEMENTATION OF A SMARTPHONE PERIPHERAL FOR BIMANUAL SKIN STRETCH FEEDBACK AND USER INPUT

by

Markus Nils Montandon

A thesis submitted to the faculty of
The University of Utah
in partial fulfillment of the requirements for the degree of

Master of Science

Department of Mechanical Engineering

The University of Utah

May 2013

The University of Utah Graduate School

STATEMENT OF THESIS APPROVAL

The thesis of Markus Nils Montandon

has been approved by the following supervisory committee members:

William R. Provancher	, Chair	3/14/2013 Date Approved
Jake J. Abbott	, Member	3/14/2013 Date Approved
Donald S. Bloswick	, Member	3/14/2013 Date Approved

and by Timothy A. Ameel, Chair of

the Department of Mechanical Engineering

and by Donna M. White, Interim Dean of The Graduate School.

ABSTRACT

Haptic interactions with smartphones are generally restricted to vibrotactile feedback that offers limited distinction between delivered tactile cues. The lateral movement of a small, high-friction contactor at the fingerpad can be used to induce skin stretch tangent to the skin's surface. This method has been demonstrated to reliably communicate four cardinal directions with 1 mm translations of the device's contactor, when finger motion is properly restrained. While earlier research has used a thimble to restrain the finger, this interface has been made portable by incorporating a simple conical hole as a finger restraint. An initial portable device design used RC hobby servos and the conical hole finger restraint, but the shape and size of this portable device wasn't compatible with smartphone form factors. This design also had significant compliance and backlash that must be compensated for with additional control schemes. In contrast, this thesis presents the design, fabrication, and testing of a low-profile skin-stretch display (LPSSD) with a novel actuation design for delivering complex tactile cues with minimal backlash or hysteresis of the skin contactor or "tactor." This flatter mechanism features embedded sensors for fingertip cursor control and selection. This device's nonlinear tactor motions are compensated for using table look-up and high-frequency open-loop control to create direction cues with 1.8 mm radial tactor displacements in 16 directions (distributed evenly every 22.5°) before returning to center. Two LPSSDs are incorporated into a smartphone peripheral and used in single-handed and bimanual tests to identify 16

directions. Users also participated in "relative" identification tests where they were first provided a reference direction cue in the forward/north direction followed by the cue direction that they were to identify. Tests were performed with the user's thumbs oriented in the forward direction and with thumbs angled inward slightly, similar to the angled-thumb orientation console game controllers. Users are found to have increased performance with an angled-thumb orientation. They performed similarly when stimuli were delivered to their right or left thumbs, and had significantly better performance judging direction cues with both thumbs simultaneously. Participants also performed slightly better in identifying the relative direction cues than the absolute.

TABLE OF CONTENTS

ACKNOWLEDGMENTS

First, I want to thank my incredible family. I would like to share my deepest appreciation to my wife Brandi and daughter Katey, who have lifted me up in difficult times, been so patient and have given me confidence when in doubt. You girls make every day an adventure. Thank you both for your love and laughter.

I need to thank my parents, Michel and Susan, for their unrelenting support and encouragement. I have always been able to look to them for examples of compassion, hard work and joy. Thank you for listening to wild and rambling ideas for all these years.

Special thanks to my advisor, Prof. William Provancher, for his technical knowledge, seasoned guidance, and reassurance. I have been pushed further than I thought possible and learned so much because of his promptings. It has been a privilege to collaborate with him through this research. Thank you for sharing all of your time and experience.

I would like to thank my lab mates for their assistance and insight. I specifically would like to thank Peter Howe for his quality programming contributions and support.

This work was supported, in part, by the National Science Foundation under awards IIS-0746914 and IIS-0904456. Support from award IIS-0746914 started during my summer research as part of the Research Experiences for Undergraduates (REU) program. Additional support was provided by a University of Utah Research Foundation *Technology Commercialization Project*.

CHAPTER 1

INTRODUCTION

Capabilities of portable and handheld consumer electronics have grown rapidly to include sophisticated visual and auditory experiences that can take advantage of increased computing power. Increasingly, the activities performed on these devices include a haptic component. Haptics has to do with the sense of touch. In current portable consumer products this is most commonly delivered as vibration feedback with programmable magnitude and timing. While this method of feedback is useful for attention-getting notification tasks and as a supplement to gaming experiences, it is limited in its capabilities compared with larger force-feedback peripherals. Consumer force feedback devices are capable of delivering haptic sensations to a user in the form of forces and motions (e.g., gun recoil on a force-feedback joystick or torque feedback on a steering wheel to portray the forces encountered when a car jumps a curb).

To make these more complex sensations available within portable handheld electronics, a tactile display (or touch feedback device) must go beyond just providing vibrational information, which can only be varied in its magnitude and temporal components. Haptic feedback through lateral skin stretch at the fingertip has been identified as a viable solution for delivering more complex modes of interaction with the user. Lateral skin stretch at the finger is accomplished through contacting the fingerpad with a small high-friction contactor (or "tactor") that limits slip between it and a user's

fingerpad. While a user's finger is restrained, this contactor is translated tangential to the skin surface to apply a small amount of skin stretch. These skin-stretch cues have been shown to allow distinct communication of four orthogonal directions to a user. The mechanism for this interface has been previously miniaturized to the approximate form-factor of a cube that is four centimeters on each side. While this skin-stretch display is functional and requires little maintenance, it has limitations in skin-stretch positioning accuracy. The form factor is also not suited for integration toward a peripheral for current slim smartphones.

Therefore, it is desirous to create a flatter skin-stretch device with a form factor more feasible for attachment to a smartphone or tablet computer. The updated design must also be capable of improved position accuracy over an enlarged workspace. This thesis outlines the design of a low-profile skin-stretch display (LPSSD) that accomplishes these improvements over the prior tactile display. As a part of this revision, the tactile display is integrated with sensors that make convenient user input possible. These sensors allow analog force and digital button input from the thumb that could be used to navigate a graphic user interface or interact with games. With this update the device is now capable of bidirectional communication consisting of finger-based force inputs to the sensors while skin-stretch feedback is provided back to the user.

The linkage and drive scheme for the new actuation mechanism are designed to minimize backlash, compliance, and hysteresis. While these measures are largely successful, the motions of the tactor within the workspace are distorted by the nonlinear kinematics of the linkage design as well as characteristics of the RC servos used in the

design. To create skin-stretch cues with linear motions for the purpose of communicating direction to the user's thumbpad these nonlinearities must be accounted for.

One of the envisioned uses of the new skin-stretch display is to provide skin-stretch cues for mobile navigation in the field. Unlike our lab's prior studies, which only examined users performance in judging direction cues from among four possible directions, we are now interested in being able to provide more subtle direction cues to nudge a user's heading slightly right or left as they are walking forward through an open field. As such we needed to characterize people's ability to interpret these subtle cues. Cues with 22.5 degree increments were chosen to communicate these subtle navigational cues.

Sixteen evenly spaced direction cues that stretch the skin radially from a center starting position in linear translations (spaced every 22.5 degrees) to portray these direction cues were programmed into the skin-stretch display. This is accomplished through an open-loop control scheme that updates the servo position commands from precompiled position trajectories via table look-up, which is implemented at a higher rate than the previous tactile display in order to create smooth trajectories. This technique results in highly consistent and repeatable tactor motions. This solution works well for a diverse set of users with varying thumb sizes and shapes. This is important as the control settings for the tactile display need not be adjusted on a per-user basis while still producing consistent tactor motions.

Finally, two of the new skin-stretch displays are integrated into a prototype smartphone peripheral for bimanual interaction with two thumbs. This prototype is used in two identification studies in which users are tested for their perception of 16 unique

direction cues. Users are tested with their thumbs in straight and angled configurations. It is determined that users are more accurate in this task while thumbs are in the angled configuration. It is also found that users are considerably more accurate when receiving cues on both thumbs simultaneously. These results are significant as they prescribe that future designs that employ thumb-based skin stretch should use handle designs that orient the user's thumbs in an angled configuration, in order to achieve increased user accuracy when interpreting directional information via skin-stretch feedback.

Three contributions were made through this research, which relate to the fields of mechatronics and haptics perception.

1. A low-profile, low-cost, compact skin-stretch tactile feedback device

   Haptic interface capable of salient and accurate skin-stretch feedback is successfully produced, based on low-cost RC-grade servos. This is possible through limiting compliance and backlash within linkages while also maintaining proper motion constraints to avoid undesired degrees of freedom. The consistency of skin-stretch tactor motion in 16 directions, across a diverse set of 10 users, suggests that the sliding tactor plate coupled with push-pull wires arrangement is capable of delivering reproducible interactions to a broad population.

2. Use of look-up tables to correct for device nonlinearities

   It is shown that workspace nonlinearity of the low-cost actuation mechanism can be compensated for with a "waypoint" table-lookup method. This high-speed open-loop control approach is demonstrated to correct workspace distortions and permit velocity control of the skin-

stretch tactor with minimal error. With expanded microcontroller capabilities this waypoint method can be further refined with improved servo control resolution and update frequency to create complex and responsive tactile cues.

3. Perceptual and cognitive data for direction perception with multiple hands that is valuable for informing portable device designs that provide tactile directional information

   Prototype of a smartphone peripheral makes use of two low-profile skin-stretch displays to test users' abilities in detecting directional skin-stretch cues at the thumbs with an assortment of test conditions. From these results, a variety of performance trends and user biases have been identified. The user accuracies of the left and right thumbs are nearly equal. Perception accuracies are significantly improved when participants received cues with both thumbs than with a single thumb. When a user's thumb is held in the angled configuration his/her direction accuracies is higher than those in the "straight" thumb configuration. Users tested with a single thumb in the straight configuration showed considerable rotation bias – answering in a direction clockwise and counterclockwise to the rendered cue for the left and right thumbs, respectively. Additionally, providing a perceptual reference increases response accuracy, especially for direction cues closest to the reference.

1.1 Thesis Overview

Chapter summaries are given below reviewing content and key results.

Chapter 2 provides a brief summary of the variety of consumer electronic products introduced over the years that have featured haptic interaction. Products in the gaming, computing, communication, and research markets are briefly reviewed. The mechanical actuation methods for these devices are discussed with notes of their advantages and shortcomings. Prior research in lateral skin slip and skin stretch are presented with summaries of results regarding human perception. The development and results for a variety of wearable and/or portable haptic interface mechanisms designed to explore skin-stretch and slip communications are given. These previous research and device-development results are used to inform an updated design for a skin-stretch display with the purpose of integration with a smartphone or tablet computer.

Chapter 3 presents an evaluation of the positioning accuracy of the prior flexure-based skin-stretch mechanism, which is used as a baseline for the design of a new low-profile skin-stretch display (LPSSD). The design and fabrication of this flat-form-factor mechanism and its actuation is presented in detail. The types of sensors embedded for user input and their integration is described. Two of these completed LPSSDs with supporting electronics are incorporated into a bimanual skin-stretch device that is wirelessly controlled with an Android smartphone. The presented design is successful in meeting some of the design goals, except that its total thickness is greater than that of current smartphones and the volume slightly exceeds the volume of the prior flexure-based design for the version that includes user input sensing.

In Chapter 4 the various sources of nonlinearity in the skin-stretch display's workspace are examined for simple cues designed for a 1.8 mm displacement and then return to center. The control scheme is detailed by which trajectories are stored and played back to create 16 linear direction cues. These direction cues are evaluated visually and through linear probe encoders to ensure cues with repeatable playback. The finalized cues are tested with 10 users, each receiving skin-stretch cues while the tactor motions are captured. The performance of the LPSSD is evaluated based on overall design criteria as well as quality of direction cues produced. Significant improvements in position accuracy and device reliability are documented for the new LPSSD design.

Chapter 5 presents two perceptual studies that evaluate users' ability to judge direction cues rendered via the newly designed smartphone peripheral, which utilizes two LPSSDs. The first study is a 16-direction absolute identification experiment with direction cues with 22.5 degree increments between direction cues. The second experiment presents a subset of the cues of the first experiment. Its stimuli consist of first rendering a forward cue, followed by the direction that is to be judged by test participants. Because each of these stimuli includes a forward reference stimuli, these experiments are called a "relative" identification experiment. The absolute and relative direction experiments are conducted with the user's left thumb, right thumb, and both thumbs in contact with the moving tactor(s). They are also conducted with the user's thumbs in a forward/straight and angled orientation. Perceived accuracy rates are computed along with an estimate of information transfer for each test case. Participants have the highest accuracies for angled-thumb orientations, where participant's when using their right and left thumbs have similar accuracies, whereas they perform

significantly better when using both thumbs simultaneously to judge direction cues. Participants also performed with higher accuracies in the relative identification tasks than in absolute identification. Information transfer estimates suggest that approximately five directions could be perfectly communicated in the angled-thumb configuration and estimates suggest that users would exhibit accuracies in an 8-direction experiment of approximately 96% or greater when using two angled thumbs.

Chapter 6 presents a summary of the work described in this thesis along with conclusions and future work. It also presents a list of the contributions of this thesis research.

CHAPTER 2

BACKGROUND

Consumer electronics with handheld interfaces have increasingly integrated haptic interaction features. Various methods of enabling tactile communication with the user have become prevalent in video game controllers, mobile phones, and research devices. These devices have employed an assortment of actuation solutions to simulate force and texture interactions with virtual objects. Mechanisms with varying levels of complexity have been employed to create a range of haptic interfaces. These interfaces are tailored to end-user markets with assorted requirements. Through advances in motor design, manufacturing, and computing, haptic interfaces with reasonably high quality and bandwidth are now found in a variety of low-cost consumer devices.

2.1 Consumer Devices with Haptic Feedback

Home video game consoles have included embedded haptics in the majority of controllers since 1997 when Nintendo introduced the Rumble Pak™. This accessory uses an eccentric weight attached to the output of a DC motor to vibrate the controller body against the user's hands. Since that time, nearly all console game controllers have adopted this method of delivering vibration feedback to the user including the Sony Dual Shock 3 controller, Nintendo Wii remote, and the Microsoft Xbox 360 controller. These vibrations are synchronized with visual displays and audio to create an improved

immersive effect. Because of the dynamics of the motor and attached weight there are limits to the responsiveness and frequency range of vibrations produced. These vibrations can be adjusted only in magnitude, which is proportional to frequency for these actuators, and timing.

Game controllers in the form of joysticks and steering wheels have also been produced for force-based haptic feedback. Motors within these controllers create forces against the hand of the user that correspond to in-game events or physics-based simulations. Joysticks that include force feedback are the Microsoft Sidewinder, Logitech Force 3D Pro, and the Saitek EVO. These joysticks are capable of delivering forces in two axes, which pivot about the base of the device. Some steering wheels featuring force feedback are the Logitech G27, Microsoft Xbox 360 Wireless Racing Wheel, and the Thrustmaster T500 RS. These driving wheels deliver rotational forces about the axis of steering wheel revolution. The Gravis Xterminator Force Gamepad is a two-handed gamepad that also feature force feedback, but within the directional input thumb pad. These controllers can recreate a range of high quality tactile effects more dynamic than through vibration from an eccentric mass motor. However, a disadvantage of force feedback is that these forces become a part of the user input to the controller and can lower the player's in-game control accuracy. Various versions of these controllers are still produced and sold but force feedback has become a niche market of gaming accessories, because of the reduction in gamer performance that usually results from the application of force feedback, which destabilizes the user's inputs.

Mobile phones and tablets have primarily followed the actuation methods used in game controllers, employing vibration through eccentric-mass motors. While sometimes

used in gaming applications on the phone, these haptic cues are primarily used for notification and user input confirmation (e.g., vibration when pressing keys on a virtual keyboard). These simple cues have been shown to improve typing ability in both quiet and noisy environments [1]. Alternate technologies are being developed for smartphone integration to allow richer, higher bandwidth, and more salient vibrations to be produced. These include electroactive polymer actuators as developed by Artificial Muscle Inc. in their ViviTouch product that is incorporated into the Mophie Pulse smartphone accessory. Piezoelectric actuators have been introduced in phone and tablets and their capability to improve multimodal interfaces are being explored [2]. The company Senseg is also developing variable friction surfaces with electrostatic fields for use in touch screens. Disney research [3] and researchers at Northwestern (e.g., [4]) have both developed methods for haptic feedback simulating textures or friction at the fingertip on a touch screen using electrovibration and ultrasonic vibration, respectively. Software initiatives such as Immersion Corporation's MOTIV API can be used to create a variety of qualitative vibration effects, such as gun fire and engine rumble, and promotes the development of unified haptic interface standards.

In 2007, Novint released the Falcon force feedback game controller to the consumer market, which is based on the device design for the Force Dimension Omega™. The Omega™ was developed to conduct research in the fields of teleoperation and virtual reality. The Falcon is one of the first commercial haptic devices to be developed that costs under $200 and is reasonable for a consumer to purchase. Its price represents a two order-of-magnitude shift in price from prior haptic devices that are capable of high

bandwidth, high resolution three-dimensional force feedback, such as the Force Dimension Omega™ and Sensable Phantom™ Premium.

2.2 Prior Finger Pad Skin Slip and Stretch Feedback Research

Previous studies in the field of "fingertip haptics" conducted by Salada and Colgate [5] have focused on slip interaction at the fingertip and its affect on velocity perception. This was done through applying a spinning Lexan surface against the finger pad to create a slipping tangential contact. The slip direction was incrementally rotated between applications of slip to the fingerpad to determine what angular differences in slip direction are noticeable. Their study resulted in 3.6 to 11.7 degrees as the "Just Noticeable Difference" (JND) threshold that could be sensed by their test participants (where the exact value depended on the surface treatment of the spinning Lexan surface and whether the slip was lateral to or along the participant's finger length.

Hayward et al. created a device capable of distributed lateral skin stretch at the fingerpad [6]. Within a 12 mm square area, an array of 112 pins is actuated through piezoelectric actuators that cause the pins to move laterally while contacting a fingerpad. This array of 0.7 mm pins could be used to convey pulsing effects and if actuated along a single row of object motion.

Translational skin stretch at the fingerpad and forearm in tangential and normal directions was tested by Biggs and Srinivasan [7]. A 1 mm diameter probe glued to the participant's finger translated up to 2.0 mm. It was found that tangential displacement between 0.45 and 0.9 mm produced similar signal response as 1.5 mm displacements in the normal direction. It is recommended that tangential forces be used when device size is limited.

Bark [8] designed a wearable haptic device that rotates to provide rotational skin stretch using two contactors that are 26 mm apart and that are held against or adhered to the user's skin. During testing, this device was worn by users on their forearm as they adjusted its rotation with an external knob to match a requested angle. Matching the requested angle was accomplished by test participants with a residual error of 5.2 degrees and standard deviation of 1.4 degrees. Further studies by Wheeler and Bark [9] have shown that this interface could be used to provide a sense of proprioceptive position and motion from a virtual prosthetic arm. Improvements in a person's ability to position the prosthetic arm, when rotational skin-stretch feedback was provided, were especially noteworthy when the user's vision is preoccupied.

Previous work to characterize tactile movement perception of lateral displacement at the fingertip has shown a just noticeable difference (JND) for fingertip angle sensitivity to be in the range of 21 to 40 degrees [10]. The Drewing et al. study users' fingers were restrained to a surface with an opening through which a 1 mm pin protrudes. This pin was translated by 1 mm by RC servo in one of eight cardinal or ordinal directions and held at that location. The user then raised his/her finger while the pin returned to center on the fingerpad. After replacing their finger the second discrimination angle cue was delivered, or rendered, and the user responded if it was perceived as either clockwise or counterclockwise of the first. These comparison angles were offset by 10 degree increments up to 90 degrees. Further studies explored the user's abilities to sense the angular difference between 1 mm lateral cues at the fingertip while the tactile display was mounted to a hyper redundant haptic display (ViSHaRD10) [11]. The user completed the discrimination experiment while the tactile display was either held static or while

performing additional exploration tasks. This study showed that the 84% discrimination threshold JND rose from 40 degrees in a static condition to a range of 50 degrees to 70 degrees while users were given exploration tasks.

In bench-top studies Gleeson [12] researched the communication capabilities for conveying direction through fingerpad skin-stretch feedback. A 7 mm diameter, high friction, rounded rubber cylinder mounted to an X-Y stage is used to deliver 0.05 mm - 1.0 mm lateral skin-stretch cues to the secured index finger. These cues were delivered with speeds between 0.5 mm/sec and 4 mm/sec in four cardinal directions. It was found that users performed with 99% recognition rates as the displacements rose to 1.0 mm. This performance also improved, though less so, with increased tactor velocity. Additional studies were completed by Gleeson [13] to determine ideal dimensions and texture for the tactor stretching the skin as well as the diameter of the rounded opening for grounding the finger. The results of this study show that a rough texture on the tactor improves communication accuracy, but the size of the tactor does not have a large effect on accuracy. Larger tactors were found by participants to be more comfortable to interact with though. A larger aperture (a conical hole used in leiu of a thimble as a finger restraint) also improves recognition rates and does not need to be adjusted to match a specific user finger size.

A portable skin-stretch feedback device was designed that was based on the findings of the above bench-top studies [14]. It is actuated using two RC hobby servos in combination with a compliant flexure. The device is approximately a 1.25 inch cube and utilized a thimble to restrain the user's finger with respect to the device. The frame of this device was originally machined from Delrin; however, the frame of these devices has

subsequently been rapid prototyped by 3D printing with no notable reduction in performance. Use of 3D printing to produce the device frame has opened up a wide range of packaging options and has permitted skin-stretch feedback to be built into a variety of devices. See Section 3.1 for further details on this device and its performance characteristics.

A multimodal study was completed to compare haptic, auditory, and visual direction cues while navigating a simple obstacle course in four directions [15]. This design utilized a 3D printed version of the device developed in [14], which allowed integration of the feedback mechanism's chassis into the handle of a hand-held device. A custom single-handed device combined these modes of communication and recorded accurate response times for each. It was found that the skin-stretch feedback was comparable with other cue types and suitable for simple mobile navigation, based on a grid course of right angle intersections.

Lateral skin-stretch feedback has also been tested within the form factor of a traditional console game controller, in which the skin-stretch tactors protrude from within the center of two analog thumb sticks; [16]. This design also utilized a 3D printed version of the device developed in [14]. Participants were tested when using two grip configurations; a straight grip with their thumbs parallel and in line with a cue given in the north (distal) direction and an angled grip, in which their thumbs were angled inward to the device centerline, as commonly found in commercial game controllers. This study showed that user grip orientation and resulting mental rotation did not affect user perception when tested in a four-direction test. Users reported preferring the angled grip due to increased comfort and thumb dexterity.

2.3 Prior Research on Portable Haptic Feedback Devices

Studies to design and characterize performance of portable and wearable haptic interfaces for fingertip or handheld use have expanded to investigate a wide variety of sensations beyond vibration. These devices have been designed to convey information including direction cues, contact location, user movement correction, temperature, and emulating human touch interactions.

Tsagarakis [17] showed that two dimensional lateral motion and velocity could be presented through two independent sliding surfaces touching the fingertip. The slide/stretch contact is made through two miniature geared motors mounted in a "V" formation with smooth outputs with little texture. The size of motors and gearboxes allow for a light and finger-mountable mechanism.

Miniaturization of a lateral-skin-stretch display to convey four orthogonal directions was demonstrated through the implementation of hobby grade servos and a custom flexure stage [14]. This process made the mechanism viable for integration into handheld and portable devices while maintaining tactor movement comparable to previous bench-top tests. A similar skin-stretch feedback device, which used the same custom flexure along with Shape Memory Alloy (SMA) actuators, was also build and fabricated [18]. While the SMA-driven design was more compact that the RC-servo-driven design, it is also more difficult to control, is less reliable, and has slower actuation speeds. For this reason, current portable skin-stretch feedback devices in the Haptics and Embedded Mechatronics Lab continue to be based on actuation by RC servos.

Solazzi [19] presents a fingertip wearable device that provides cutaneous contact surface orientation information to one or more fingers simultaneously. With the addition

of kinesthetic feedback this allows for immersive pinching interactions with virtual environments.

Pressure and shear at the fingerpad have been used to simulate fingertip surface contact and lateral skin stretch due to gravity through a fingertip wearable apparatus that uses two motors to tighten or shear a band of fabric on the fingerpads [20], [21]. These devices were found to recreate approximations of the sensations experienced due to gravity and contact without the accompanying grounded kinesthetic feedback.

Wearable actuators for replicating social human interactions have been designed for the wrist. A device with the form factor of a watch was built and tested to create a sensation of a hand squeezing the wrist or a finger tapping the back of the hand [22]. In a similar study four separate wearable devices were produced and had their performance characterized [23]. Each device was capable of either tapping, dragging, squeezing, or twisting interactions with the user's wrist. Both of these projects resulted in positive feedback from users for use in attention-getting tests and delivering natural tactile cues.

Designed for individuals with visual impairments, a haptic alert system couples an ultrasonic range sensor with vibrotactile feedback to warn of low-hanging obstacles was developed [24]. Preliminary results show that users' ability to navigate an obstacle course was greatly aided through this intuitive feedback.

CHAPTER 3

DESIGN OF A LOW-PROFILE SKIN-STRETCH DISPLAY AND SMARTPHONE PERIPHERAL

Ongoing studies in skin-stretch tactile feedback require mechanisms with increasingly responsive and compact actuation. A skin-stretch display that delivers this feedback in a lower-profile form factor more compatible with current smartphones or tablets is desirable. A flatter mechanism could be more readily used as a peripheral with these devices and with further miniaturization be directly embedded into consumer electronic devices. Expanded user input capabilities, by integrating a force sensor with the skin-stretch feedback device, would also allow a greater range of user interaction. We have developed a smartphone peripheral (see Fig. 3.1) that utilizes a new low-profile skin-stretch feedback display that embodies the above traits and describe the design of this new mechanism and the resulting smartphone peripheral below.

3.1 Prior Skin-Stretch Device Overview and Performance Summary

The mechanism used in previous and ongoing fingertip skin-stretch experiments was designed by Gleeson and Horschel [14]. This device is reliable in its operation and features compact dimensions. The moving components have a long usable life without need for maintenance. The small footprint and vertical height of the device is ideal for integration within taller handheld devices such as a joystick. The overall dimensions of

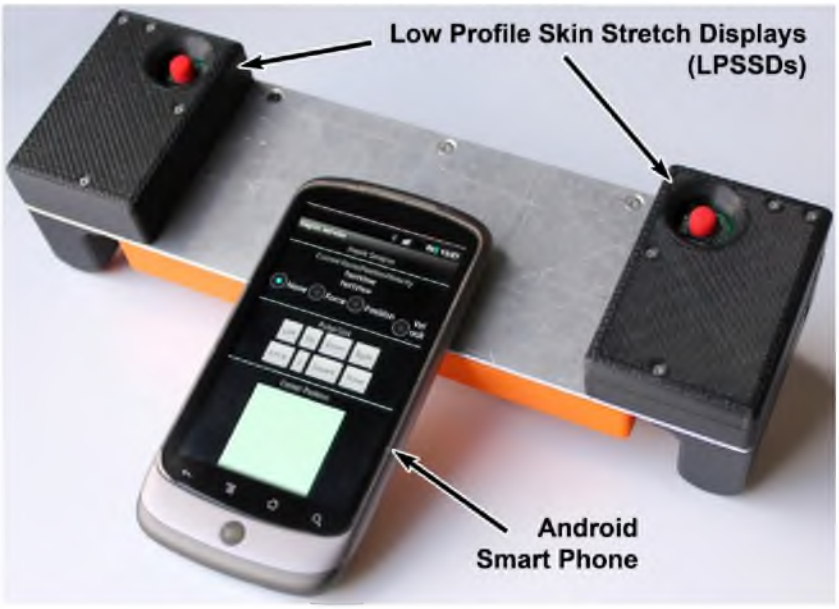

Figure 3.1 Completed smartphone peripheral with bimanual skin-stretch feedback and user input capabilities. This peripheral uses two low-profile skin-stretch displays, which interface with an Android smartphone.

this design, which is shown on the left of Fig. 3.1, are 32.4 mm x 39.4 mm x 44.1 mm tall.

This device makes use of two servos mounted under a polymer flexure stage that moves a red IBM TrackPoint™ cap, which contacts a user's fingerpad and stretches the skin laterally (see Fig. 3.2). This flexure translates the two servos' rotational motions into orthogonal, translational motions that lie within a plane that is parallel to the top surface of the tactile feedback device. The flexure stage also acts to decouple the motions of the devices two (orthogonal) axes of motion (referred to as the x and y axes of motion, as shown in Fig. 3.2. The small rotation angle required from the servos delivers a nearly consistent velocity through the tactor's range of travel. The shear display is capable of moving the tactor within a 4.0 mm x 4.0 mm planar square workspace. The

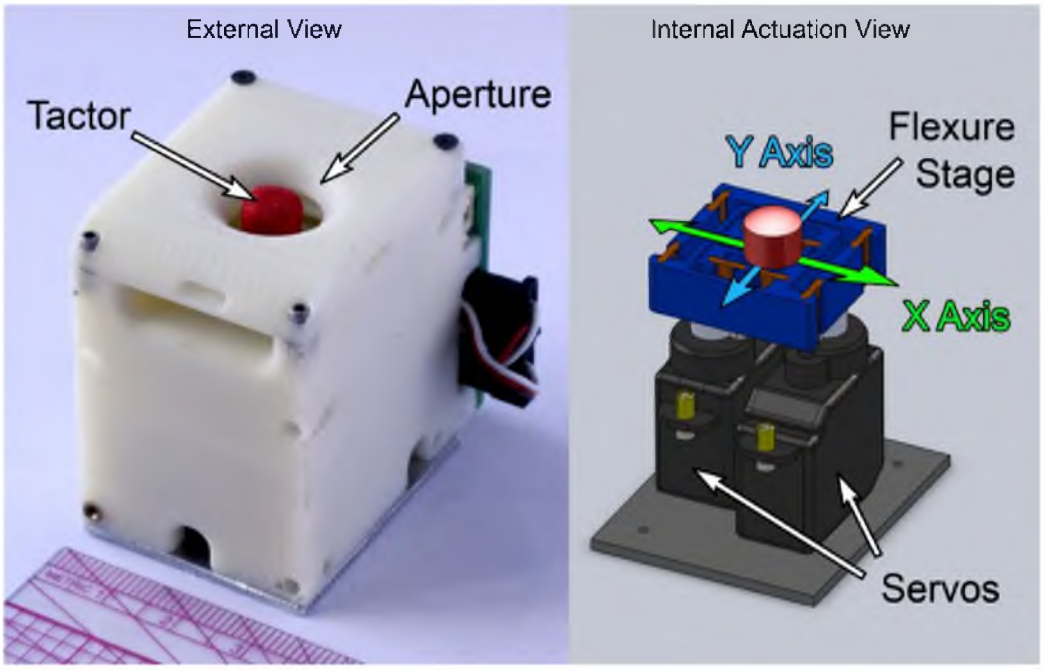

Figure 3.2 External view of prior skin-stretch display with tactor and finger-restraint aperture opening (left). Internal component view showing actuation components (right). Figure used with permission of Gleeson *et al.* [14].

full range of the workspace is not commonly used to prevent accidentally stalling a servo against the device's hard stops and lowering the servo's functional life.

This design has some shortcomings in its position accuracy and the consistency of how skin-stretch is rendered via the device's tactor to the user's fingerpad. This is due to device compliance and backlash. The physical interface between the device's servo outputs and flexure stage include up to 0.25 mm of compliance and backlash (for the device shown in Fig. 3.1). The flexure stage also undergoes out-of-plane angular rotation of the tactor post when a finger is held against the tactor during normal operation. This is due to the force couple created between where the servos interface at the bottom of the flexure and the resistance of stretching the user's skin at the top of the tactor, which is attached to the top of the flexure (see Fig. 3.3). This tactor post rotation is responsible for

up to an additional 0.55 mm of position error. These two types of error combine to permit up to 0.8 mm of position error and hysteresis when the tactor is commanded 2.0 mm from center in the north-south axis. In previous tests a user is given a direction cue by placing his/her thumb on the tactor and aperture. The tactor then translates stretching the fingerpad laterally 1.0 mm before it returns to the start position and releases tension on the skin. These direction cues were given in four cardinal directions (i.e., the equivalent of North, South, East, and West) [25].

The backlash and tactor post deflection made it necessary to implement a custom position controller (to compensate for device backlash) as direction cues rendered by the tactor did not always reach the desired outbound position. This effect was more prevalent in the north and south directions where skin stiffness is generally greater. These losses in travel can be as high as 45% of the commanded distance when stretching the thumbpad in the north or south directions, while only about a 7% loss is observed when the tactor stretches across the thumb's width. As an example, in order to achieve approximately 1 mm of net tactor motion (and resulting skin stretch) it is necessary to command 1.9 mm of servo motion in the north/south directions while only 1.1 mm of servo motion is required in the east/west directions for the same net tactor motion. Part of this loss in travel is due to the spring-like resistance of the finger against the tactor (see [14]); however, a stiffer actuator mechanism will limit these losses.

On the return path to the tactor's center position, the hysteresis within the system required the tactor to be commanded past the center position to reduce the final position error (i.e., hysteresis compensation). The skin-stretch feedback display was calibrated over multiple trials across different users, to determine the amount of hysteresis

Figure 3.3 The force couple between grounded thumb pad and the servo input to flexure results in tactor post rotation.

compensation required. This led to a prescribed average level of hysteresis compensation for the device; however, variations between people's skin properties results in imperfect hysteresis compensation for these devices.

3.2 Design Targets for Low-Profile Skin-Stretch Display

An alternate design for a skin-stretch display should maintain or improve upon the performance of the previous skin-stretch device, delivering consistent tactile cues while accommodating additional requirements in several areas:

1. Slim form factor. The design of a skin-stretch mechanism as a peripheral for a slim smartphone or tablet computer would require the mechanism take on a slimmer form factor.
2. Reduced size. For this same reason, the overall volume of the device ought to decrease.

3. Larger workspace. The tactor's planar workspace should increase to allow for more distinct or complicated tactile cues.
4. Improved tactor position accuracy. The tactor's location accuracy should be increased throughout this workspace.
    a. Reduced device backlash. Tactor backlash or tactor post rotation should be minimized.
5. Integrated user input. The tactor should be capable of accepting thumb-based input for interaction compatible with modern user interfaces.
6. Tactor velocity. The device's tactor movement should allow translation velocities of at least 12mm/sec that the previous mechanism is capable of.
7. Silent actuation. Reducing the volume of the device actuation would assist in limiting distractions to the user.

The metrics and corresponding goals for some of these improvements are given in Table 3.1. The desired target specification for a 9 mm device thickness originates from the thickness of common smartphones such as the Apple iPhone 4S and Samsung Galaxy Nexus. The goal to decrease overall spatial volume by approximately half is motivated by the desire to move toward integration into portable consumer electronics. By doubling the workspace area the display would be capable of larger more salient and complex tactile and even kinesthetic cues. Ideally the final device could be used to interact with a modern graphical user interface. As such, it must have methods for cursor control and item selection similar to a computer mouse. The audible volume of the device's actuation would ideally be silent, but any mitigation of the sound of the servo gears would be of aid. This final goal is not of primary concern for the updated device.

Table 3.1 Design goal specifications for a low-profile skin-stretch display for the display's physical dimensions, and capabilities and characteristics of the directional cues provided. "Spec. of Prior Flexure Design" indicates specifications from the prior flexure-based skin-stretch display. "Design Spec. Target" lists specification targets for the updated low-profile device design.

Skin Stretch Display Characteristics			Spec. of Prior	Design	
Type	Desired	Metric	Flexure Design	Spec. Target	Goal
Form Factor	Low Profile/Flat	mm thick	44.1	9	Comparable to smart phone
Size	Small Volume	cm^3	56.30	30.00	No larger than flexure design
Workspace Size	Larger Travel Area	mm^2	16	32	Grow to usable skin stretch limit
Methods for Input	Analog or Digital	NA	Neither	Both	Functional for modern GUI
Direction Characteristics for Cue with Finger Applied			Spec. of Prior	Design	
Type	Desired	Metric	Flexure Design	Spec. Target	Goal
Cue Travel	Small Travel Losses	% travel loss	7 - 45	10	Minimal, consistent in all directions
Cue Angle Error	Small Absolute Error	avg deg. error	8	2	Half error of flexure design
Cue Path Width	Small Path Width	avg width mm	0.21	0.1	Linear and narrow completed path

The remaining goals pertain to skin-stretch cue characteristics for simple direction cues that are commanded on an outbound linear path before returning to center, ideally, along the same path. The profile of this roundtrip outward and return path can be used to describe the quality of the directional skin-stretch cue. By enclosing this complete path within a fitted box the overall length and width of the path may be determined. A large path width indicates a potential for causing confusion while delivering tactile signals to the user, as the outbound path may be dissimilar to the return. If travel losses due to finger skin-stretch resistance and display compliance are minimized, less compensation will be required to ensure proper skin-stretch displacements. As there is no direct measurement of the tactor location during normal operation, only some of the device compliance and backlash can be compensated for. The tactor's angular error and path width should be limited when delivering direction cues to ensure distinct cues as close to the intended cue angle as possible. The velocity of the tactor's translation ought to match or improve upon the speeds of the original device. This will provide a more direct

comparison of cue saliency between the devices as well as allow for more responsive and complex cue paths.

3.3 Low-Profile Skin-Stretch Display Design and Fabrication

Several design changes were made in going from the prior flexure-based design to the LPSSD. These changes include going to higher performance servos and using a sliding-plate mechanism design that is actuated by push-pull wires. Details of LPSSD are described below.

To improve tactor responsiveness and accuracy the Futaba S3114 analog servos of the prior flexure-based design were replaced with Futaba S3156MG digital servos that feature a 300 Hz internal update rate and all metal gears. This allows the digital servos to receive and make updates to their position at up to 300 Hz, which is significantly faster than the 50 Hz maximum update rate of the prior analog servos. Rated torque of the digital servos is increased from 1.5 kg·cm to 2.0 kg·cm. They are, however, marginally slower than the prior analog servos (time for 60 degrees of rotation changed from 0.10 seconds to 0.13 seconds when powered at 4.8 V). These servos are still sufficient to surpass velocities tested as perceivable [25]. These servos have been reliable, are compact, and offer sufficient torque and velocity to create salient tactile cues.

The actuating servos are oriented flat on their sides with their largest dimensions parallel with the desired tactor motion, thus creating a lower-profile device. The x-axis and y-axis servos are positioned such that their wiper rotational outputs are aligned horizontally and vertically with the tactor's center, respectively, as seen in Fig. 3.4. To further minimize the footprint, the mounting tabs of the servos are trimmed away and the servos are installed with a light press fit into the housing structure. The cavities that hold

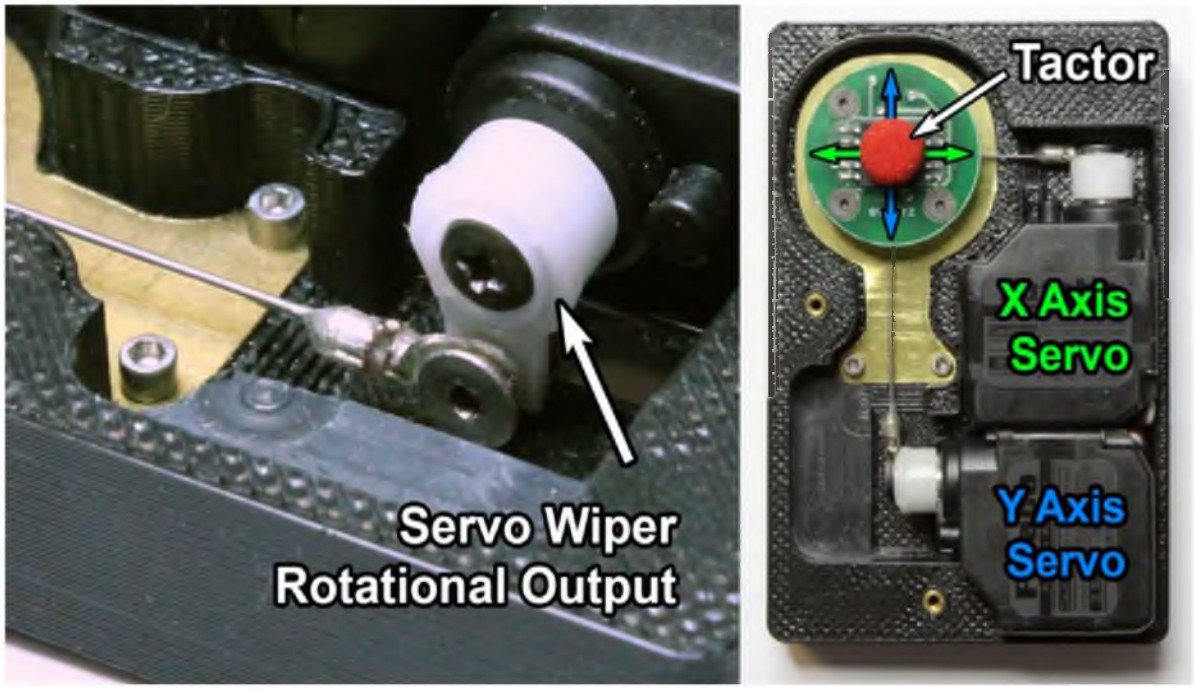

Figure 3.4 Servo wiper rotational output (left). Servo orientation and servo wiper output alignment with plate/tactor centered (right).

the servos were sized to leave a 0.076 mm gap around the perimeter of the footprint of these servos. These tight tolerances allow the servos to be held in place by friction and stop servo rotation within the cavity. The ceiling of this cavity, which resides in the upper half of the housing material, was designed with a 0.36 mm overhead space. This thru-thickness gap maintains servo placement without compressing and deflecting the side walls of the servo, which can lead to binding in the internal servo mechanism. The housing for the mechanism is printed on a Dimension SST 1200es 3D printer with an ABS plastic material. The housing also includes an open cavity that accommodates the sliding tactor plate plus 6.2 mm x 6.2 mm of tactor plate motion. The overall housing dimensions of the skin-stretch feedback mechanism are 42.7 mm x 65.5 mm x 14.0 mm.

The primary design change for the current design was to mount the tactor post to a circular sliding plate to be constrained to planar motion by top and bottom sliding surfaces. By mounting the tactor to this rigid plate the restraints provided by the two sliding surfaces minimize any out of plane rotation to the tactor post. These planar constraints allow the tactor sliding plate to translate and rotate within the plane of the plate cavity (see Fig. 3.5). A plate diameter of 20.0 mm was chosen to be twice the height of the final tactor-to-finger contact location at 7.0 mm. This was chosen to allow a ratio between the moments created by the finger to not cause wedging to occur between the sliding plate and the top and bottom constraint surfaces, based on "rules of thumb" from precision machine design. The device's top face includes a 16.0 mm opening (which we refer to as an aperture) where the tactor protrudes from the sliding tactor plate. The geometry of the aperture opening matches the geometry used in prior skin-stretch-feedback experiments [13]. The surface surrounding the aperture provides support for the user's finger so that he/she may steady his/her finger while the tactor delivers skin stretch to the fingerpad.

To achieve higher accuracy tactor positioning and motion, a more rigid transmission between the motors and tactor is required. A decision was made to continue to use RC hobby servos. The new linkage that connects the servo to the sliding tactor plate is made of 0.50 mm spring steel push-pull wires. These push-pull wires deflect and bend laterally when the mechanisms mating, orthogonal push-pull wire is actuated. These wires maintain a rigid linkage along their respective axes from the servo wiper to the sliding plate (see Figs. 3.4 and 3.5). The tactor plate is not constrained from rotating along the axis perpendicular to the plane of motion except by the combined rotational compliance

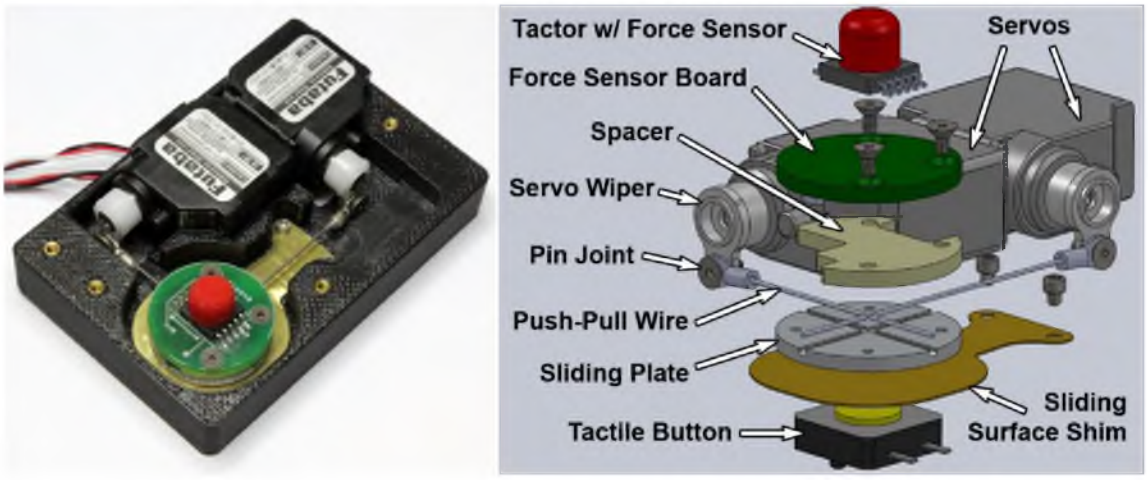

Figure 3.5 Completed low-profile skin-stretch display with top cover removed (left). Exploded internal view of actuation and sensor components of LPSSD (right).

of the two orthogonal push-pull actuation wires.

The sliding tactor plate is cut from 1.6 mm thick aluminum using a water jet cutter (see Fig. 3.6). A center hole is cut in the plate for mounting a tactor post. To firmly attach the spring steel push-pull wires to the sliding plate, grooves are cut into the aluminum sliding plate to create channels that partially embed the wires within the thickness of the plate. This prevents the push-pull wires from slipping relative to the tactor plate and does not require additional mounting hardware, which could catch on the sliding surfaces. The path of these grooves includes a right angle that is designed to cross at the center of the tactor plate. The actuation wires are then bent to a matching angle so that once laid in the channel they do not slip and the distance from the tactor to the servo wiper remains constant. The fastener that is used to attach the tactor post is also used to clamp the push-pull wires to the sliding tactor plate (see Fig. 3.6).

The tactor post is made of a 4.5 mm length piece of 10-32 threaded brass rod and is center drilled and threaded with a 2-56 internal thread. This center-drilled thread

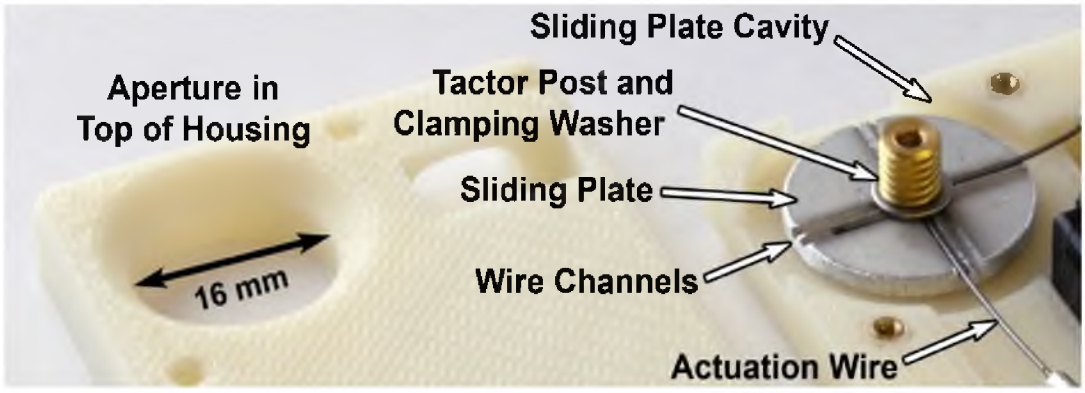

Figure 3.6 Aperture in device housing cover, internal view of actuation components (note that this image is of a prior design with actuation only that does not include the sensor hardware discussed in Section 3.4, which replaces the tactor post and clamping washer. See Section 3.4 for details.)

connects the post to the sliding plate with a flat-head socket screw that passes through the plate. Between the tactor post and the top of the sliding plate, a 2-56 flat washer distributes the clamping force across a wider area of the actuation wires that are resting in their respective channels. For this reason, it is desired that the channels be shallower than the wire's diameter. This allows the clamping washer beneath the tactor post to make direct contact with the region of the actuation wires that protrude above the top surface of the sliding plate.

Making a partial depth cut in the aluminum tactor plate for the push-pull wires required some trial and error testing and used the "scribe" cutting settings on the water jet cutter. Several cutting tests were run on the water jet cutter to calibrate the process for making the wire grooves and to determine a proper cutting speed to create etched channels of the desired depth of 0.35 mm to be cut into the sliding plate. The water jet cutter left a rough finish within these channels, which provided the unexpected benefit of

creating a higher friction surface to clamp the wires against. Once the grooves had been scribed and the sliding plate was cut out of the stock material, manual finishing of the plate was also done. Rough edges at the water jet cuts were filed down, a countersink was made on the underside of the plate to contain the head of a 2-56 flat head socket screw and top, and the bottom edges on the outer diameter of the plate were chamfered. These chamfers help the plate to slide smoothly and keep the plate from catching on the edge of the top aperture opening while returning to center from the workspace limits. The wire grooves were also cleaned up with a hand file where "scribe" lines had overlapped in order to create a clean space for the curved corner of the bent actuation wires.

The means of attachment of the actuation wires to the servos' wiper outputs also require special measures to ensure minimal backlash and compliance. These push-pull wires are linked to the respective servo wipers via two ring terminals, which are normally used as an electrical interconnect component (see Fig. 3.7(right)). The ring terminal has a 0.64 mm wide slot in the side of the crimped tube section cut by a wire electrical discharge machine (EDM) cutter (see Fig. 3.7(left)). The end 0.8 mm segment of the push-pull wire is bent at a right angle to better allow it to be fixed to the eyelet. The end of the push-pull wire is inserted into the tubular section of the terminal ring and the 0.8 mm bend is pushed radially outward to protrude through the slot and creates a rigid mechanical joint along the axis of actuation. An additional 0.4 mm length of spring steel wire 0.64 mm in diameter is then press fit into the ring terminal crimp tube, which holds the protruding section of the actuation wire firmly in place within the slot. The end of the spring-steel wire is abraded to create a quality surface to be attached to the terminal with

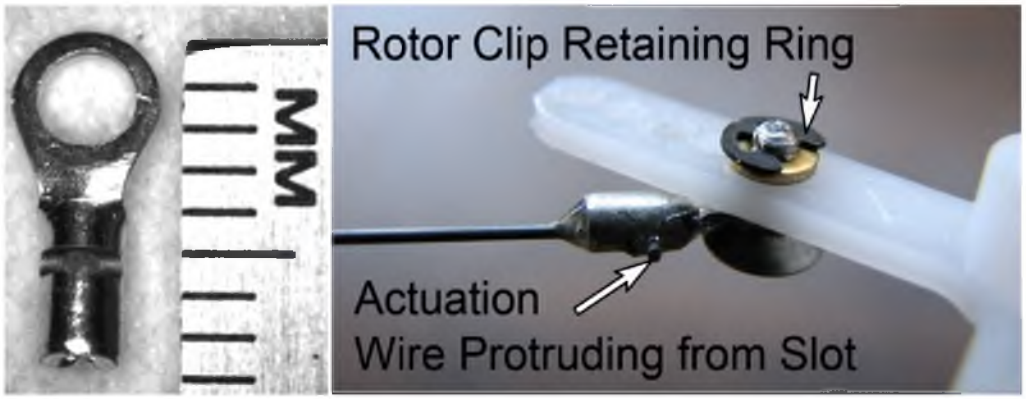

Figure 3.7 Eyelet with slot cut on wire EDM cutter (left). Pin-joint between actuation wire and servo wiper (right). Custom pin with tapered head held secured with rotor clip retaining ring and connection between actuation wire and ring terminal.

epoxy. The wire and ring terminal are bonded with epoxy throughout the terminal tube and cut slot (see Fig. 3.7 (right)).

This ring terminal is then attached to the wiper with a custom machined pin that runs through the ring terminal and nylon wiper as shown in Fig. 3.7. This pin is turned down on a lathe, by starting from a flat head 2-56 screw to remove its threads, to a diameter of 1.575 mm. The corresponding hole in the servo wiper is reamed to 1.55 mm that requires the nylon to stretch to receive the pin. The eyelet holes are used as received from the manufacturer. The tapered head of the pin is pressed against the ring terminal's inside diameter to reduce backlash. While the nylon wiper is under compression, a brass washer and rotor clip retaining ring are installed on the pin end, which keeps the joint from loosening, while not inducing excess friction at the interface.

When the opposing axis is actuated, a minimal amount of rotation occurs at this completed joint due to torsion of the nylon wiper in combination with deflection of the terminal ring in the plane of the sliding plate motion. Extensive testing has shown that

this joint provides smooth rotation and maintains a secure mechanical connection between the servo and push-pull wire. Furthermore, we have not observed any measureable increase in backlash over the course of time, due to the servo-eyelet-wire joint.

With the push-pull actuation wires clamped to the sliding plate, the wires are anticipated to deflect similar to a cantilever beam at the edge of the sliding plate, where they are rigidly attached within the channels. The push-pull wires bend laterally and pivot at the wiper output. Because of the attachment at each end of these wires, it is expected that when the tactor is commanded along a single axis the motion of the sliding plate will translate and rotate along arcs about the opposing servo wiper (see Fig. 3.8). Because of these characteristics, the x and y axes of motion are no longer decoupled as in the previous flexure-stage design. This effect needs to be accounted for in the control scheme of the new device to avoid presenting curved direction cues that may be confusing to the user. Special controller modifications were implemented on the LPSSD mechanism to correct these curved paths, using the dsPIC microcontroller from the prior flexure-based design. New travel limits were also set to avoid forcing the sliding plate into the hard stops. Further details of device control are provided in Section 4.4.

Users familiar with the flexure-based shear display were tested with the skin-stretch mechanism given direction cues in cardinal directions and asked for their qualitative feedback. Responses were positive that the device created prominent cues with a stiff feeling tactor that did not flex or roll under the thumb. The convenient form factor and compact design were also noted.

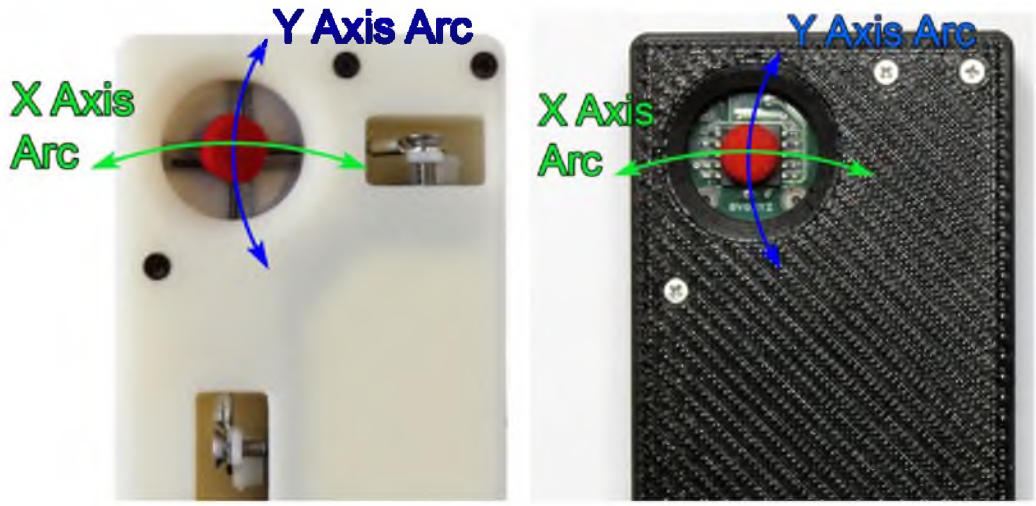

Figure 3.8 Curved tactor paths result from pivots about the anchor point of the push-pull wires at each servo wiper. (left) Prior design in which wiper attachment pivots are visible. (right) Final mechanism design with servo outputs facing back of device and hidden.

3.4 Integrated User Input Interfaces

Two LPSSDs were combined with custom electronics to form a smartphone peripheral that has been configured to communicate with an Android smartphone via Bluetooth serial communication. The smartphone peripheral can both deliver tactile information (i.e., give tactile feedback to the user) as well as receive input from a user through the integration of additional sensors to the LPSSD. Two methods of user input are embedded into the device's tactile interface. These inputs were selected based on their functionality and compatibility with a user fingertip's consistent contact with the tactor. The first method of input is through a momentary tactile switch activated through the depression of the tactor similar to the clicking of a computer mouse (analogous to clicking the button under the current MacBook's touch pad). The second mode of input senses lateral force input on the tactor from the users finger and uses the same force sensor as the IBM TrackPoint™ mouse interface found in laptop computers.

To facilitate the tactile button interface a button cavity in the housing is created below the lower surface of the sliding-plate cavity. A momentary-on tactile switch (Omron model B3W-4005) is installed in this space. The 12.0 mm x 12.0 mm switch features a 350 g actuation switch force that assists in limiting accidental depression of the switch. To maintain a quality sliding surface between the tactor plate and button, a custom thin cantilever plate is made from 0.25 mm thick brass shim material with a water jet cutter. This shim plate is attached to the housing below the south push-pull wire using two 0-80 socket-head cap screws. These screws keep the shim from rotating and catching on the walls of the sliding-plate cavity (prior designs utilized floating shims). By positioning these mounting screws away (by 23.0 mm) from the tactor, the shim is capable of moving up and down upon the button with minimal angular travel. The buttons upward spring force also serves to provide a small upward preload on the sliding tactor plate against the top sliding surface. This preload was adjusted through adding shims below the tactile button and tested to maintain salient tactile button depression. This preload also helps reduce the button travel required to register a "click." We also considered using flat spring washers to increase the required force to depress the tactile button, but this proved unnecessary once the brass shim sliding surface, shown in Fig. 3.9(right), was added to the device design.

To incorporate two-dimensional force input, a TrackPoint™ force sensor with integral strain gage sensors is fitted under and within the tactor cap. The selected CTS SurfStik™ 109 strain gage had been successfully used in a prototype using the previous flexure mechanism (note that the CTS 109 is no longer manufactured and future designs should consider using the NMB "LightPoint™" touch stick force sensor). The TrackPoint™ cap

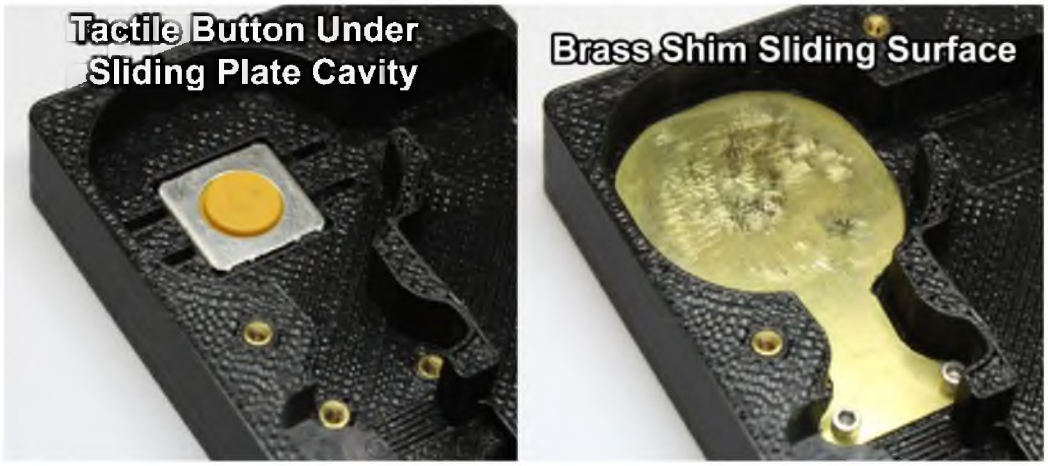

Figure 3.9 Tactile button beneath sliding-plate cavity (left). Cantilever 0.25 mm thick brass shim sliding surface (right).

is mounted to the top of the sensor's strain sensing post with an included plastic adapter. This sensor is surface-mounted to a round printed circuit board (PCB) designed to match the diameter of the tactor plate. Three holes in the PCB accept 0-80 flat-head hex screws for attachment to the sliding plate. The countersunk holes allow the screw heads to be flush with the circuit board's top face that acts as the sliding surface within the plate cavity. These screws run through the force sensor PCB, a printed plastic spacer, and are then fastened into the threaded sliding plate (see Fig. 3.5). The plastic spacer creates a physical space for electrical components on the underside of the PCB while also providing distributed clamping force to the actuation wires against the plate channels (see Figure 3.10).

The skin-stretch prototype with embedded sensors has dimensions of 45.9 mm x 67.7 mm x 18.5 mm. The fully assembled device has been run through extended assessment of its actuation with the tactile button and force sensor in place to ensure dependable operation. The addition of these sensors did not create a drastic difference to

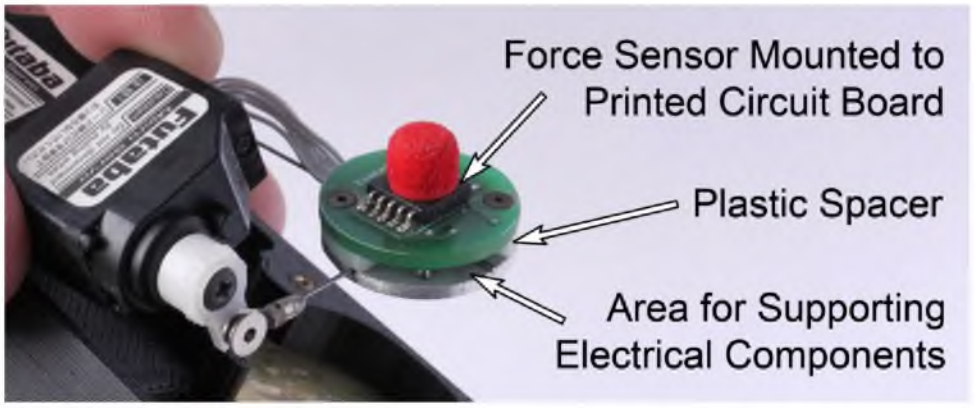

Figure 3.10 Force sensor and printed circuit board attached to sliding plate

the quality of tactor motion or stiffness. Upon concluding this qualitative testing, the hardware had reached a feature set and performance consistency suitable for calibration in preparation for user experiments.

3.5 Electrical Components

The LPSSD is supported by three circuit boards, two of which are custom-built by our lab and one that is a commercially available Bluetooth communications board (see Fig. 3.11). The primary board features a Microchip dsPIC30F4011 microcontroller and manages servo controls, sensor input readings, and communications. The board is capable of serial communications at logic and PC RS-232 logic levels simultaneously. The second custom board reads force sensor data from the strain gauge within the tactor. These signals are amplified and balanced before passing these analog signals to the dsPIC. The third commercially available board is a Bluetooth modem module that makes wireless communication possible (model BlueSMiRF Silver). This modem is connected to the logic-level serial lines of the microcontroller.

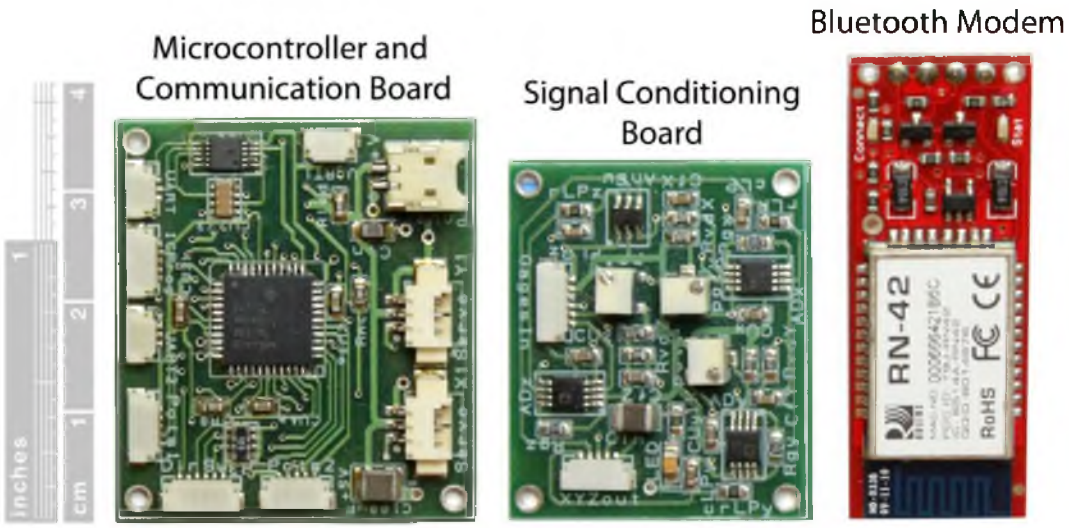

Figure 3.11 Microcontroller/communication printed circuit board (left), force sensor signal conditioning board (middle), and Bluetooth serial modem (right).

3.6 Android Interface and Control

Control of the skin-stretch display is completed over a Bluetooth serial interface between the dsPIC microcontroller and a smartphone (HTC Nexus One) running the Android operating system. This interface is capable of transmitting the tactor force input, current servo position (if appropriate), and tactile button sensor data to the phone. A simple graphical user interface (GUI) on the smartphone is used to issue a variety of commands to the skin-stretch display tactor and to read the LPSSD's sensor data as shown in Fig. 3.12. The LPSSD can be commanded to provide tactile cues in one of the 16 preprogrammed directions as well as run through a list of these cues. The tactor can also be moved to an arbitrary position in the workspace through input on the phone's capacitive touch screen. Parameters for the how the LPSSD's force sensor data is interpreted and settings of the microcontroller program can also be modified from the smartphone interface.

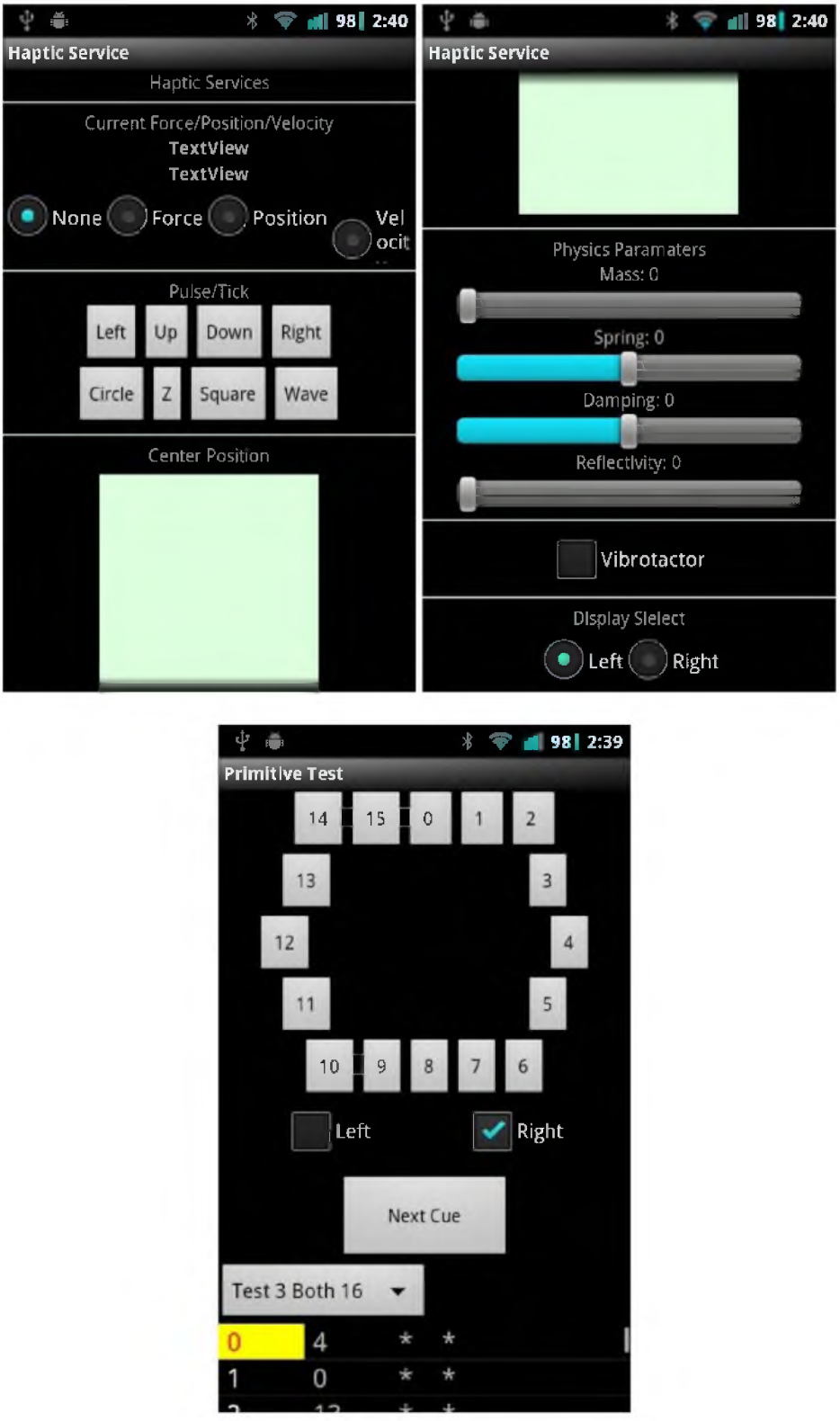

Figure 3.12 Android phone GUI for reading force sensors, modifying microcontroller parameters, manually positioning tactor, or commanding predefined direction cues.

The wireless interface is also capable of sending larger segments of code from the phone, which has large amount of expandable memory, to the microcontroller which has limited memory. Phone-to-dsPIC communication includes the ability to run a cyclic redundancy check (CRC) between the phone and microcontroller to ensure the accurate transmission of data. This feature allows the microcontroller to preload complex tactile cues from the phone as they are needed while ensuring responsive playback of those cues.

Because of latency and potential for error in serial transmission over Bluetooth (which can be caught and resent via CRC checks), the connection is not used for real-time control of the tactor from the smartphone. All tactile movements commanded by the phone to the skin-stretch display are either preprogrammed or are preloaded to the microcontroller before playback to ensure reliable cues.

An example of a simple preprogrammed tactile cue is termed a "tick". For the tactile "tick" command, the tactor is commanded to move in 1 of 16 directions to create the skin stretch equivalent sensation of a button click or detent. After a 20 ms delay the tactor is instructed to return to the start position. This creates an abrupt and short tactor movement, which is perceived as a succinct tapping sensation at the fingertip that contains little directional information. Because the timing and position specifics of this cue are already programmed at the microcontroller, the request for playback from the phone only need include the cue type and direction.

The "pulse" is an example of a more complex cue that requires preloading from the phone before it can be delivered to the user. The pulse motion has a longer tactor movement of approximately 1.8 mm. It can be sent in 1 of 16 directions, using a set of

tactor trajectory waypoints. A preset list of waypoints is transferred to the microcontroller in order to control a skin-stretch cue whose path is adjusted to account for the nonlinear kinematics of the LPSSD. Once the trajectory information is loaded and the integrity of the data is confirmed with a CRC check, the microcontroller can "playback" this tactile cue as instructed by the tactor positions and timings given in the "playback list." This process is described in further detail in Section 4.4. This type of preloaded cue is also capable of complex, nonlinear tactor paths shapes

3.7 Bimanual Skin-Stretch Device Assembly

To test bimanual usage of the LPSSD, two of the completed displays (one of them is mirrored) are mounted into a portable phone peripheral configuration (see Fig. 3.1). The chassis of the two-handed peripheral is made of 1.6 mm thick aluminum plate. Each skin-stretch display is affixed to the top of this plate at its ends for use with the left hand, right hand, and bimanual use. Two grips on the underside of the aluminum chassis provide a location for users to wrap their index and middle fingers to position their thumb over the tactor and promote the desired hand orientation. Each grip contains a vibrating pager motor and two AAA sized NiMH batteries to power the skin-stretch servo actuators. These vibrotactor components are functional and provide salient sensation, but are not used as a part of the current research. On the underside of the aluminum plate and between these two grips is an enclosure, which holds supporting electronics and an additional battery pack as displayed in Fig. 3.13. This Li-Ion battery powers the microcontroller, signal conditioning boards, and force sensors and is electrically isolated from the battery that powers the Bluetooth communications module and RC servos in order to avoid inducing noise onto the sensitive force-sensor signal-conditioning circuits.

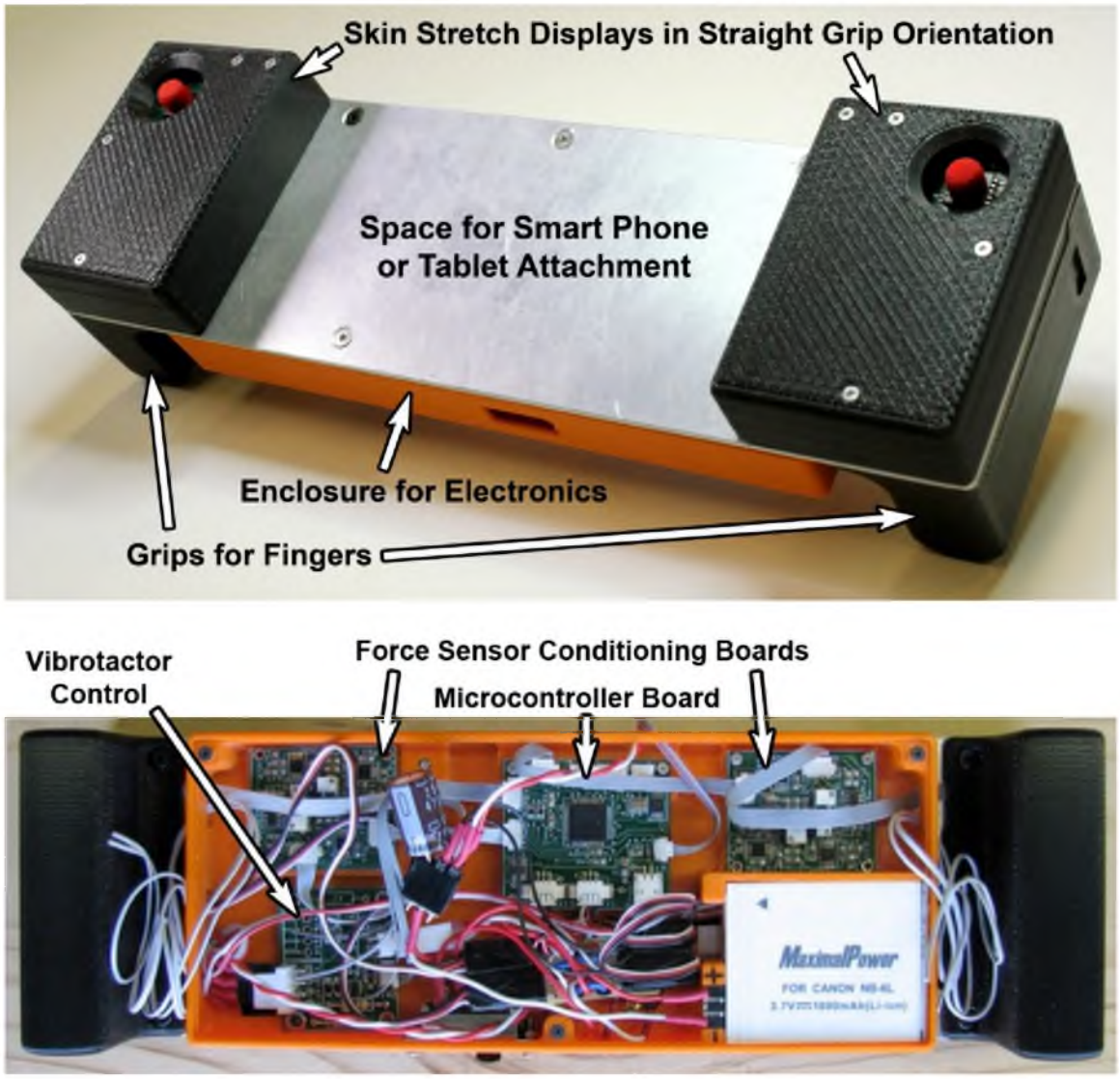

Figure 3.13 Assembled smartphone peripheral with bimanual skin-stretch displays in straight grip orientation (top). Bottom view of enclosure containing supporting electronics and battery within phone peripheral (bottom).

An empty space between the two skin-stretch displays is left for adding a smartphone in landscape orientation or a tablet in portrait.

Previous skin-stretch studies have been completed with the user's finger oriented in the forward direction and aligned with the coordinate system that the direction cues were being delivered in [13]. In this orientation, a forward or "north" direction cue points

directly down the center line of the finger toward the fingertip. To allow testing of users with their thumbs angled toward the center, similar to a console game controller, as well as in a straight-thumb configuration, the chassis is designed such that the left and right skin-stretch mechanisms can be swapped and mounted at opposite ends. Fig. 3.13 shows the peripheral in the straight grip orientation.

3.8 Additional Microcontroller and Android Development for Input Sensor Integration

The software capabilities of the microcontroller and associated Android application are amended to take advantage of the additional features afforded by the smartphone peripheral. These include the simple abilities to accept tactile button inputs or toggle the vibration motors within the finger grips.

More substantial development was required to allow the Android phone to accept inputs from the two force sensors within the tactors of the completed bimanual peripheral. A microcontroller program and accompanying Android application was completed to transmit the current readings from the LPSSDs force sensor to the smartphone. These force readings have a weighted moving average filter applied to the raw force data at the microcontroller before sending to the phone. This filtered force input was then fed into a simplified physics simulation running on the smartphone. Results of this simulation are then transmitted back to the LPSSDs to generate haptic feedback at the tactor.

The overall goal of this effort is to take advantage of the increased computing power of the phone to create high-fidelity virtual simulations that could feed into responsive and complex haptic interactions with the LPSSD tactor. However, the communication

reliability and rates afforded by the Bluetooth serial communication are not sufficient for sustaining responsive haptic rates. This "round trip" transmission method results in lagging tactor motions and unpredictable instability if data is corrupted during transmission.

In a second attempt to explore simple interactions between the tactor motion and embedded force sensor, a program was created to run at the microcontroller to give a basic approximation of a physics simulation. This was done so that a high-speed and consistent communication solution between the microcontroller and smartphone would not be needed. This method is largely successful in creating a responsive tactile interaction with a virtual spring, mass, and damper system. The variables for these effects can be adjusted at the smartphone in real time. The interface for this variable control is shown in Fig. 3.12.

This communication bandwidth limitation could be resolved through a faster and more reliable communication protocol. Updating the current Bluetooth serial communication being used to Bluetooth v2.0 + EDR, would increase the data rate from 57600 bit/sec to 2.1 Mbit/sec.

CHAPTER 4

DEVELOPMENT OF DIRECTIONAL CUES AND DEVICE CALIBRATION

4.1 Calibration Hardware and Initial Direction Cues

To analyze the tactor position and path profile, as presented to a user, it is necessary to capture its x-axis and y-axis translations over time. These paths are captured by securely mounting the skin-stretch display to specially designed calibration hardware to record the two-dimensional travel within the planar workspace. The hardware features two linear probe encoders (model US Digital PE-500-2-I-S-L) mounted orthogonally to read the x and y axes (see Fig. 4.1). These encoders have a travel of 50.8 mm and a resolution of 0.0127 mm. Calibration wires, 18 cm in length and made of 0.5 mm diameter spring steel, are attached at the tactor cap in a fashion that allows free rotation in the plane of motion. These long calibration wires keep position error to a maximum of 0.0011 mm due to the actuation of the opposing axis of 2 mm perpendicular displacement at the tactor. This potential error is an order of magnitude smaller than the encoder's resolution and is thus neglected during device calibration. A microcontroller records position data from both encoders simultaneously at 333 Hz, which is logged to a computer through a serial connection. By logging the position on both axes, a two-dimensional path and corresponding velocity profile of the tactor are produced.

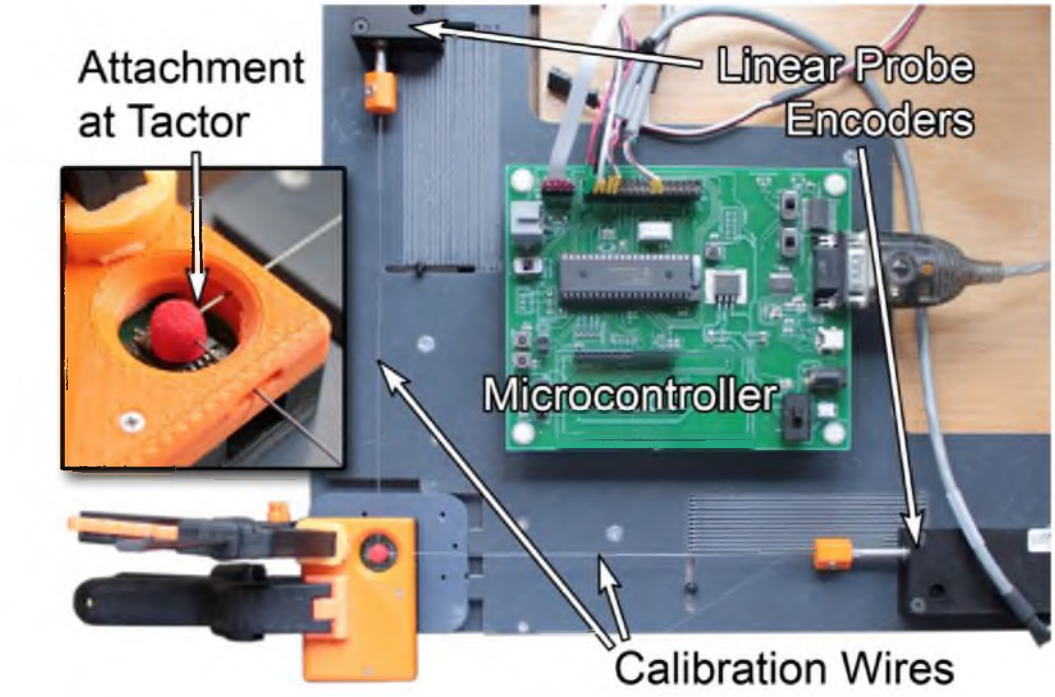

Figure 4.1 Skin-stretch display mounted for calibration and patch capture

The calibration hardware is used to record simple tactile directional cues programmed to move the tactor (e.g., in the cardinal directions; north, south, east, and west). These cues are based on those used by Gleeson et al [25] in a bench-top study that found 99% accuracy was attainable with direction cues of 1.0 mm length delivered to the right-hand index finger. Based on pilot test results of B. Gleeson [25] and the research of J. Craig [26] the outbound tactor translation is held static for 300 ms before returning to the starting position. This is done to avoid any masking effects caused by the onset of two tactile stimuli being too close in proximity. A diagram of the tactor's outbound and return motions is shown in Fig. 4.2.

Because the LPSSD is interacted with in a hand-held configuration similar to a smartphone, in which the user is often distracted with additional sensory input or

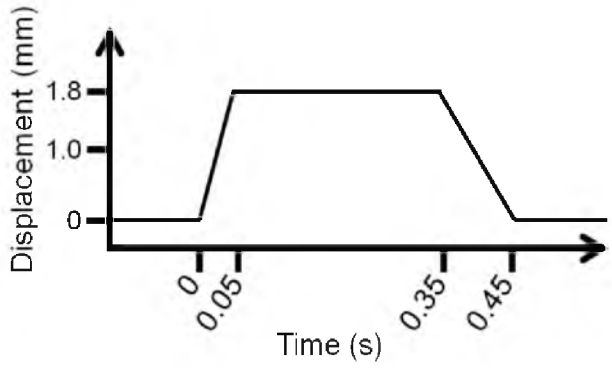

Figure 4.2 Outbound and return path displacement motion of single direction cue.

multitasking, the cue distances are extended to be even more salient. The new mechanism's expanded workspace makes translations of up to 3.0 mm possible. However, as this travel distance increases to 2.0 mm and beyond the chance of a user interaction with the tactor to transition from stretch to slip greatly increases. This slip effect creates an undesired effect as it shifts the contact location on the user's fingerpad and their center reference point is lost. If slip occurs during the outbound portion of a direction cue, the return path induces skin stretch at center position while the user waits for the next cue. For this reason, direction cues are limited to tactor motions of 1.8 mm of outbound travel.

4.2 Sliding-Plate Workspace Curvature and Cardinal Directions

To measure the expected arcing sliding-plate motion, the tactor's path is recorded with the calibration hardware for the cardinal directions with 1.8 mm travel without a user's thumb in place. The distortions of these paths are evident from this data as shown in Fig. 4.3. The greatest deflection recorded, while moving along the y-axis, is 0.254 mm east at end of the north-most tactor motion. In the x-axis of translation, the greatest

position error due to the arced tactor motion is observed when the tactor is moved west, where the tactor's path deflects south by 0.090 mm. These deflections are in range of those expected due to the sliding-plate rotation about the servo wiper attachment point. However, note that tactor motions are slightly asymmetric on each axis, which is most likely due to the asymmetrical lateral stiffness of the eyelet-to-servo-wiper interface. Also, as the tactor motions shown in Fig. 4.3 only actuate a single servo at a time, their return paths remain in line with the outbound paths.

Brief informal testing was done using the LPSSD prior to correcting these curved tactor motions. Users who experienced these curved tactile cues did not make any

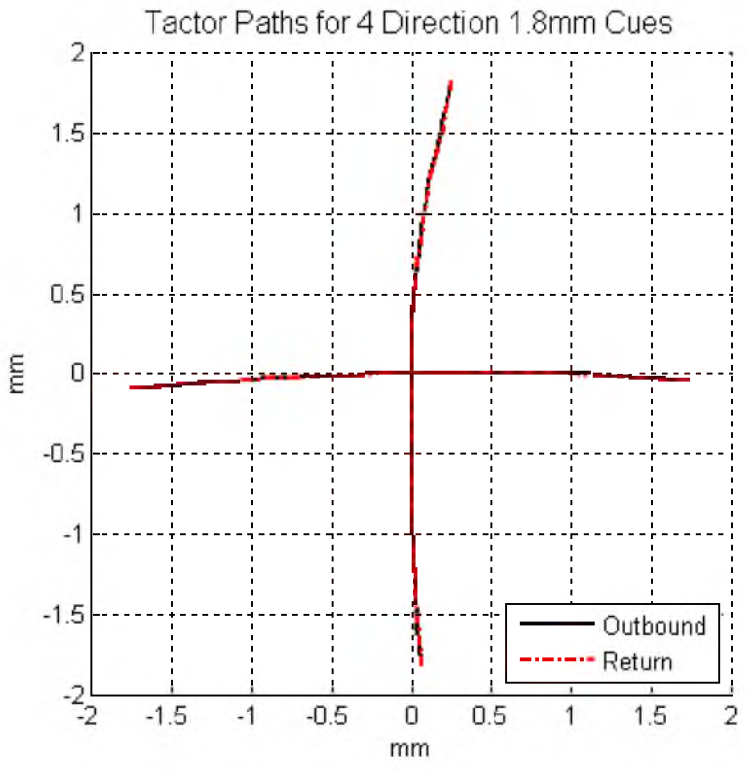

Figure 4.3 Tactor paths for outbound and return direction cues commanded to 1.8mm. X-axis is horizontal (E-W directions) and y-axis is vertical (N-S directions).

comments that the paths were not orthogonal and consistently responded correctly when asked to identify their perceived direction. However, this may be because they were only provided with cues in one of four directions. If direction cues were given in a denser radial array, the arced paths present a greater chance for confusion. Effort was therefore taken to correct these arced paths in order to create straighter tactor motions, which likely will result in clearer direction cues.

4.3 Path Quality of Angular Direction Cues

As a starting point for the skin-stretch display to compliment a wider variety of interfaces on smartphones and other handheld devices, the display must be capable of more versatile direction cues than solely the cardinal directions. A device with a similar tactile interface utilizing lateral movement of pins has resulted in just noticeable differences of 21 to 40 degrees [10]. For sliding feedback at the fingertip the angular JND has a reported average of 14 degrees [27].

To assess how fine of resolution of direction cues can be provided to a person, we have decided to assess more than the four-cardinal directions explored in our lab's past studies [25]. Based on the above JNDs, angular tactile direction cues are programmed in 22.5 degree increments between the cardinal and ordinal directions, to create a total of 16 direction cues. The commanded final outbound positions of all 16 cues are adjusted to reach the desired overall travel distance of 1.8 mm and correct trajectory angle. Each servo is simultaneously commanded with its respective trajectory. Initially, tactor motions were simply based on commanding both servos to their respective endpoints.

As an initial assessment of the motion of the 12 off-axis direction cues (on-axis cues were previously shown in Fig. 4.3), their trajectories were captured with the calibration hardware and plotted (see Fig. 4.4). These motions were simply based on commanding both servos to their respective endpoints. The path types fall into two categories. The first group includes the four ordinal direction cues which have destinations with relatively equal x and y components (i.e., NE, SE, SW, and NW directions). This results in completed paths which are relatively straight and narrow with the widest path approximately 0.3 mm in width (NE direction) and the majority of the path widths measuring 0.1 mm. The remaining eight paths fall into a second group of oblique angle cues which are given end point objectives with disproportionate x and y translations (e.g., NNE, ENE directions). The completed paths of these cues create elliptical leaf shapes. Because both servos are given the commanded endpoint position at the same time, the servo that requires a shorter translation reaches its goal first for each outbound or return portion of these paths. This leaves the opposing servo to finish travelling primarily in one axis. Some curvature remains due to the previously discussed arc motions about the servo-wiper pivots and the combined dynamics of the two deflecting actuation wires. These effects put the tactor on paths with overall widths of exceeding 0.6 mm in width. These paths all leave the center points along the same trajectories as the 45 degree angular cues (since both servos move during the initial portion of each direction cue) and the last portion of their return to center is along the cardinal directions (since only one servo is moving at the end of each motion).

During informal testing, users were again asked to respond with their perceived direction to these cues felt on their thumb. Users reliably gave confident and correct

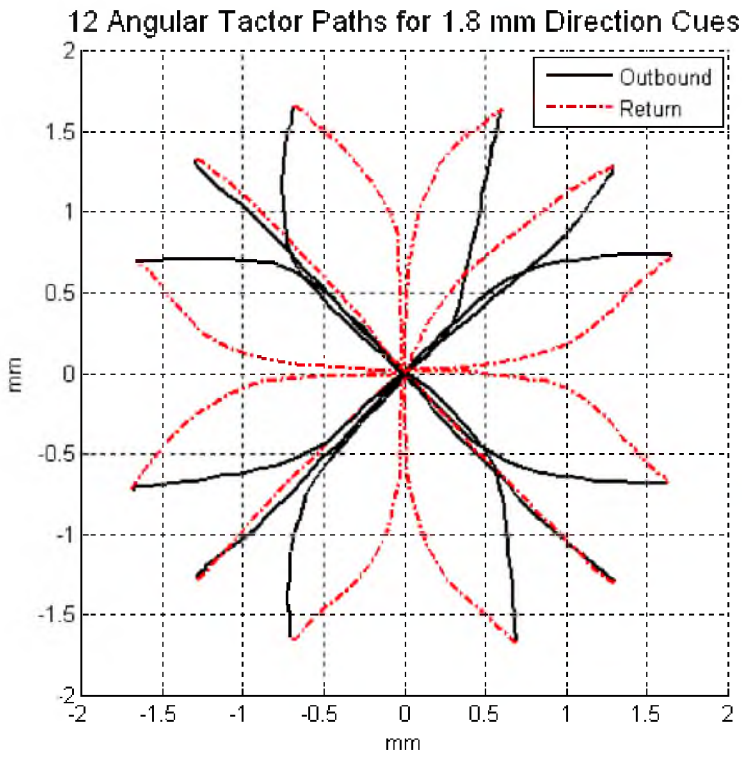

Figure 4.4 Tactor path of 12 angular tactile direction cues to 1.8 mm

answers when given a cue in one of the four ordinal directions (northeast, northwest, southeast, southwest) that maintained overall linear paths. The remaining elliptic leaf path cues confused participants and led to unsure and often incorrect responses. Though only the last group of eight oblique cues is indiscernible/perplexing to users, the tactile cues in all directions were adjusted for consistency by using multiple waypoints to define the paths of each direction cue, which is described in the next Section 4.4.

4.4 Multiple Waypoint Path Correction and Control Setup

Developing linear direction cues in 16 directions necessitates finer tuning of the servos' positions and velocities as well as coordination between the servos of each axis. Ideally a microcontroller would be used to manage the tactor position, and tracking errors

would be minimized by altering characteristics of the servo's internal control law. However, hobby-grade servos predominantly feature a preprogrammed internal control scheme that does not permit later adjustment or real-time access. Servos that do offer custom programming options are currently not available in compact sizes. The skin-stretch display has no ability to sense the tactor position outside of the servos' internal potentiometers, which are not readily accessible. For these reasons, the various sources of path error (i.e., arced tactor path and asynchronous servo motion) are accounted for by supplying a preprogrammed list of waypoint coordinates. These waypoints are commanded to the servos for each of the 16 direction cues (open loop control). This control scheme sends multiple position waypoints during tactor translation, which requires higher-frequency updates than the flexure-based design's Futaba S3114 is capable of. The S3114 and most standard analog servos update at 50 Hz.

The Futaba S3156MG digital servo is rated to read a pulse width modulated (PWM) signal with a carrier frequency of up to 300 Hz. This servo was tested capable of reliably reading pulse width modulation (PWM) at a frequency of up to 600 Hz for extended periods. This test resulted in no hardware or communication failure; however, the servo's internal update rate to the motor remained consistent at 300 Hz. These results reveal the upper-bound update rate from the microcontroller to the servos of 300 Hz.

The S3156MG servos were tested to characterize their responsiveness and resulting path for direction cues commanded with a various number of waypoints between the starting and final outbound position. The waypoint list is read by the microcontroller and each point in the list is encoded with two bytes as the desired change in position for each axis along with the associated timing delay before the next waypoint update. Hence each

waypoint update actually encodes the relative velocity of the tactor. Each 16-bit waypoint is made up of two 6-bit segments to command movements on each of the two axes with 32 signed increments of movement. Each increment equates to approximately 0.04 mm of tactor travel. The remaining 4 bits are used set the length of timing delay before applying the following waypoint. The timing delay parameter can be set from 10 to 170 ms. Multiple waypoints without servo commands can be used to establish longer delays. The number of waypoints used within a tactile cue is only limited by the memory capacity of the microcontroller.

Based on data size restrictions in the waypoint code format and available microcontroller program memory, the length of timing delay is in units of 10 ms delay blocks, which is the rate at which the dsPIC currently implements the device's haptic updates. The microcontroller is configured to generate the servo control PWM signal at a 300 Hz frequency.

To enable sufficient resolution for path trajectory course adjustments, the microcontroller's servo PWM control signal is adjusted to both match the sliding plate's range of motion and also allow higher than the standard 8-bit position resolution that servos are normally controlled with across their total rotational range. This enables smaller distance adjustments, but also requires multiple waypoints to reach the device's total workspace limits, since the device range exceeds the 6-bit value that is encoded within each x and y trajectory update. These increases in control resolution and timing make fine-tuning of the path trajectory possible.

4.5 Development of Direction Cue Tactor Paths

An initial attempt at compensation to create the ideal linear trajectory began with a single waypoint between the start and end locations. Subsequently, to further improve the tactor trajectories, the number of waypoints was increased and timing delays between waypoints in the range of 10 ms to 90 ms were used. The paths are captured and then analyzed for linearity and velocity uniformity. From these test paths control guidelines are ascertained for the purpose of creating direction cues that are 1.8 mm length in 16 directions.

These trials helped to determine a set of control parameters capable of inducing a range of velocities while maintaining the desired linear path. It is concluded that outbound direction cue paths can include as many as seven waypoints with 10 ms delays to create a 1.8 mm linear path without limiting the tactor velocity. To emulate previous tactile cues [25] and induce a slower return path, it is possible to use up to 18 waypoints in combination with 20 ms delays to reduce the velocity by up to 75% while maintaining a steady velocity and a tactile cue that is free from perceptible grittiness or jitter (see Fig. 4.5). Note that for the 14 and 18 waypoint paths shown in Fig. 4.5, undulations can be seen in the tactor's path, but these are quite difficult to perceive tactilely.

From these observations, a range of velocities could be set for a 1.8 mm linear translation. For example, by employing seven waypoints with 10 ms delays a corrected path could be created with 100% of the original servo velocity. Alternately, up to 18 waypoints with 20 ms delays could be used to attain a slower linear path with 25% of the uncorrected path tactor speed.

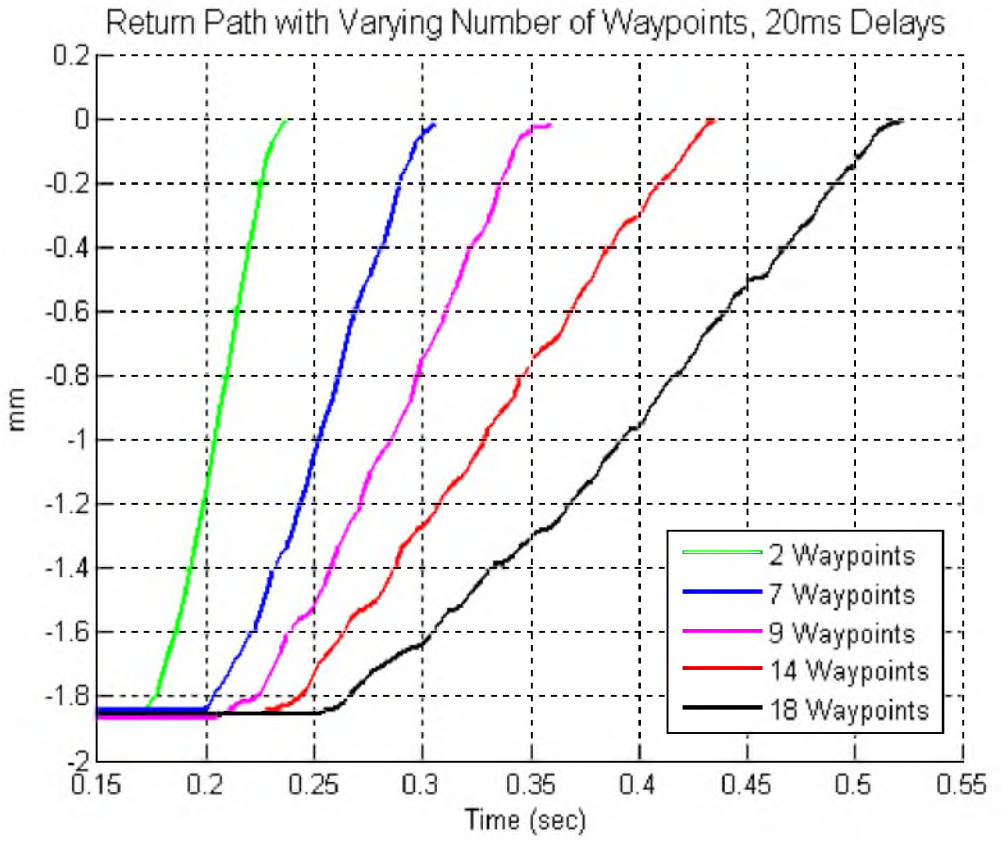

Figure 4.5 Return path of south direction cue versus time, with varying number of waypoints. All depicted tactor motions use 20 ms delays between waypoints.

The 16 cues can be categorized into three groups based on their differing ratios of required x and y actuation. Cardinal directions are driven with almost exclusively a single axis with minor corrective input from the perpendicular servo. Ordinal directions are commanded with relatively equal displacements from each axis. The remaining eight oblique directions, which left uncorrected create elliptic leaf shapes, call for 92% of the actuation of a cardinal in the direction of major translation and 38% in the orthogonal direction. The methods for waypoint distribution and timing vary greatly between these three types of cues to create linear paths. Uniformity between the groups is checked for travel distance and velocity (see Fig. 4.6).

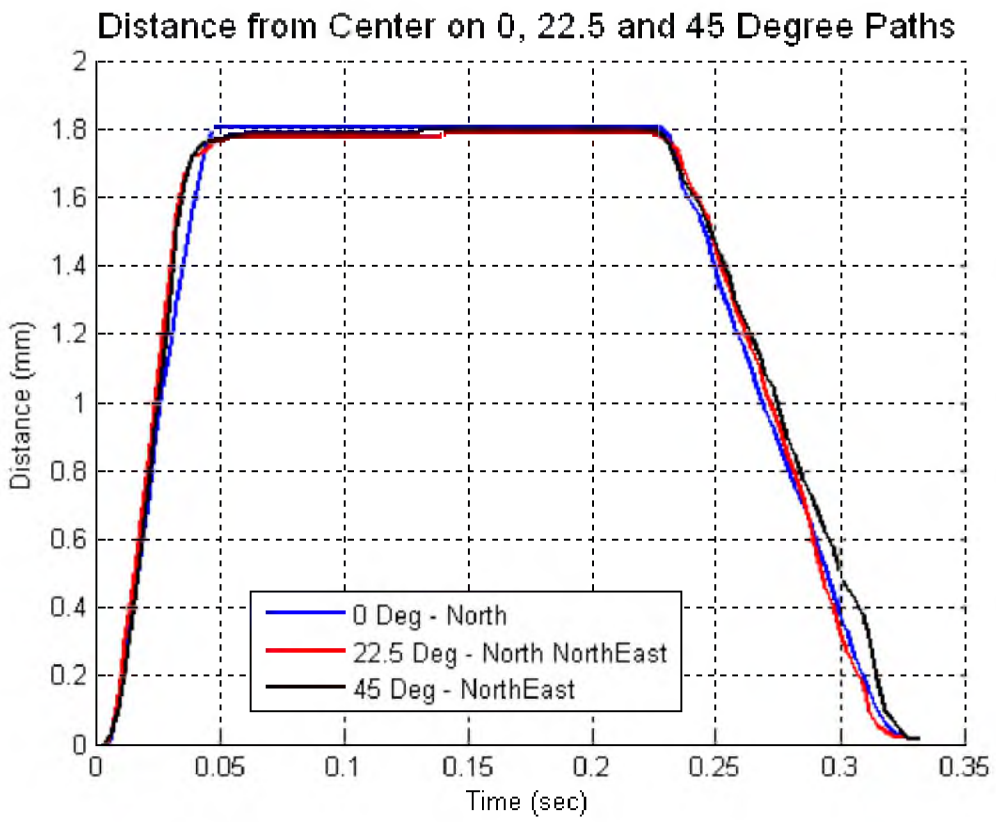

Figure 4.6 Sample plot of distance from center for three cues of varying angles over time to ensure consistent velocities between cues (note that delay in finalized direction cues was extended from a 150 ms hold in the outbound position that is shown above, to 300 ms by use of additional delay time in the waypoint specification. As expected, this change did not affect translation velocity).

The manually tuned and programmed direction cues are created for the 16 directions. Each direction cue is comprised of 23 total waypoints. In sequence, five waypoints direct the outbound path. Three waypoints create the 300 ms delay before the final 15 waypoints are used to return the tactor to center at 50% of the outbound speed. These cues are tuned through visual inspection of their recorded paths checking for velocity consistency, outbound displacement, and overall path linearity. This process begins by initially distributing the timing and x-axis and y-axis translations evenly across the 5 outbound or 15 return waypoints in the desired cue angle for a 1.8 mm. The position data

are recorded for this direction cue on the custom-calibration apparatus shown in Fig. 4.1. The plotted path is inspected and waypoint parameters are adjusted. With repeated cycles of trial and adjustment, the path is adjusted to improve linearity from the start of movement to the end of the return translation. The chosen waypoints provide consistent velocities, relatively linear paths, and accurate endpoints for each of the 16 directions (see Figs. 4.7 and 4.8 for comparison).

A second vertically mirrored LPSSD enables symmetrical two-handed testing. Mirroring existing waypoint lists in software created a starting point for a second set of 16 direction cues for this opposing hand device. Further waypoint adjustment created similar path quality on the second mechanism. The requirement for a separate set of waypoints is expected to be due to manufacturing inconsistencies in the lengths between right angle bends on the actuation wires and slot positions cut in the terminal rings. The waypoints for the second device's 16 direction cues were fine tuned and tested for the same path qualities as the original set. Characterizations of the tactor's motions are presented in the next sections.

4.6 Visual Verification of Calibration Hardware and Direction Cues

To ensure the encoder hardware provides reliable position data and to check that the off-axis bending of the calibration wires only results in minute errors, a set of visual measures are also made. The tactor center and the 16 direction cue endpoints are captured visually through a high-resolution digital camera (model MT1000) attached to an AmScope trinocular stereo microscope (model SM-3T) with an alternate TrackPoint™ cap marked at its center (see Fig. 4.9). Measurements of multiple in-image features are

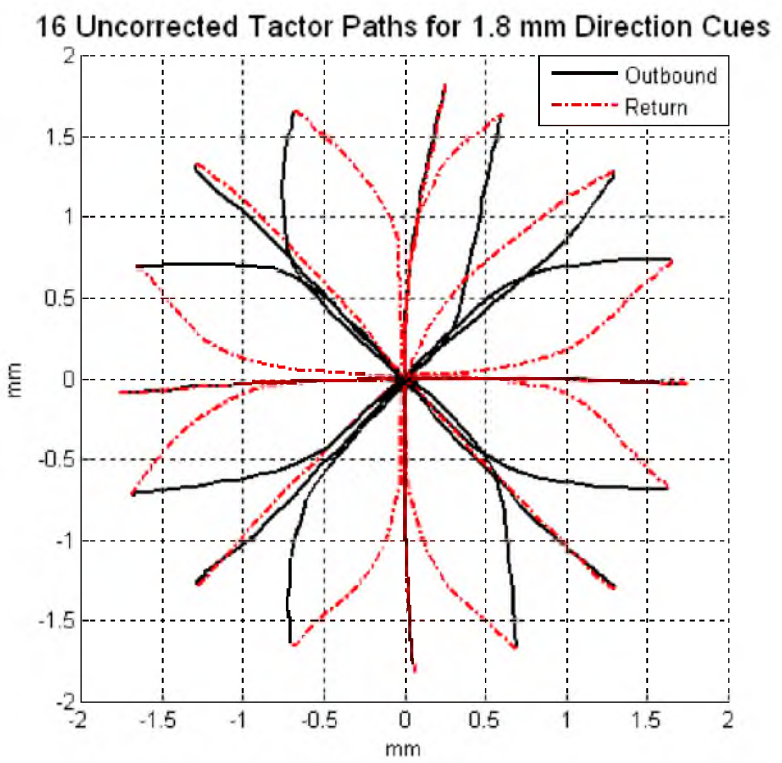

Figure 4.7 Uncorrected path direction cues in 16 directions. Outbound positions are adjusted only for proper travel distance.

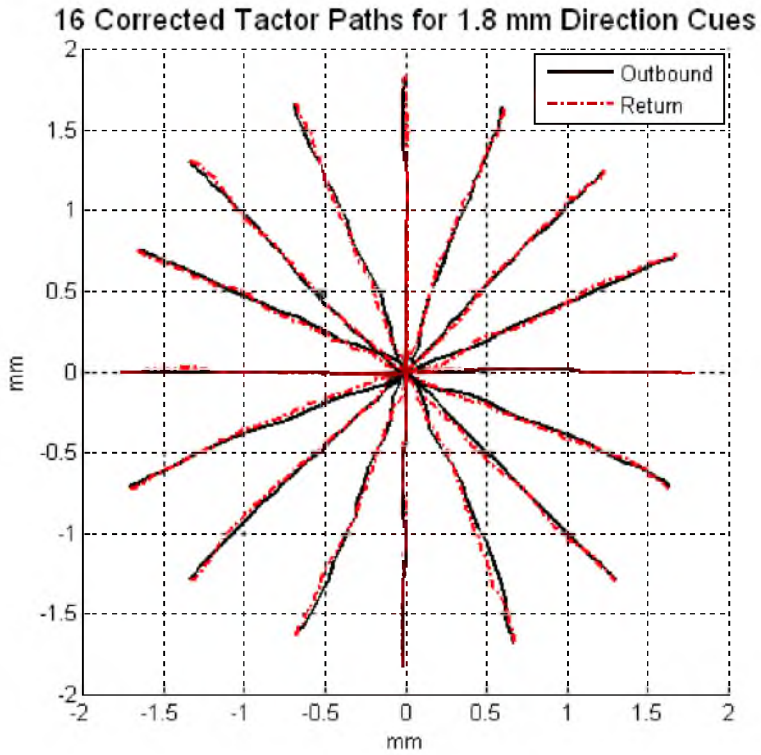

Figure 4.8 Corrected outbound and return paths for 16 directions.

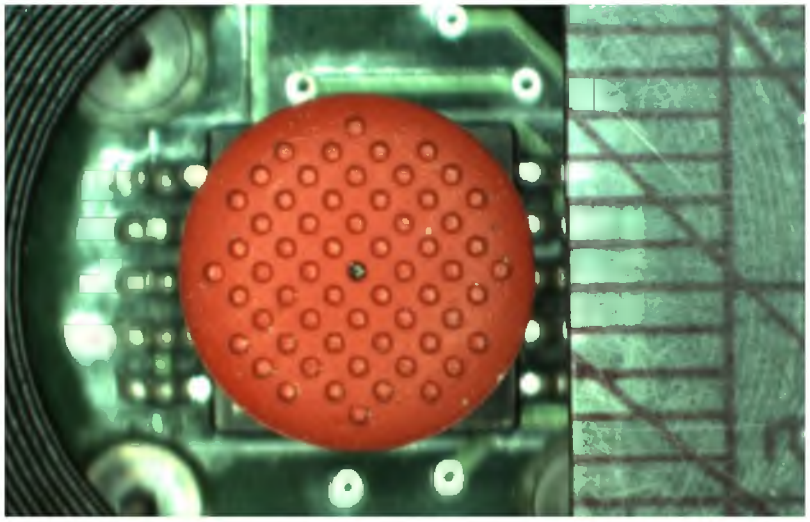

Figure 4.9 Sample scope image used for visual check of direction cue endpoints with millimeter scale in image.

used to create a conversion scale of pixels to millimeters as well as confirm that any lens distortion found throughout the frame do not affect the accuracy of this check. The maximum trajectory error from center to the endpoints of the trajectory was found to be 1.91 degrees counterclockwise (CCW), with average error, as measured by the endpoint of each of the 16 trajectories, of 0.47 degrees CCW error and 1.00 degree standard deviation. Mean cue distance was found to be 1.82 mm long with a standard deviation of 0.06 mm. These results validate the data collected with linear encoders and calibration hardware setup.

4.7 Low-Profile Skin-Stretch Display Performance

The LPSSD is tested to investigate skin-stretch characteristics while operated by end users. The path data for all 16 directions for the "right-hand" were analyzed with the device in the "free state" as well as when a user's thumb is held firmly in contact with the

tactor and aperture ("loaded" state). The thumb is held in a straight orientation such that the thumb tip aligns with the north direction cue. While tactor motion is captured, the user's thumb is visually monitored to ensure a proper grounding contact at the aperture that does not allow movement or slipping of the entire thumb.

For statistical purposes, the measurement of the tactor's motion in the free and loaded states was repeated 10 times in each of the 16 directions. The loaded tactor measurements were performed with the thumbs from 10 different participants : five male, five female, between 23 and 46 years old. The "left-hand" device was also tested 10 times in each direction in the "free" state to test for consistency with the right-hand version of the device. The left-hand device's tactor motion was also tested in the "loaded" condition with one user (for a quick comparison to loaded tactor motion of the right-hand LPSSD).

Metrics for characterizing the device's motions include: average signed angular error, average absolute angular error, average absolute error, average width of the bounding box for each rendered tactor path, and average cue length. A sampling of these bounding boxes encapsulating the tactor's outbound and return paths is shown in Fig. 4.10. The angular error is determined as the difference in orientation of the best fit line to each path trajectory and the intended path orientation. The 95% confidence intervals are also reported for each of these metrics.

The most important of these metrics is the rendered angle of each cue, as this will directly affect the perceived direction of each cue. The best representation of this metric is the absolute angular error. The average absolute angle error in tactor paths, averaged across all 16 directions, including 10 repetitions, was 0.73 +/- 0.08 degrees for the right

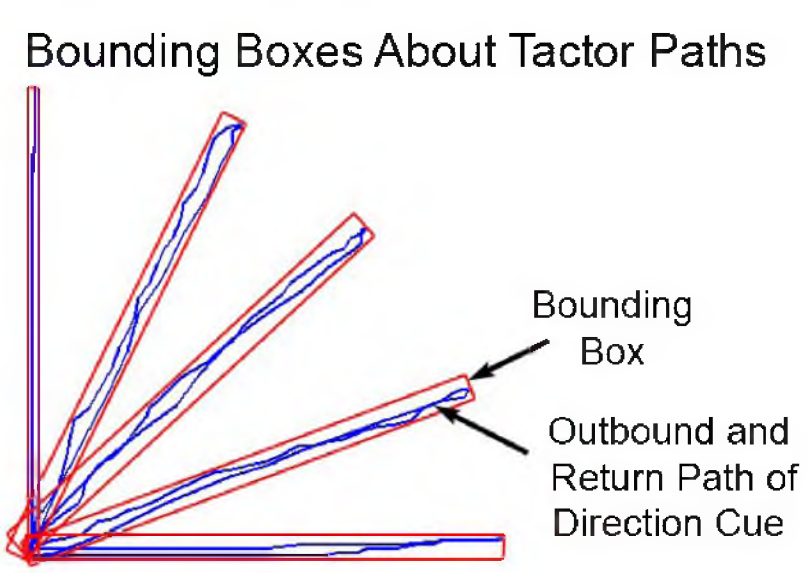

Figure 4.10 Sample plot of complete outbound and return path with calculated bounding boxes used to determine width of bounding box and rendered cue length.

hand device in the "free" (unloaded) condition and was 1.67 +/- 0.06 degrees for the 10 repetitions on each of 10 users in the loaded condition, where the +/- number represents the 95% confidence interval. Note that the error and variance is expected to be slightly higher in the loaded state. Similarly, the left-hand device had an average absolute error for direction cues in the free state of 0.74 +/- 0.11 degrees. For the one user that was tested in the loaded state the device delivered cues with an average absolute error of 1.33 +/- 0.16 degrees. See Table 4.1 for more detailed results of this characterization.

The metrics from the 1600 samples recorded over 10 users' thumbs on the right-hand device were checked for worst-case outliers. It was found that the greatest angle error is 6.51 degrees. The shortest cue length measures 1.394 mm and the widest path bounding box is 0.131 mm. The largest average absolute error from a path's best-fit line is 0.0359 mm.

Table 4.1 Direction cue path characteristics of LPSSDs while in the "free state" (i.e., not contacted by and loaded by a thumb). Data was collected from 10 repetitions of both devices in the free state. Ten users were tested on right device in the loaded condition each with 10 repetitions, whereas the left device was only tested in the loaded condition for one user, to provide a quick verification that both devices perform similarly. The mean and 95% confidence interval are reported for each measurement type.

Low Profile Skin Stretch Mechanism - Tactor Path Charterisitics with 95% Confidence					
		"Right Hand" Device		"Left Hand" Device	
Metric	Units	Free State	Loaded 10 Users	Free State	Loaded 1 User
Average Signed Angular Error	degrees	-0.26 ± 0.13	-0.02 ± 0.10	0.02 ± 0.16	-0.87 ± 0.22
Average Absolute Angular Error	degrees	0.73 ± 0.08	1.67 ± 0.06	0.74 ± 0.11	1.33 ± 0.16
Average Absolute Error	μm	12.2 ± 0.83	13.4 ± 0.31	12.74 ± 0.80	16.8 ± 1.69
Average Width of Bounding Box	μm	37.0 ± 2.62	36.0 ± 0.89	37.6 ± 2.93	42.4 ± 3.81
Average Rendered Cue Lenth	μm	1779 ± 4.72	1547 ± 3.17	1800 ± 4.47	1599 ± 7.63

4.8 General Compensation for Workspace Correction

We have also explored a more general solution to correct the LPSSD's nonlinear tactor movement. This method uses the microcontroller of the calibration hardware to control the skin-stretch mechanism servos. Linear probes from the calibration device shown in Fig. 4.1 allow the microcontroller to capture the tactor's actual position for each corresponding servo command. While this same feedback could be used for closed-loop control, this would not solve workspace irregularities after the LPSSD is dismounted from the calibration hardware. Instead we use these measurements as the basis for specifying a lookup table that can be interpolated by the microcontroller to provide corrected tactor positions once the LPSSD is removed from the calibration device.

Within the microcontroller program, a square grid pattern is mapped to the desired physical workspace limits as shown in Fig. 4.11. This pattern is made up of a five-by-five grid of evenly spaced rows of points across the workspace. The microcontroller commands the tactor to each grid intersection location from a center starting position.

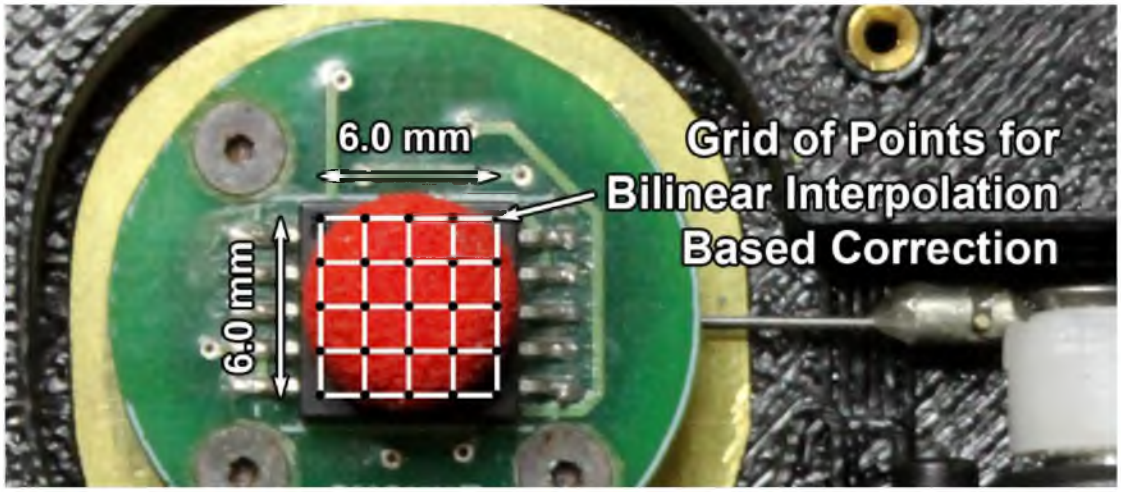

Figure 4.11 Grid of points mapped to skin-stretch workspace for exploring a more generalized methodology for correcting the LPSSD's nonlinear kinematics.

After each trial translation to a point, the tactor endpoint position is recorded along with the corresponding servo PWM signals used for that motion. The microcontroller calculates position error and adjusts the servo commands for the next trial. This process is repeated until the error falls below a 0.038 mm threshold (or three increments on the linear encoder). Requiring a lower threshold led to an extended calibration process with comparable results. This is completed for all 25 intersections on the grid. This results in a table of nominal servo commands that match the physical grid of tested tactor locations with little error.

To command the tactor to any location within the 6.0 mm x 6.0 mm workspace the microcontroller can determine which of the 16 grid regions the desired position falls within. The microcontroller can then recall from a table look-up the four corners of this area and interpolate to determine a pair of x and y servo commands to be issued. This table could be created once and then stored on the microcontroller for future reference.

Figure 4.12 shows an example of the servos' calibrated corner positions (A, B, C, D), which are stored in the look-up table, and the area subsections (w, x, y, z) are displayed that would be used for this bi-linear interpolation. The bi-linear interpolation scheme would be in the form of:

$$PWM = \frac{PWM_A \cdot area_z + PWM_B \cdot area_y + PWM_C \cdot area_x + PWM_D \cdot area_w}{area_{total}} \quad (1)$$

The implementation of this correction process was explored, but is relegated to future work. When attempted, the quality of the correction could be further improved through a denser grid of points as well as explicitly compensating for the small amount of device hysteresis, as was previously done in [14].

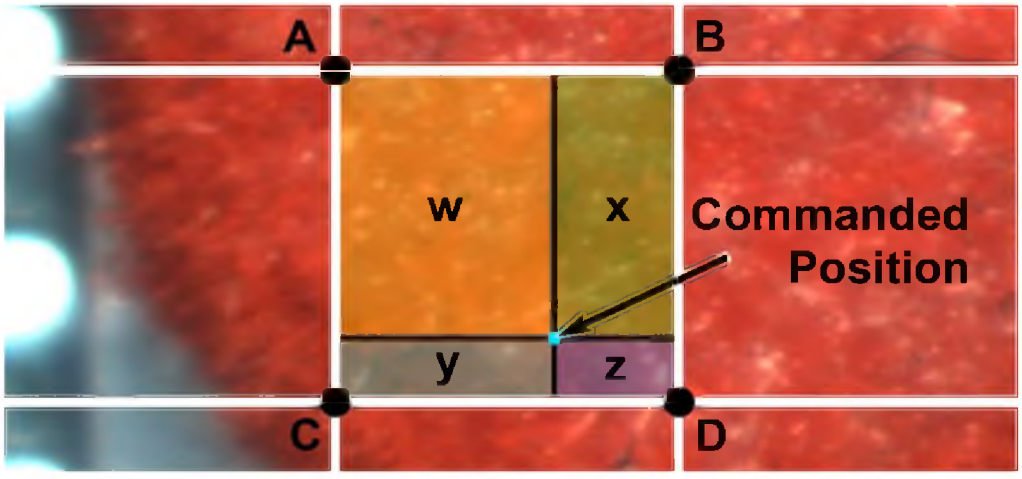

Figure 4.12 Close up of single area on grid used for bilinear interpolation. Each corner of square correlates to the PWM values obtained by automated calibration process.

4.9 Overall Device Design Performance

The overall design and performance of the LPSSD is evaluated based on the original goals of the redesign as shown in Table 4.2. Performance of an actuation-only LPSSD prototype that does not contain a button switch or force sensor is also included in this table. The through-thickness dimension was minimized to 18.5 mm and 14.5 mm for the sensor-embedded and actuation-only LPSSDs, respectively. While short of the 9 mm thickness goal, the physical dimensions and flatter form factor of the LPSSD are much more in line with that of a smartphone. A direct visual comparison is given in Fig. 4.13. The tactor-workspace-area goal was reached in the new display, which increased by 140% due to the increased travel and reduced device transmission compliance. The successful integration of both analog and digital sensors allows for a multimodal interface that keeps the finger in consistent contact with the tactor. The audible volume of servo actuation during tactor translation is not diminished in this design.

The LPSSD's actuation mechanism features more rigid linkages that permit consistent tactile cue playback. Angle error has been reduced to less than 25% of the prior design and absolute average tactor path width for outbound and return motions of the tactor has been drastically reduced down to 0.036 mm. Losses due to the resistance of skin stretch and device backlash/compliance are limited to 13% and are consistent throughout the 16 directions. The LPSSD maximum tactor velocity is approximately 30 mm/sec while under the load of a user's thumb, over twice the speed of the previous device's 12 mm/sec. Furthermore, the two current prototype LPSSD mechanisms have each performed over 10,000 direction cues to user thumbs without need for maintenance or adjustment.

Table 4.2 Performance of prior flexure mechanism compared to final LPSSD with embedded input sensors as well as LPSSD actuation mechanism without these sensors. Visual comparison given in Fig. 4.12.

Skin Stretch Display Characteristics			Spec. of Prior	Design	LPSSD	LPSSD
Type	Desired	Metric	Flexure Design	Spec. Target	with Sensors	Actuation Only
Form Factor	Low Profile/Flat	mm thick	44.1	9	18.5	14.5
Size	Small Volume	cm^3	56.30	30.00	57.49	39.16
Workspace Size	Larger Travel Area	mm^2	16	32	38.44	38.44
Methods for Input	Analog and Digital	NA	Neither	Both	Both	Neither
Direction Characteristics for Cue with Finger Applied			Spec. of Prior	Design	LPSSD	LPSSD
Type	Desired	Metric	Flexure Design	Spec. Target	with Sensors	Actuation Only
Cue Travel	Small Travel Losses	% travel loss	7 - 45	10	13	13
Cue Angle Error	Small Absolute Error	avg degrees error	8	2	1.7	1.7
Cue Path Width	Small Path Width	avg width mm	0.21	0.1	0.036	0.036

Figure 4.13 Form-factor comparison of (left) prior flexure stage design, (middle) LPSSD with embedded sensors, and (right) intermediate prototype without sensors.

CHAPTER 5

DIRECTION IDENTIFICATION USER EXPERIMENTS

To characterize recognition rates for users with the updated skin-stretch display, several perception experiments are conducted in which users are tested in identifying directional skin-stretch cues. An initial pilot study is used to aid in forming ideal testing criteria for the more in-depth "Main Experiment."

5.1 Pilot Test Method and Procedures

An initial evaluation of user perception capabilities of skin-stretch directional cues is obtained through a pilot test in which a single LPSSD device is held in a user's hand (see Fig. 5.1). Two identification tests are administered to eight users. In the first test the user is given skin-stretch cues from the complete set of 16 directions. In the second test, this set is pared down to the eight cues in the cardinal and ordinal directions. Within each test, the cues are given in random sequence and the user receives each direction twice (i.e., two repetitions of each direction cue within the pilot test). Eight males with a mean age of 28 participated in the pilot study. One user is left handed by self report. These two tests are run on each participant's left and right thumbs.

Participants are directed to hold the prototype in front of them. The LPSSD is held relatively level with a small amount of rotation allowed that corresponds with tilting a smartphone screen toward the user's view. Users are seated in a chair that does not

Figure 5.1 Test participant seating orientation showing the divider with arrow display obscuring the user's view of his hand (left). Straight grip used for left hand pilot test (center). Straight grip used for right hand pilot test (right).

permit rolling or swiveling. A divider is used to obscure the user's hand from view to avoid seeing any small thumb movements (see Fig. 5.1). The user is presented with an arrow printout as visual reference of the set of directions being tested for (see Fig. 5.2). Headphones playing white noise are used to mask distractions. Each user is familiarized with the skin-stretch cues during a brief practice session in which each direction is felt twice. Upon sensing a direction cue, the user responds verbally the number label that corresponds to the perceived direction. All tests were completed under Institutional Review Board approved human subjects protocol.

5.2 Pilot Test Results

The results of this pilot test are presented in confusion matrices shown in Tables 5.1 and 5.2 (refer to Fig. 5.2 for direction of numbered cues). A confusion matrix provides the set of rendered stimuli on the left and the corresponding answers that test participants gave across the top row. Correct answers, in which the user perceived the same direction

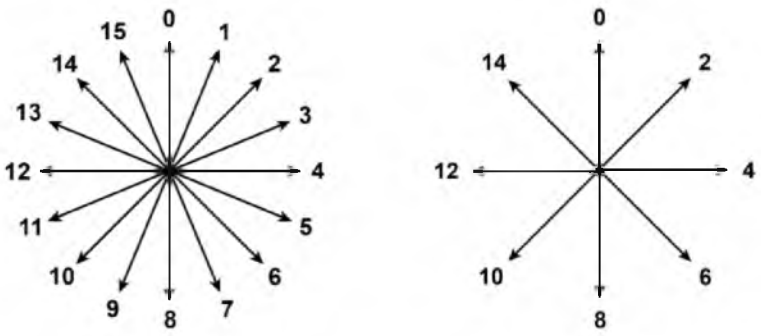

Figure 5.2 Arrow printouts displayed to users during pilot testing for identification capabilities in 16 and 8 directions.

that was rendered to the skin-stretch mechanism, appear on the highlighted diagonal of these tables. Answers are clustered around these diagonal cells showing that incorrect answers in the 8-direction tests are generally within one step, 45 degrees angle away from the correct response. In the 16-direction test, most incorrect answers fall within two increments, again corresponding to being off by approximately 45 degrees. Accuracy percentages are shown in the right vertical column in which the user responded on the same direction as rendered to the finger. For the 16-direction tests, a special case was calculated in which answers given one increment away from the correct answer were also counted as a valid response, which is tabulated on the right-most column of Table 5.2. Further explanation of this calculation and its relevance are given in section 5.4.1.1.

The direction of these errors is also relevant. Both left-hand tests show that incorrect answers are heavily weighted to appear on the off diagonal that is above and to the right of the main diagonal, which corresponds to answers being perceived as clockwise (CW) of the correct direction. Correspondingly, the incorrect answers in the right-handed tests fall on the off-diagonals that are below and to the left of the main diagonal. This indicates that direction cues rendered to the right hand are most often confused as being

Table 5.1 Eight-direction confusion matrices for left and right hands

Left Hand - 8 Direction

	Percieved								
Rendered	0	2	4	6	8	10	12	14	Total
0	11	5							16
2		7	8	1					16
4			10	6					16
6				11	5				16
8					13	3			16
10						10	6		16
12						1	11	4	16
14	6					1		9	16
Total	17	12	18	18	18	15	17	13	

Right Hand - 8 Direction

	Percieved								
Rendered	0	2	4	6	8	10	12	14	Total
0	16								16
2	3	12						1	16
4		2	14						16
6		1	1	14					16
8					16				16
10				1	1	14			16
12						3	12	1	16
14	1						3	12	16
Total	20	15	15	15	17	17	15	14	

more counter clockwise (CCW) than the rendered direction. Therefore users are identifying direction cues, rendered to their thumbs, as rotated such that north direction cues are perceived as rotated inward toward the user's center or sagittal plane, when their thumbs are oriented to face straight forward.

Accuracy was also examined per user and per test condition. Comparing accuracy between users within a test condition shows relatively little fluctuation and has very few outliers. For the 8-direction test, the average percent correct at the left thumb was 64.1% and 85.9% with the right thumb. In the 16-direction test, users average 30.5% correct with the left thumb and 46.1% with the right. Both tests show a significant improvement in accuracy with the right hand. This effect was also noted on a per user basis in 81.25% of the test comparisons. This result was somewhat unexpected and led us to continue testing both thumbs in our main experiment, whose test methods are discussed in the next section.

During pilot testing some users commented on the occasional awkward grip orientation required to put their left thumb in the requested orientation. These

Table 5.2 Sixteen-direction confusion matrix for (a) left hand and (b) right hand.

Left Hand - 16 Direction

	Percieved																	Accuracy	
Rendered	0	1	2	3	4	5	6	7	8	9	10	11	12	13	14	15	Total	On	On +/-1
0	8	5	1												1	1	16	50%	88%
1		7	8	1													16	44%	94%
2			4	8	2	1					1						16	25%	75%
3			1	3	9	2						1					16	19%	81%
4					3	9	4										16	19%	75%
5					1	1	9	4		1							16	6%	69%
6							5	10	1								16	31%	94%
7							1	4	9	2							16	25%	88%
8									11	4		1					16	69%	94%
9									3	8	4	1					16	50%	94%
10											8	3	4	1			16	50%	69%
11											1	2	8	5			16	13%	69%
12													4	6	5	1	16	25%	63%
13													1	6	7	2	16	38%	88%
14	2		1											2	3	8	16	19%	81%
15	10	2													3	1	16	6%	88%
Total	20	14	15	12	15	13	19	18	24	15	14	8	17	20	19	13		30.5%	81.6%
																		Avg. Accuracy	

a)

Right Hand - 16 Direction

	Percieved																	Accuracy	
Rendered	0	1	2	3	4	5	6	7	8	9	10	11	12	13	14	15	Total	On	On +/-1
0	7	3													1	5	16	44%	94%
1	6	7														3	16	44%	81%
2		7	8	1													16	50%	100%
3		1	13	2													16	13%	94%
4			1	4	11												16	69%	94%
5				1	6	7	1									1	16	44%	88%
6					1	6	6	2		1							16	38%	88%
7						2	2	10	2								16	63%	88%
8							1	4	9	2							16	56%	94%
9								2	7	7							16	44%	88%
10									2	5	8	1					16	50%	88%
11										3	7	5	1				16	31%	81%
12											1	7	7	1			16	44%	94%
13													5	8	3		16	50%	100%
14	1													4	11		16	69%	94%
15	3													1	7	5	16	31%	94%
Total	17	18	22	8	18	15	10	18	20	18	16	13	13	14	22	14		46.1%	91.0%
																		Avg. Accuracy	

b)

comments may be related to the poorer performance users had when judging direction cues with their left thumbs. Other user comments included a desire for better ergonomics for the placement of the fingers that are not on the tactor (i.e., the fingers holding the LPSSD) as well as a request for either padding or additional rounding of the LPSSD's corner that presses against the thenar eminence at the base of the thumb.

5.3 Absolute Identification and Relative Identification Test Methods for Main Experiment

To further investigate the initial results of the pilot test and to characterize user capabilities with other patterns of simple direction cues, two more tests are designed. These more in-depth tests make use of the complete bimanual smartphone peripheral shown in Fig. 3.13. This device encourages consistent hand positioning and allows for convenient ergonomics, similar to those found in portable gaming devices. In addition, the peripheral allows for testing of the left hand, right hand, or both hands simultaneously.

Design of the first test was based on user subjective feedback and the results of the pilot test and were also designed to parallel the studies performed by [16]. As such, all test conditions are administered twice – with the user's thumbs in one of two different configurations. In the straight-thumb configuration the user's thumb is aligned with the north/forward direction cue as shown in Fig. 5.1 (right). The second configuration has the user's thumbs angled inward similar to current video game controllers as displayed in Fig. 5.3. This was accomplished through switching the LPSSDs to opposite ends of the peripheral. It was observed that this configuration induces thumb angles between 23 and 47 degrees off the north/forward direction when held naturally by users. The average

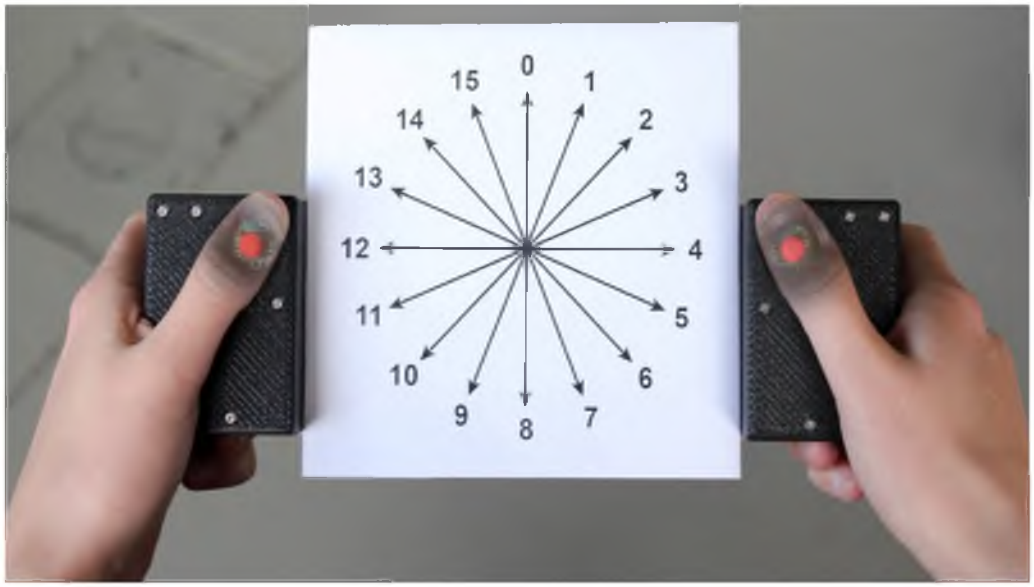

Figure 5.3 Angled grip orientation on bimanual smartphone peripheral with tactor positions shown through partially transparent thumbs.

thumb angle from all test participants is 33.3 degrees. By running all tests with both grip types, it may be determined if one style has an accuracy advantage.

Two tests are run on the device. A diagram of the potential directions being rendered in each test is attached to the peripheral; samples of these printouts are shown in Figs. 5.3-5.5. The first test type is an *absolute* identification paradigm in which the user is given a single cue in one of the 16 directions, consisting of the tactor's outward skin stretch, a 300 ms delay, and a return to center at half the outbound speed (see Fig. 4.2). Each of the 16 directions is repeated 10 times in random order (160 total direction cues). The user verbally responds with the number label of the direction perceived (i.e., they will state a number that is between 0 and 15. See Fig. 5.3).

The second test is a *relative* identification test in which the subject receives a sequence of two separate direction cues separated by a 600 ms pause. The first cue is

always a north (0) direction cue and the user is informed as such so that it may be used as a reference. After the 600 ms pause, a second cue is delivered from the upper subsection of 16-direction diagram – starting with west (12) direction through east (4) direction (see Fig. 5.4(right)). These nine sequences are each repeated 10 times within the random series (90 sequences total). The user responds verbally to identify only the second cue delivered.

Because the first cue delivered in the relative identification test is a consistent direction and already known to the user it can be used as a perceptual anchor. It is expected that this anchor can be used to improve the recognition rates of the second direction cue.

Another motivation behind the relative identification test is to match a potential need for mobile walking navigation, where giving subtle heading corrections could be advantageous. In such a situation the user receives steadily timed updates in the forward

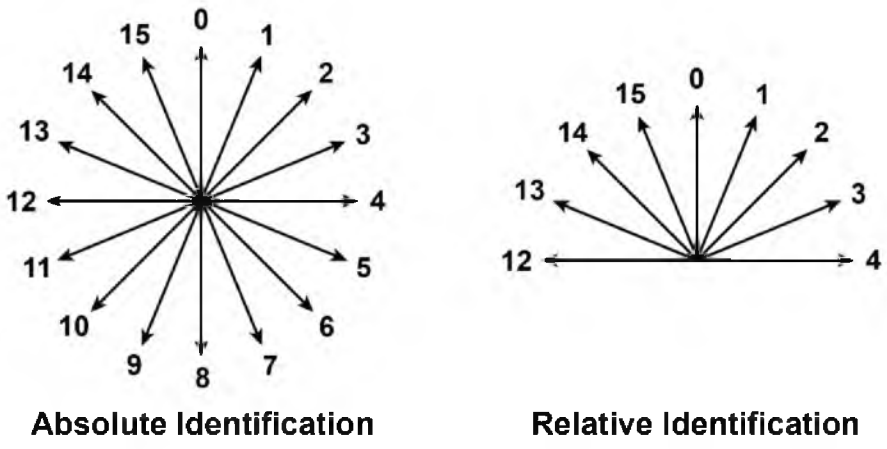

Figure 5.4 Directions cues delivered in *absolute* and *relative* identification experiments. The absolute identification test renders a single tactile cue in one of the 16 directions while the relative identification test first delivers a north '0' direction cue followed by one of the nine directions shown in the right diagram above.

(0) direction that confirm that he/she is supposed to continue their current walking direction. Once the user begins to stray to the left or right of the desired heading, a second direction cue would be interleaved with the existing steady pattern of forward cues. This correction cue is then detected based on its irregular timing with the consistent updates and its offset to one side of north is used for course adjustment by the user.

The 8-direction test used as part of the pilot test was not pursued for further testing as it was decided that many of the trends could be extracted from results of the 16-direction test.

For both the absolute and relative identification tests, the user is tested with left, right, and both hands in both the straight- and angled-thumb configurations. The ordering in which participants complete the tests based on which hand is tested is balanced with a Latin squares design. Half the participants are tested first with their thumbs in the straight configuration while the other half start with the angled-thumb configuration. All users complete the second half of their testing in the opposing thumb configuration. Participants wear headphones playing brown noise to limit distractions and mask the sound of the servos during tactor movement. Small aluminum plate covers are attached to the peripheral as shown in Fig. 5.5 to restrict the subject's view of their thumbs and avoid any visual feedback of the tactor motion. After each verbal response, a pause of approximately one second, controlled by the test proctor, was given before delivering the next cue. This is done to avoid pressuring the subject to respond with a priority of speed over accuracy.

These tests are completed for 12 users (6 male, 6 female) of which two participants are left handed by self report. Average participant age is 32.8 years with a standard

Figure 5.5 Example of seated position for absolute and relative identification tests. The participant's thumbs are in the angled configuration.

deviation of 11.2. Tests were completed over two sessions per user, each session in either straight or angled-thumb configuration. Sessions lasted an average of 75 minutes including approximately 30 minutes of instruction, training, and breaks between tests. Graphical representations of the directions being tested were printed out and given associated numbers in order to facilitate verbal responses of the test participants' perceived directions. These printouts were attached to the smartphone peripheral to disallow any rotation or translation of the graphic relative to coordinates in which the LPSSDs delivered their cues.

Experiment participants, once seated, were given guidance before testing sessions:

- Keep both hands and thumbs in the requested orientation, even if only one thumb is being tested.

- Hold the tactile display device with forearms about parallel with the ground with hands 10 to 30 cm in front of chest. Do not tilt the device about the dorso-ventral or antero-posterior axes (i.e. do not rotate due to one hand further away from body or due to one hand raised higher than the other). Minimal tilting in the left-right axis is permitted for comfort at wrists and to allow easy viewing of directional arrow graphic.
- The device can be held with hands rested on a table, forearms rested on lap or without support.

Users were given a brief training session before each experiment and hand configuration (12 training sessions total per user). In this training the user experienced each cue two times, once in sequence and then in a random order to simulate the test environment. The user is verbally informed the direction they will be given prior to its playback. The user is then given a short trial period in which they verbally respond to tactile cues in the identical fashion as the complete test. These responses are checked by the test proctor. Users were given feedback on their performance and directions with incorrect responses were retested. This trial period was on average one minute long, though some users did require up to two minutes under certain test configurations before feeling comfortable.

The average completion time for an absolute identification test of 160 cues is approximately 9.5 minutes, or 3.5 seconds for each cycle consisting of cue, verbal response and delay before next cue. For the relative identification test of 90 samples, the average time to finish is about 7 minutes, or 4.7 seconds per cycle. This is expected as the relative direction cues take 1.6 seconds to play back while the single-direction cue of

the absolute identification test takes 0.5 seconds. All tests were completed under Institutional Review Board approved human subjects protocol.

5.4 Main Experiment Results

Results for the absolute identification tests are given for the straight and then angled-hand configurations in sections 5.4.1 and 5.4.2, respectively. Sections 5.4.3 and 5.4.4 similarly contain results for straight and angled hand configurations, but for the relative identification experiment. Within each of these subsections the results are presented in confusion matrices, bar graphs showing accuracy for each rendered direction, and followed by polar plots of average signed error per rendered direction.

The confusion matrices display the rendered direction down the left column and user responses across the top. The values inside the matrix give a tally of the number of responses for each direction stated by participants for each rendered direction cue. The highlighted diagonal row indicates correct answers. For the results of these experiments, incorrect answers in each row to the right of the highlighted diagonal are perceived as clockwise of the rendered direction and those to the left were perceived counterclockwise relative to the provided cue. Note that the 16-direction confusion matrices have a horizontal wrap around effect that is most notable for directions 0, 1, 14, and 15. Further explanation of additional calculations on these tables is given starting in Section 5.4.1.1. Overall comparisons of accuracy with confidence intervals for the absolute and relative tests are given in Sections 5.4.2.1 and 5.4.4.1, respectively, for all handedness conditions and both straight and angled thumb orientations.

Bar graphs are used to gauge average user accuracy on a per direction basis. For each test direction, accuracy results are given for left, right, and bimanual test configurations

for convenient for comparison between hand configurations. This graph also allows for a visual check of accuracy trends across directions.

The final sets of figures within the first four primary subsections of absolute and relative identification test results are polar plots of signed mean error. These plots show the same direction biases present in the confusion matrices, but simplified into a single value showing participants' mean error for each rendered direction, plotted as a dashed arrow in the same coordinates that the tactile cues were given. These plots present the relative magnitude of errors and general trends of user confusion. Note that these plots are split into pairs to ease readability and make user tendencies more evident.

Bar graphs are also used in Section 5.4.5 to compare user accuracy in the directions shared between the absolute and relative identification experiments. While not a precise comparison, these plots give a general sense as to the increase in direction identification accuracy when users are supplied with a known perceptual reference with which to compare subsequent tactile cues.

Information transfer test results and equations are given in tables of Section 5.4.6. These values estimate the skin-stretch displays communication bandwidth, in bits, for each test. It also gives a sense as to the maximum number of directions that could be used with a goal of 100% accuracy.

Differences in the way that participants perceived and responded to direction cues in cardinal and ordinate directions were compared to the remaining oblique direction cues in Section 5.4.7. The counts of participant responses in each of the directions are used to calculate if users prefer to answer in the subset of eight cardinal/ordinal directions as opposed to the remaining 8 directions that are not multiples of 45 degrees. The results for

these calculations for user direction bias are given within tables of Section 5.4.7. The accuracy of users when given cues in these 'preferred' directions are compared to the remaining eight directions for each test condition. Relations to the "oblique effect" are discussed.

A metric for the bias free measure of accuracy, d', was also calculated for each test condition. These results echo the results reported based on the reported percent accuracies, but also account for false alarm rates given by participants to more accurately identify participants' best performance conditions.

5.4.1 Results for Absolute Identification Experiment with Straight-Thumb Orientation

5.4.1.1 Confusion Matrices

Participant responses are first presented using confusion matrices. Confusion matrices are presented in Tables 5.3, 5.4 and 5.5 for the straight grip absolute identification test for the left, right and both hands cases respectively. Rendered skin-stretch cues in directions 0 through 15 are given on the left column and can be referenced in Fig. 5.4. The perceived directions users verbally responded with are displayed across the top row. The cells shaded diagonally across the response tallies are the cells corresponding to correct answers (i.e., user responded in the direction identical to rendered). The accuracy rates for this case are listed in the first accuracy column labeled "On".

A special case is calculated for the results listed in second accuracy column labeled "On +/- 1" to create an estimate of user performance in an 8-direction test. These are calculated by also considering user responses that are in error by a single increment (+/- 22.5 degrees off) to be correct answers (i.e. user responses 3, 4, and 5 are considered

Table 5.3 Confusion matrix showing the pooled responses for all 12 participants for absolute identification left hand, straight grip

Left Hand Absolute Identification Straight Grip

	Percieved																Acurracy	
Rendered	0	1	2	3	4	5	6	7	8	9	10	11	12	13	14	15	Total	On	On +/- 1
0	35	44	33										1		1	6	120	29%	71%
1	9	30	58	17	4											2	120	25%	81%
2		4	39	40	29	7	1										120	33%	69%
3		1	6	27	50	26	9	1									120	23%	69%
4			1	9	42	40	27	1									120	35%	76%
5				1	7	27	57	26	2								120	23%	76%
6			1		1	9	32	59	14	4							120	27%	83%
7						1	7	39	63	7	2	1					120	33%	91%
8							1	10	59	32	18						120	49%	84%
9								1	13	36	49	18	2	1			120	30%	82%
10								1	1	13	24	42	28	9	1	1	120	20%	66%
11										3	10	20	46	26	13	2	120	17%	63%
12		1									1	1	21	44	47	5	120	18%	55%
13	3												3	19	62	33	120	16%	70%
14	31	3	1			1								6	35	43	120	29%	70%
15	58	15	2									1		1	12	31	120	26%	84%
Total	136	98	141	94	133	111	134	138	152	95	104	83	101	106	171	123		27%	74%
Percent	7%	5%	7%	5%	7%	6%	7%	7%	8%	5%	5%	4%	5%	6%	9%	6%		Avg. Accuracy	

Avg Absolute Error	
1.0396	Increments
23.39	Degrees

Table 5.4 Confusion matrix showing the pooled responses for all 12 participants for absolute identification right hand, straight grip

Right Hand Absolute Identification Straight Grip

	Percieved																	Accuracy	
Rendered	0	1	2	3	4	5	6	7	8	9	10	11	12	13	14	15	Total	On	On +/- 1
0	41	4												2	28	45	120	34%	75%
1	61	38	9	1		1								1	2	7	120	32%	90%
2	17	55	41	6												1	120	34%	85%
3	1	14	61	34	8										1	1	120	28%	86%
4		4	36	51	29												120	24%	67%
5			9	27	63	18	3										120	15%	70%
6			2	13	26	46	26	7									120	22%	66%
7				3	2	11	34	44	26								120	37%	87%
8						1	11	27	69	11	1						120	58%	89%
9							1	9	54	48	8						120	40%	92%
10							1	5	12	50	48	4					120	40%	85%
11								1	1	34	62	17	5				120	14%	70%
12						1			2	6	34	47	22	5	3		120	18%	62%
13										1	14	25	48	18	14		120	15%	67%
14	1										3	4	26	52	24	10	120	20%	72%
15	4												3	14	63	36	120	30%	86%
Total	125	115	158	135	128	78	76	93	164	150	170	97	104	92	135	100		29%	78%
Percent	7%	6%	8%	7%	7%	4%	4%	5%	9%	8%	9%	5%	5%	5%	7%	5%		Avg. Accuracy	

Avg Absolute Error	
0.9896	Increments
22.27	Degrees

Table 5.5 Confusion matrix showing the pooled responses for all 12 participants for absolute identification both hands straight grip

Both Hands Absolute Identification Straight Grip

	Percieved																	Accuracy	
Rendered	0	1	2	3	4	5	6	7	8	9	10	11	12	13	14	15	Total	On	On +/- 1
0	74	19	4											1	2	20	120	62%	94%
1	21	45	47	7													120	38%	94%
2		8	65	43	2	2											120	54%	97%
3			22	52	39	7											120	43%	94%
4			9	29	72	9									1		120	60%	92%
5			1	20	51	41	7										120	34%	83%
6				1	8	30	62	18	1								120	52%	92%
7						1	34	54	30	1							120	45%	98%
8							4	7	83	23	2	1					120	69%	94%
9								2	27	41	42	8					120	34%	92%
10								1	1	21	62	27	7		1		120	52%	92%
11										4	25	51	32	8			120	43%	90%
12											3	14	72	22	9		120	60%	90%
13											2	5	30	54	27	2	120	45%	93%
14													4	30	68	18	120	57%	97%
15	18	2												10	39	51	120	43%	90%
Total	113	74	148	152	172	90	107	82	142	90	136	106	145	125	147	91		49%	93%
Percent	6%	4%	8%	8%	9%	5%	6%	4%	7%	5%	7%	6%	8%	7%	8%	5%		Avg. Accuracy	

Avg Absolute Error	
0.5896	Increments
13.27	Degrees

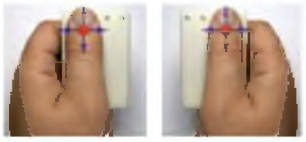

correct answers for a cue rendered in the 4 direction). This span of three increments of answers covers a range of angles slightly greater to the range of perceived directions for answering correctly in an 8-direction test as depicted in Fig. 5.6. This accuracy calculation is evaluated as approximately 67.5 degrees if summing the full range of the single correct answer plus the angular range of each of the adjacent directions. While not a direct predictor of an 8-direction experiment, it is a reasonable approximation as will be explained next, based on the pilot test data.

The average accuracies for the 8-direction pilot tests, in which the user's thumbs were in the straight configuration, are 64.0% and 85.9% for the left and right hands respectively. As the poorer performance for the left hand is likely an artifact of the poor ergonomics of the device used for the left-hand pilot tests, we will take 85.9% as the more appropriate accuracy estimate of a single handed, straight configuration, 8-direction experiment. This 8-direction accuracy estimate is similar to the 16-direction pilot test's averages of a "On +/- 1" column for the same configurations, which are 81.6% and 91.0% – for left and right hands, respectively. Again, due to ergonomic issues for the left hand tests, 91.0% for the right hand "+/- 1" 16-direction pilot test is the best number for comparison to the 85.9% accuracy numbers for the 8-direction pilot test. Based on these observations, the number reported in the "On +/- 1" columns for our 16-direction experiments provides a reasonable approximation (and perhaps a slight overestimate) of the predicted user performance for an 8-direction experiment.

For reference, the "On +/- 1" columns of the main experiment's averages for the same straight-thumb configurations are 74% and 78% (left and right hands, respectively), which are lower than the "On +/- 1" 16-direction accuracies of the pilot test. However,

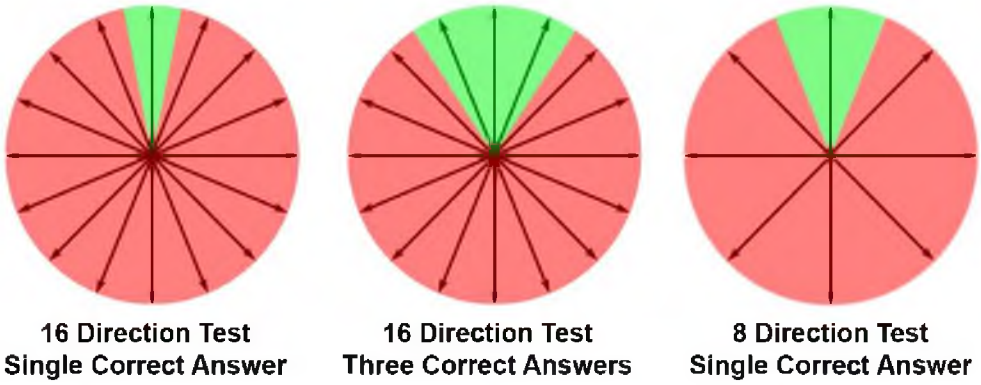

Figure 5.6 Response ranges used for predicting results of an 8-direction experiment based on the accuracy results of the 16-direction absolute identification experiment. Using the responses from the adjacent bins in a 16-direction is expected to be a slight overestimate of what would be found if conducting an 8-direction experiment.

the main experiment was conducted with fewer participants, all of whom performed above average in the main experiment. Therefore, the "On +/- 1" 16-direction accuracies is still believed to be a reasonable estimate of expected accuracies of an 8-direction experiment, though probably a small overestimate, as indicated by a comparison of the middle and right-most images in Fig. 5.6.

Unless noted, all statistics reported are performed on the accuracies reported in the "first accuracy column" reported on the lower right side of each confusion matrix, which tallies only correct answers for the 16-direction experiments.

The bottom left of each confusion matrix reports the average absolute error in direction increments, which we also refer to as "bins" (e.g., a value of 1.0 for this error would correspond to users responding with an answer that is on average one bin away from the correct answer). This value is multiplied by the direction cue spacing (22.5 degrees) to give a sense of the overall absolute average error that users are making, measured in degrees.

Looking first at the confusion matrices for the left hand, straight configuration, it can be seen that people responded with an average accuracy of 27%, which is far better than a chance response accuracy, but certainly not a level that would be considered as reliable for communicating direction information. It can also be seen that when grouping correct responses with the responses given in the next nearest direction, which is a reasonable predictor of performance for an 8-direction test, that the reported accuracy goes up to 74%. This rate is also lower than what is desirable. Table 5.3 also shows that the average absolute error to be 23.93 degrees. In contrast to the pilot tests, similar though slightly improved performance can be found for the right hand, straight configuration in Fig. 5.4 for the 16- and 8-direction accuracies and absolute error.

Returning to Table 5.3, it can be seen that when participants answered incorrectly for the left hand, that their answers tend to fall on the off-diagonal that is above and to the right of the main (correct response) diagonal, which indicates a clockwise confusion. The opposite trend is shown for the right hand, straight configuration as shown in Table 5.4. This same observation with respect to the appearance of rotational bias when presenting direction cues to a participant when their thumb is extended forward was found in our pilot tests and in a prior study [13].

Accuracy rates for the straight configuration when both hands receive direction cues increases from the high twenties up to 49% average accuracy for the 16-direction test. Including the neighboring responses as a correct response (to get an estimate of the accuracy if an 8-direction experiment were to be conducted) yields an 93% accuracy level, which is nearing an accuracy level one would consider for communicating direction information in a consumer device such as a handheld GPS unit.

In addition to the higher accuracy rates observed when both hands are used, it should also be noted that the rotational biases that were observed when single thumbs received direction cues in the straight configuration, that such bias is no longer observable when both hands are used in the straight configuration.

A one way between subjects ANOVA is conducted to compare the effect of handedness and number of hands used on accuracy in the absolute identification test with straight-thumb orientation for left hand, right hand, and the both hands conditions. There is a significant effect of handedness on accuracy at the $p<.05$ level for the three conditions [$F(2,5757) = 136.77$, $p < 0.001$]. As it is found to be significant, a post hoc test is computed using a Tukey's honest significance difference (HSD) method. It is designed to compare each condition to every other condition. The post hoc comparisons using the Tukey's HSD test indicate that the both-hands configuration is significantly more accurate than either the left or right hand conditions ($p <= .001$). However no significant difference was found between the left and right hand accuracy. A plot of these accuracies and confidence intervals can be found in Secion 5.4.2.1 alongside results of the absolute identification test with angled thumbs.

Further observations can be made about the straight hand configuration results by examining the plots in the next section.

5.4.1.2 Accuracy and Polar Plots

Figure 5.7 shows bar graphs that display accuracy levels, compared by direction, of the straight grip absolute identification test for each hand configuration. The substantially improved performance when the user is tested with both hands is clearly

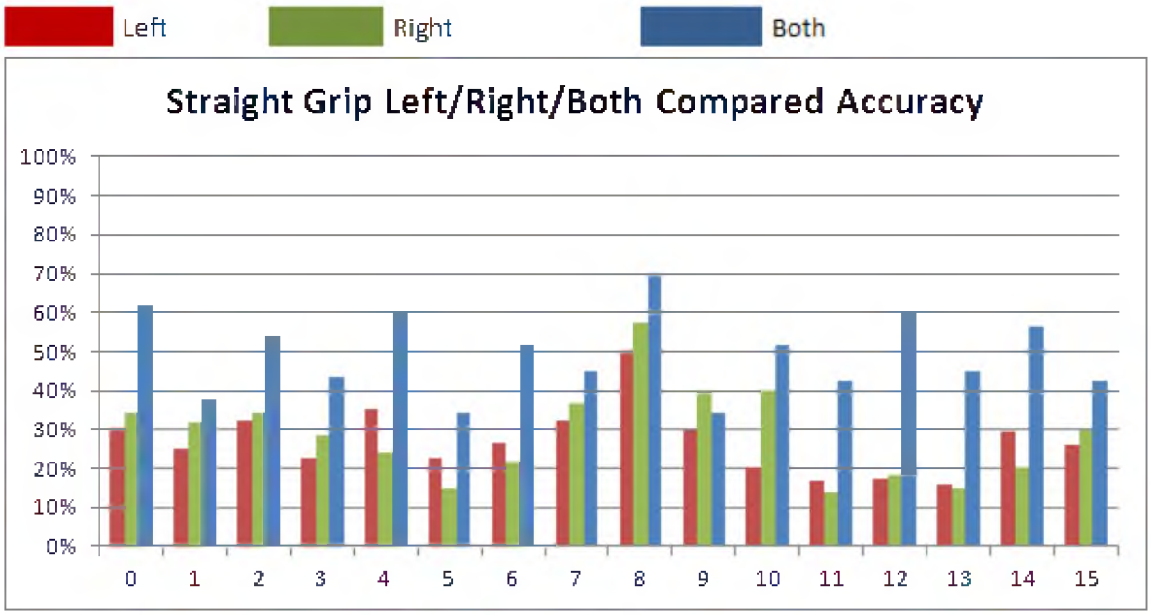

Figure 5.7 Bar graph showing the pooled accuracy levels for all 12 users per direction comparing left, right and both hands for straight grip absolute identification.

visible by the taller, blue bar shown for every cue direction. Another distinguishable trend seen for all hand configurations are the peaks in accuracy found at the south or '8' direction that taper off with adjacent bins. This may suggest that user responses are being affected by the mechanical attributes of the skin-stretch, the physical interaction of the tactor with the thumb, or some other perceptual user bias. This peak is most prevalent in the single hand tests. Also worth noting is that the four cardinal directions (0, 4, 8, and 12) have the four highest accuracies in the dual hand ("both") configuration.

In Figs. 5.8, 5.9 and 5.10 polar plots are given for the average signed mean angular error per direction compared to the direction rendered. These plots are split into even and odd directions for greater readability, but each horizontal pair are plotted from the same experimental conditions. For tests in which all mean error's follow the same CW or CCW trend, an overlaid circular arrow indicates this direction of bias. The left hand,

Left Straight

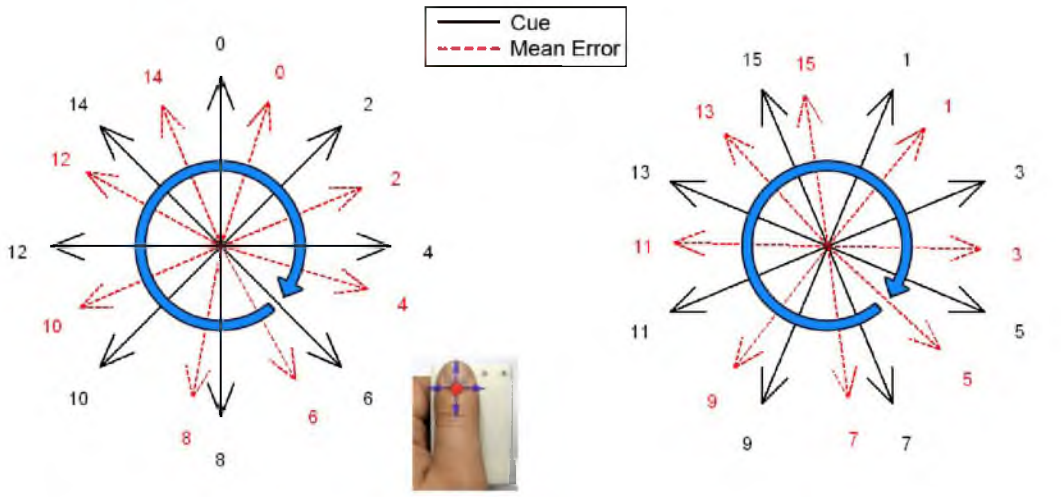

Figure 5.8 Polar plots pooled for all 12 participants showing the mean response direction for each rendered direction for the left hand, straight configuration of the absolute identification experiment. The curved blue arrow indicates the bias direction that participants generally responded in relation to the actual rendered direction cues. Participants' responses indicate a clockwise confusion pattern when they answered incorrectly for the left hand, straight configuration.

Right Straight

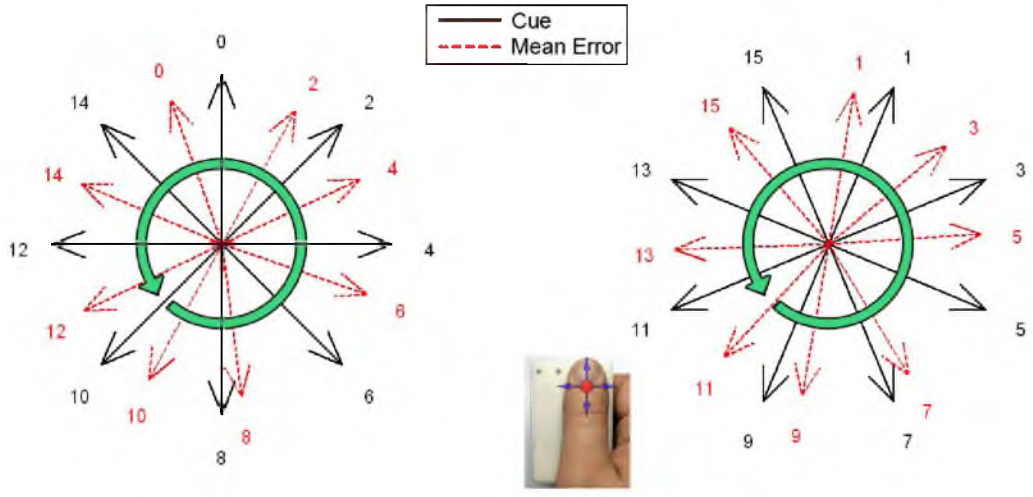

Figure 5.9 Polar plots pooled for all 12 participants showing the mean response direction for each rendered direction for the right hand, straight configuration of the absolute identification experiment. The curved green arrow indicates the bias direction that participants generally responded in relation to the actual rendered direction cues. Participants' responses indicate a counter clockwise confusion pattern when they answered incorrectly for the right hand, straight configuration.

Both Straight

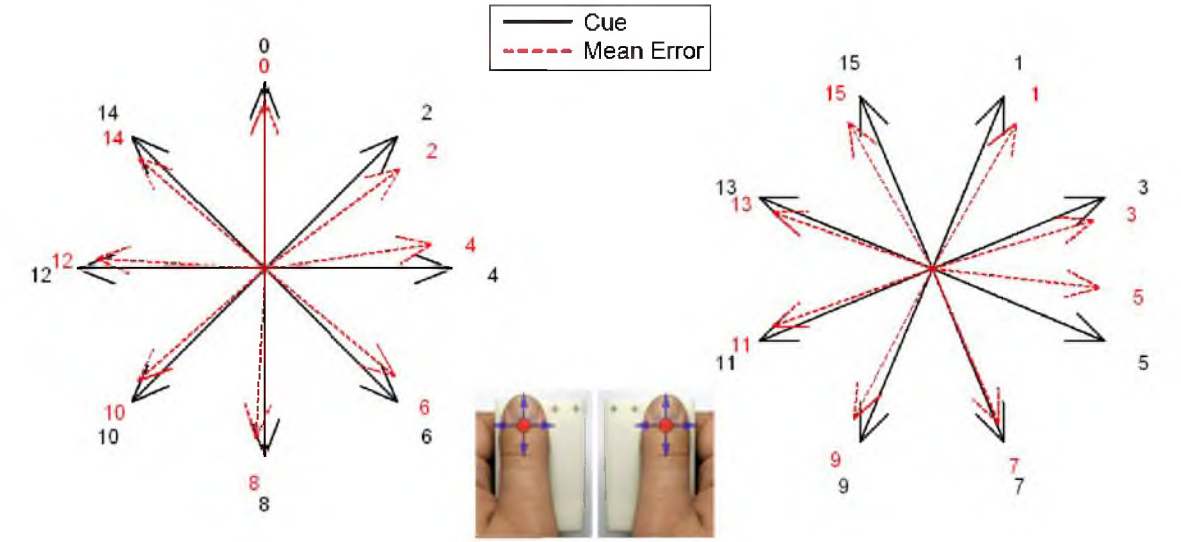

Figure 5.10 Polar plots pooled for all 12 participants showing the mean response direction for each rendered direction for both hands, straight configuration of the absolute identification experiment.

straight configuration results of Fig 5.8 feature a consistent CW response bias for all 16 directions with an average of 23.39 degrees as calculated in the bottom left of Table 5.3. The right thumb, straight configuration plots show the opposite rotation bias in all directions with an average mean error of 22.27 degrees CCW. Both the left and right, straight-thumb configurations are being interpreted, on average, one "bin" of rotation away from the intended direction rendered.

Figure 5.10 shows the polar plots of mean errors for the two-handed, straight-thumb configuration. Consistent with the confusion matrix in Table 5.5 there is little or no angular bias in user responses to this test. The mean errors plotted are similar to the direction intended. The absolute average angular error is 13.27 degrees. Therefore, the

effects of rotational biases in skin stretch direction perception, with thumbs in a straight configuration, can be minimized when stimuli are provided to both thumbs.

5.4.2 Results for Absolute Identification Experiment with Angled-Thumb Orientation

5.4.2.1 Confusion Matrices

Confusion matrices for the absolute identification test in the angled grip orientation are shown for the left, right, and both hands in Tables 5.6, 5.7 and 5.8. The confusion matrix in Table 5.6 for the left hand with angled grip shows errors much more symmetrical about the main diagonal (correct answers) compared to the left/straight-thumb configuration results. A similar reduction of rotational bias of responses can be found when comparing the right angled-thumb to the right straight-thumb configuration. The angled left and right thumb configuration result in higher accuracies of 41% and 42%, respectively, up from 27% and 29% in the corresponding thumbs in straight alignment. The estimated 8-direction "On +/-1" accuracy for left and right straight-thumbs also improves from 74% and 78%, respectively, to 89% and 91% for the same in angled. Again, this is expected to be a slight overestimate as explained in Section 5.4.1.1 and in Fig. 5.6.

Note the similarity in accuracy between the left and right hands. This continues the trend of similar perception levels between the two thumbs that was seen in the angled-thumb configuration. Therefore, it can be assumed that the disparity in performance that was seen between the single thumb cases in the pilot test is due to inconsistent hand grip angles used. Despite both thumb pads being aligned straight with the aperture the hand orientation cannot be ignored. Due to this effect and the improved accuracy seen going

Table 5.6 Confusion matrix showing the pooled responses for all 12 participants for absolute identification left hand angled grip

Left Hand Absolute Identification Angled Grip

	Percieved																Acurracy	
Rendered	0	1	2	3	4	5	6	7	8	9	10	11	12	13	14	15	Total	On	On +/- 1
0	66	22	8												7	17	120	55%	88%
1	40	38	32	6	2											2	120	32%	92%
2	2	22	59	23	12	1										1	120	49%	87%
3			20	34	57	5	3	1									120	28%	93%
4		1	3	18	47	26	22	3									120	39%	76%
5				4	13	32	53	18									120	27%	82%
6				1	2	9	54	50	3	1							120	45%	94%
7						2	17	53	46	2							120	44%	97%
8								20	75	22	3						120	63%	98%
9								5	46	48	17	4					120	40%	93%
10							1	1	9	35	48	23	3				120	40%	88%
11										14	27	44	30	5			120	37%	84%
12										2	2	14	47	40	13	2	120	39%	84%
13												2	18	22	65	13	120	18%	88%
14	11	2											2	6	56	43	120	47%	88%
15	41	3												2	17	57	120	48%	96%
Total	160	88	122	86	133	75	150	151	179	124	97	87	100	75	158	135		41%	89%
Percent	8%	5%	6%	4%	7%	4%	8%	8%	9%	6%	5%	5%	5%	4%	8%	7%		Avg. Accuracy	

Avg Absolute Error	
0.7161	Increments
16.11	Degrees

Table 5.7 Confusion matrix showing the pooled responses for all 12 participants for absolute identification right hand angled grip

Right Hand Absolute Identification Angled Grip

	Percieved																Accuracy	
Rendered	0	1	2	3	4	5	6	7	8	9	10	11	12	13	14	15	Total	On	On +/- 1
0	63	25	3	1											3	25	120	53%	94%
1	14	47	56	2												1	120	39%	98%
2	4	37	65	13	1												120	54%	96%
3		12	52	45	10	1											120	38%	89%
4		1	21	47	35	9	7										120	29%	76%
5			1	5	32	43	32	7									120	36%	89%
6					3	25	64	24	4								120	53%	94%
7						1	16	54	41	6	2						120	45%	93%
8							2	24	64	26	3	1					120	53%	95%
9								4	45	51	20						120	43%	97%
10									4	51	54	11					120	45%	97%
11										23	61	31	5				120	26%	81%
12											19	45	50	5	1		120	42%	83%
13											2	4	52	31	29	2	120	26%	93%
14	3											4	12	26	57	18	120	48%	84%
15	29	4												3	33	51	120	43%	94%
Total	113	126	198	113	81	79	121	113	158	157	161	96	119	65	123	97		42%	91%
Percent	6%	7%	10%	6%	4%	4%	6%	6%	8%	8%	8%	5%	6%	3%	6%	5%		Avg. Accuracy	

Avg Absolute Error	
0.6792	Increments
15.28	Degrees

Table 5.8 Confusion matrix showing the pooled responses for all 12 participants for absolute identification both hands angled grip

Both Hands Absolute Identification Angled Grip

	Percieved																	Accuracy	
Rendered	0	1	2	3	4	5	6	7	8	9	10	11	12	13	14	15	Total	On	On +/- 1
0	69	19	3												6	23	120	58%	93%
1	12	55	49	4													120	46%	97%
2		15	68	33	4												120	57%	97%
3			20	65	28	6	1										120	54%	94%
4			3	15	81	21											120	68%	98%
5					23	63	32	2									120	53%	98%
6						16	76	25	3								120	63%	98%
7							19	65	33	3							120	54%	98%
8							2	11	89	16	2						120	74%	97%
9								1	31	68	19	1					120	57%	98%
10									2	34	70	13	1				120	58%	98%
11		1								6	42	51	18	2			120	43%	93%
12											7	22	67	21	3		120	56%	92%
13											1	3	29	53	28	6	120	44%	92%
14		1											5	21	74	19	120	62%	95%
15	22	2												5	32	59	120	49%	94%
Total	103	93	143	117	136	106	130	104	158	127	141	90	120	102	143	107		56%	96%
Percent	5%	5%	7%	6%	7%	6%	7%	5%	8%	7%	7%	5%	6%	5%	7%	6%		Avg. Accuracy	

Avg Absolute Error	
0.4896	Increments
11.02	Degrees

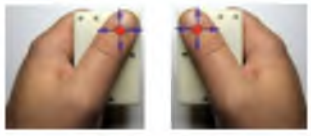

to an angled-thumb configuration, future device design and testing of finger-based skin stretch in 16 directions should be mindful of overall hand orientation. This conclusion appears to be in conflict with the results of a mental rotation study using similar lateral skin-stretch cues at the fingertip in four orthogonal directions [28]. Their study determined that accuracy and response times were not greatly affected by hand orientations angled up to 40 degrees inward of straight forward. However, Gleeson and Provancher were only considering user responses when cues were presented to the index fingertip. The angled thumb configuration does appear to address the rotational bias observed for the straight thumb configuration that is discussed in Section 5.4.1 and in a prior study [13].

Looking at Table 5.8, the benefits of using two hands in angled configuration can be seen in the improved accuracy of 56% and 96% for 16-direction and approximate 8-directions, respectively. These compare favorably to the straight two handed accuracies of 49% and 93% but are not vast improvements. Symmetry and narrow spread of errors within the angled matrix do indicate less user confusion in this configuration.

One way ANOVA is computed for comparing the effect of handedness on accuracy in the absolute identification test now with an angled-thumb orientation for left hand, right hand, and the both hands conditions. A significant effect is found for handedness on accuracy at the $p < 0.05$ level for the three conditions [$F(2,5757) = 56.35$, $p < 0.001$]. Tukey's HSD test post hoc analysis indicates that again that the both-hands configuration is significantly more accurate than either the left or right hand conditions ($p < 0.001$) with angled thumbs. Similarly, no significant difference was found between accuracies for the left and right hand conditions. Figure 5.11 shows the mean accuracies and confidence

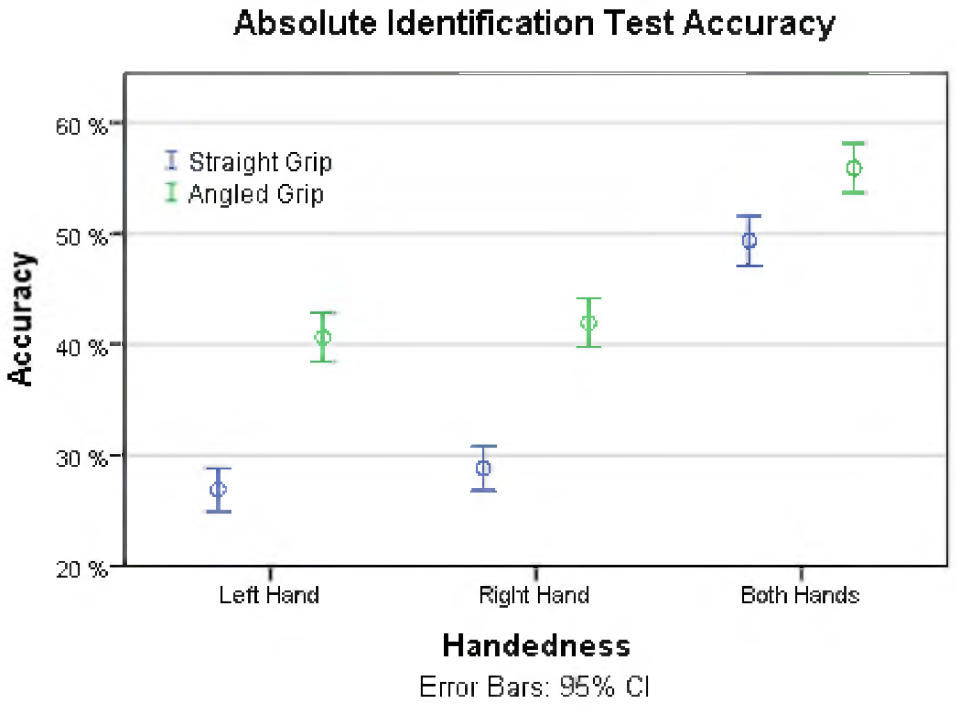

Figure 5.11 Mean accuracy and confidence intervals for the absolute identification test under left, right, and both hand configurations with both straight and angled grips.

intervals for the absolute identification test with both straight and angled thumbs and all handedness conditions. While no difference was found between single thumb conditions, the significant improvements through delivering cues to both thumbs can readily be seen for both the straight and angled grip conditions.

A separate ANOVA is computed to study the effect on accuracy of straight versus angled thumbs in the absolute identification test. Significance is found for thumb orientation on accuracy at $p < 0.05$ [$F(1,11518) = 150.30$, $p < 0.001$]. Giving directions to users with thumbs angled is ideal for increasing accuracy in the absolute identification task.

5.4.2.2 Accuracy and Polar Plots

The bar graph in Fig. 5.12 compares the absolute identification accuracy of the left, right, and both hands cases while in the angled orientation. The improvement in accuracy for using both thumbs in the angled configuration over single thumbs is evident but not nearly as substantial or uniform as was seen in the straight-thumb case of Figure 5.7. Direction '8' continues to show increased apparent accuracy of responses, though again not as drastically as in straight-thumb tests. The cardinal directions (0, 4, 8, and 12) for both hands again have the highest accuracies within that test, all greater than 60%.

Polar plots of Figs. 5.13, 5.14 and 5.15 show the mean error per direction of the absolute identification test of the left, right and both hands while in the angled orientation. No consistent rotational bias can be seen in any of the angled-thumb absolute identification tests. Signed mean angle errors are overall reduced by moving

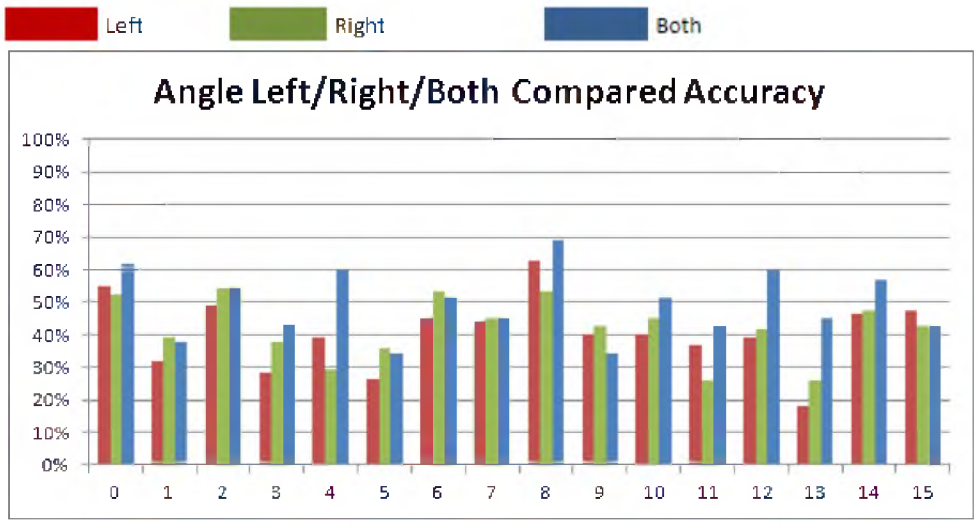

Figure 5.12 Bar graph showing the pooled accuracy levels for all 12 participants per direction comparing left, right and both hands configurations for angled grip absolute identification.

Left Angled

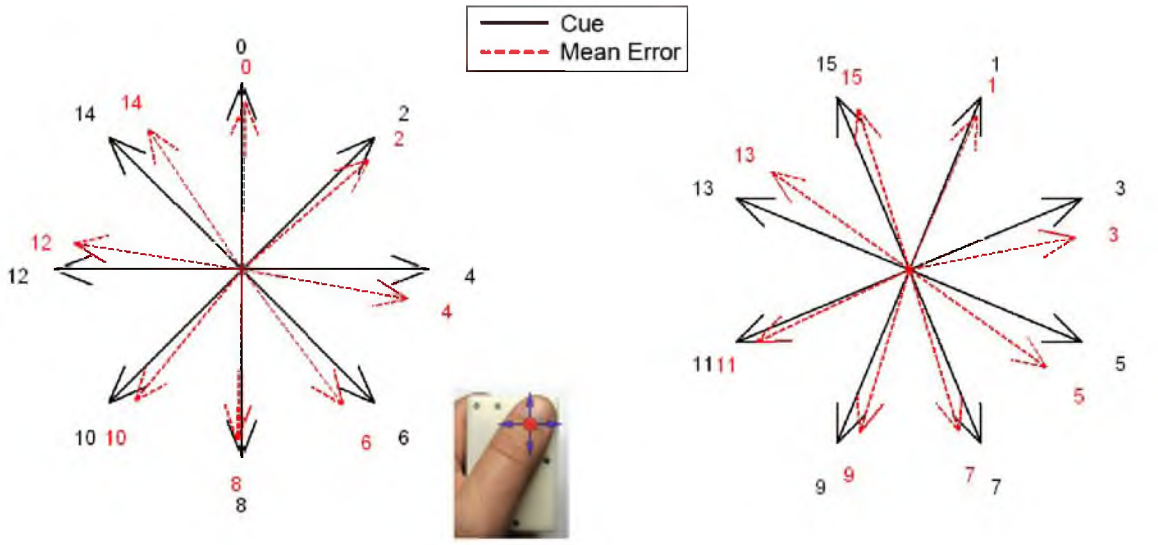

Figure 5.13 Polar plots of mean error per direction for absolute identification experiment with angled left hand. No consistent pattern of rotational bias is observed.

from the straight configuration to angled as also supported by the absolute average angle errors calculated on the corresponding confusion matrices.

There are several characteristics of note visible within these single angled hand polar plots. First, the cues rendered in line with the distal axis of thumb orientation (towards the tip) show very small mean errors. These are direction '1' for left angled thumb and '15' for right angled thumb. This could indicate that increased direction sensitivity may align with the tip of the thumb. Secondly, the mean response error for directions '7' and '9' are all gravitated towards '8'. This lends to the idea that an additional aspect of interaction is taking place at the south direction. Lastly, the mean errors for angle error at east '4' and west '12' are rotated similarly to the participants' thumb orientation/rotation. These mean errors align more closely with the local lateral axis of the thumbpad.

Right Angled

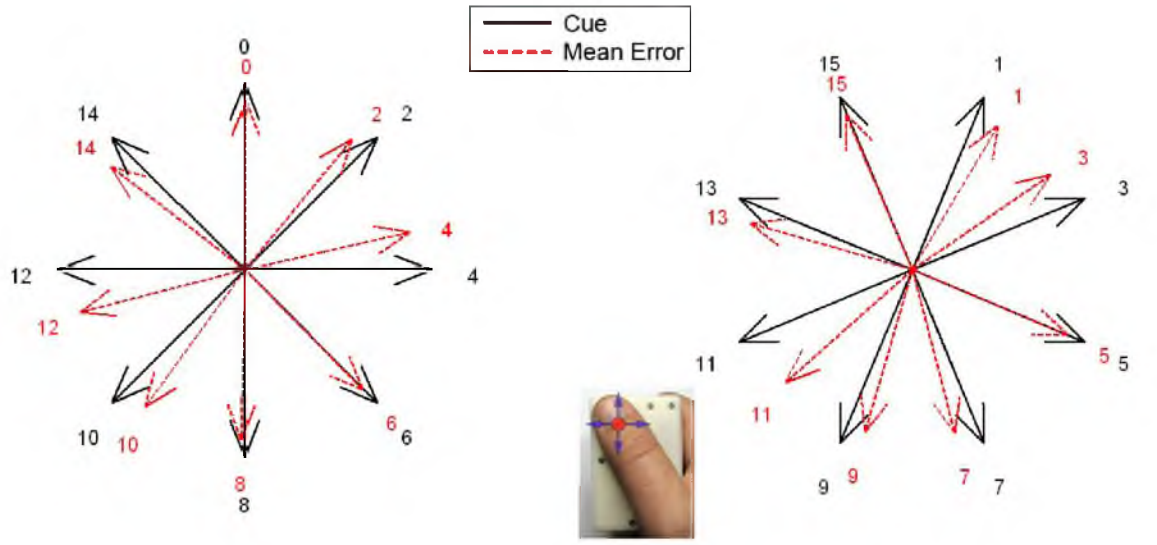

Figure 5.14 Polar plots of mean error per direction for absolute identification experiment with angled right hand. No consistent pattern of rotational bias is observed.

Both Angled

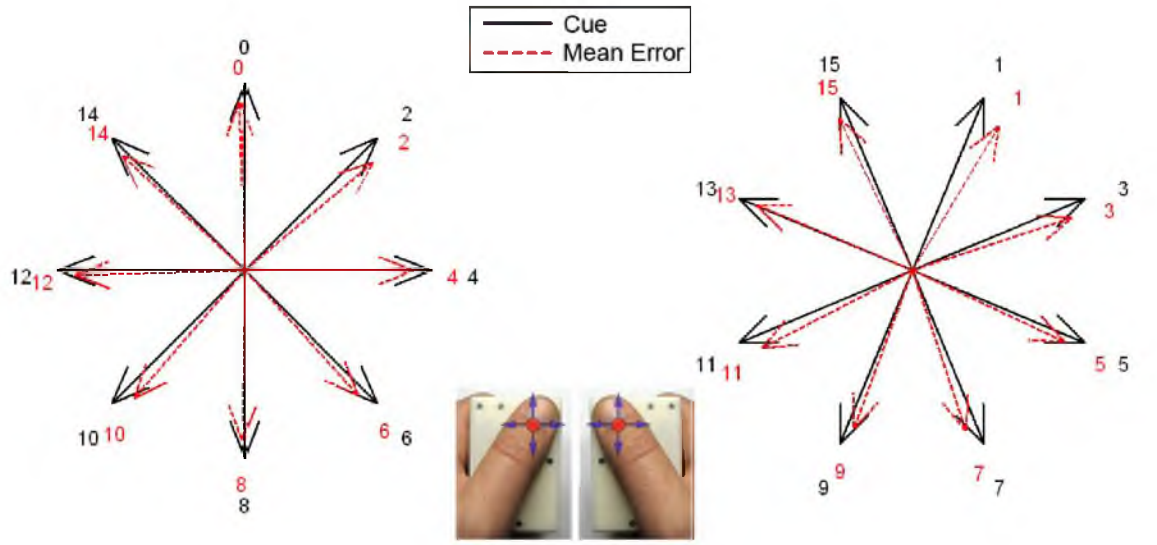

Figure 5.15 Polar plots of mean error per direction for absolute identification experiment with angled left hand. Responses show very little error or uniform rotational bias.

5.4.3 Results for Relative Identification Experiment with Straight-Thumb Orientation

5.4.3.1 Confusion Matrices

In Tables 5.9 and 5.10 are the confusion matrices for the relative identification test with straight grip for left, right, and both hands. Note that the ordering of directions starts with 12 (west) and continue through to 4 (east). Reference for these directions can be found in Fig. 5.4. In Table 5.9 the responses offset from diagonal indicate rotational bias is present for left and right hands in the straight configuration in CW and CCW rotations, respectively. Average accuracy for the single hands conditions are 41% for left and 50% for right. While these averages improve upon those seen in the absolute 16-direction test, they are less consistent across directions, ranging 18% - 83% on the left thumb and 17% - 90% on the right. To compare, the largest span of accuracies in the absolute test with straight grip is from 14% - 58% at the right hand and all accuracies are more closely grouped for both hands. This can be seen in the direction comparison of absolute and relative accuracies in Section 5.4.5. In Table 5.10 the both hand condition again removes broad rotational bias effects and results in a moderate increase in correct answers. The level of performance also more evenly distributed across directions in the two-handed case.

A one way ANOVA is calculated comparing the effect of handedness on accuracy in the relative identification test with straight-thumbs for left hand, right hand, and the both hands conditions. A significant effect is found for handedness on accuracy at the $p < 0.05$ level for the three conditions [$F(2,3237) = 34.87$, $p < 0.001$]. Post hoc Tukey's HSD indicates that the right hand is significantly more accurate than the left hand

Table 5.9 Confusion Matrices showing the pooled responses for all 12 participants for relative identification left hand (top) and right hand (bottom) straight grip

Left Hand Relative Identification Test Straight Grip

	Percieved										Acurracy	
Rendered	12	13	14	15	0	1	2	3	4	Total	On	On +/- 1
12	21	43	45	10					1	120	18%	53%
13	2	22	69	25	1	1				120	18%	78%
14		2	41	66	5	6				120	34%	91%
15		2	8	46	55	7	2			120	38%	91%
0			1	14	68	32	5			120	57%	95%
1				1	12	63	33	9	2	120	53%	90%
2						12	42	51	15	120	35%	88%
3						1	13	36	70	120	30%	99%
4							1	20	99	120	83%	99%
Total	23	69	164	162	141	122	96	116	187		41%	87%
Percent	2%	6%	15%	15%	13%	11%	9%	11%	17%		Avg. Accuracy	

Avg Absolute Error	
0.7509	Increments
16.90	Degrees

Right Hand Relative Identification Test Straight Grip

	Percieved										Acurracy	
Rendered	12	13	14	15	0	1	2	3	4	Total	On	On +/- 1
12	108	9	2	1						120	90%	98%
13	48	51	19	1				1		120	43%	98%
14	7	34	63	15	1					120	53%	93%
15		9	25	71	14	1				120	59%	92%
0			1	23	91	5				120	76%	99%
1				4	50	61	5			120	51%	97%
2					11	55	50	3	1	120	42%	90%
3						24	62	24	10	120	20%	80%
4						10	48	42	20	120	17%	52%
Total	163	103	110	115	167	156	165	70	31		50%	89%
Percent	15%	10%	10%	11%	15%	14%	15%	6%	3%		Avg. Accuracy	

Avg Absolute Error	
0.6278	Increments
14.13	Degrees

Table 5.10 Confusion Matrix showing the pooled responses for all 12 participants for relative identification both hands straight grip

Both Hands Relative Identification Test Straight Grip

	Percieved										Acurracy	
Rendered	12	13	14	15	0	1	2	3	4	Total	On	On +/- 1
12	77	33	10							120	64%	92%
13	18	53	40	9						120	44%	93%
14	4	17	77	22						120	64%	97%
15		3	21	80	15	1				120	67%	97%
0		1		14	94	9	2			120	78%	98%
1				1	27	68	21	3		120	57%	97%
2						22	65	32	1	120	54%	99%
3						2	31	56	31	120	47%	98%
4							15	45	60	120	50%	88%
Total	99	107	148	126	136	102	134	136	92		58%	95%
Percent	9%	10%	14%	12%	13%	9%	12%	13%	9%		Avg. Accuracy	

Avg Absolute Error	
0.4657	Increments
10.48	Degrees

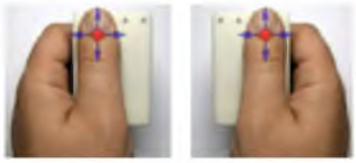

configuration ($p < 0.001$). The both hand condition is significantly more accurate than both the left and right hands alone ($p < 0.001$). The average accuracy and confidence interval for the relative identification tests for all hand conditions and both straight and angled thumbs are given at the end of Section 5.4.4.1.

The straight-thumb relative identification test is the only experimental condition in which a significant accuracy difference can be found between the left and right thumbs. The accuracy disparity seen between single thumbs in the pilot test can be primarily attributed to the difference in the hand ergonomics used during the preliminary trials as has been previously discussed. There are potential grounds for finding significance in the

full relative identification straight-thumb experiment between hands. It could be partly due to the imbalance of left and right handed participants tested (10 right handed and two left handed). Also the interaction of the rotational bias with the nature of the relative test, as discussed in the following section, might have additional interactions based on handedness. It is expected that with further trials with a more balanced subject sample this difference would become less pronounced.

5.4.3.2 Accuracy and Polar Plots

Figure 5.16 compares the accuracy rates for left, right, and both hands with thumbs in the straight orientation for the relative identification test on a per direction basis. Because the range of angles used in the relative experiment is not continuous through the bottom range of directions, the rotational bias seen in the 16-direction test creates a final bin with an outlying level of performance. This can been seen for direction '4' on the left thumb, in which test the user cannot select '5' as a rotationally biased response, and at '12' on the right thumb where '11', the rotationally biased response, is not an option. If these two thumb/direction cases are ignored the improved accuracy is uniformly evident at each direction 'bin' moving towards the perceptual reference in the center at '0' for single thumb tests. If again ignoring the two outlying cases, both straight-thumbs consistently produces the best results in this relative experiment.

Figure 5.17 contains three sets of polar plots corresponding to the average signed response error for left, right and both hands in the relative identification test with straight-thumbs. Curved arrows indicate general bias direction of error. Exceptions to this are at

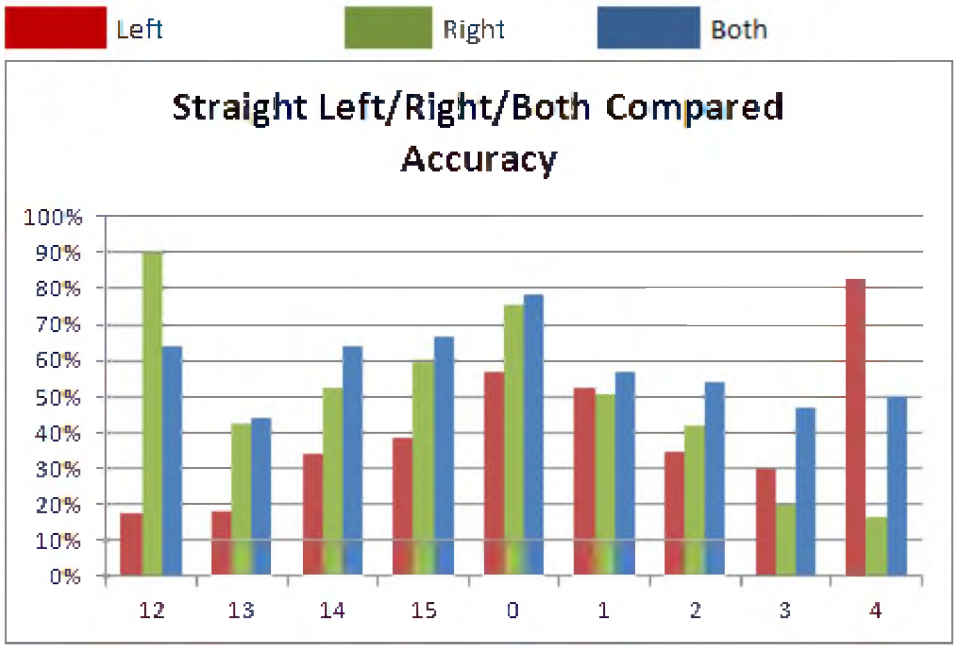

Figure 5.16 Bar graph showing the pooled accuracy levels for all 12 participants per direction comparing left, right and both hands configurations for straight grip relative identification.

the previously discussed conditions at direction 4 in the left thumb case and direction 12 for the right hand. Because there are no available responses past these directions the overall rotation bias is not possible at these two locations. The greatest mean error is found at the opposite directions of these two cases for the same reason.

Both thumb testing produces little mean error for directions '14' through '3'. This is promising as the symmetric subset of directions '14' to '2' could be put to use for GPS walking navigation studies in which varying degrees of correction magnitude could be communicated while a user navigates an unstructured outdoor course. The corresponding confusion matrix shows that the approximated 8-direction accuracy for these directions is no less than 97%.

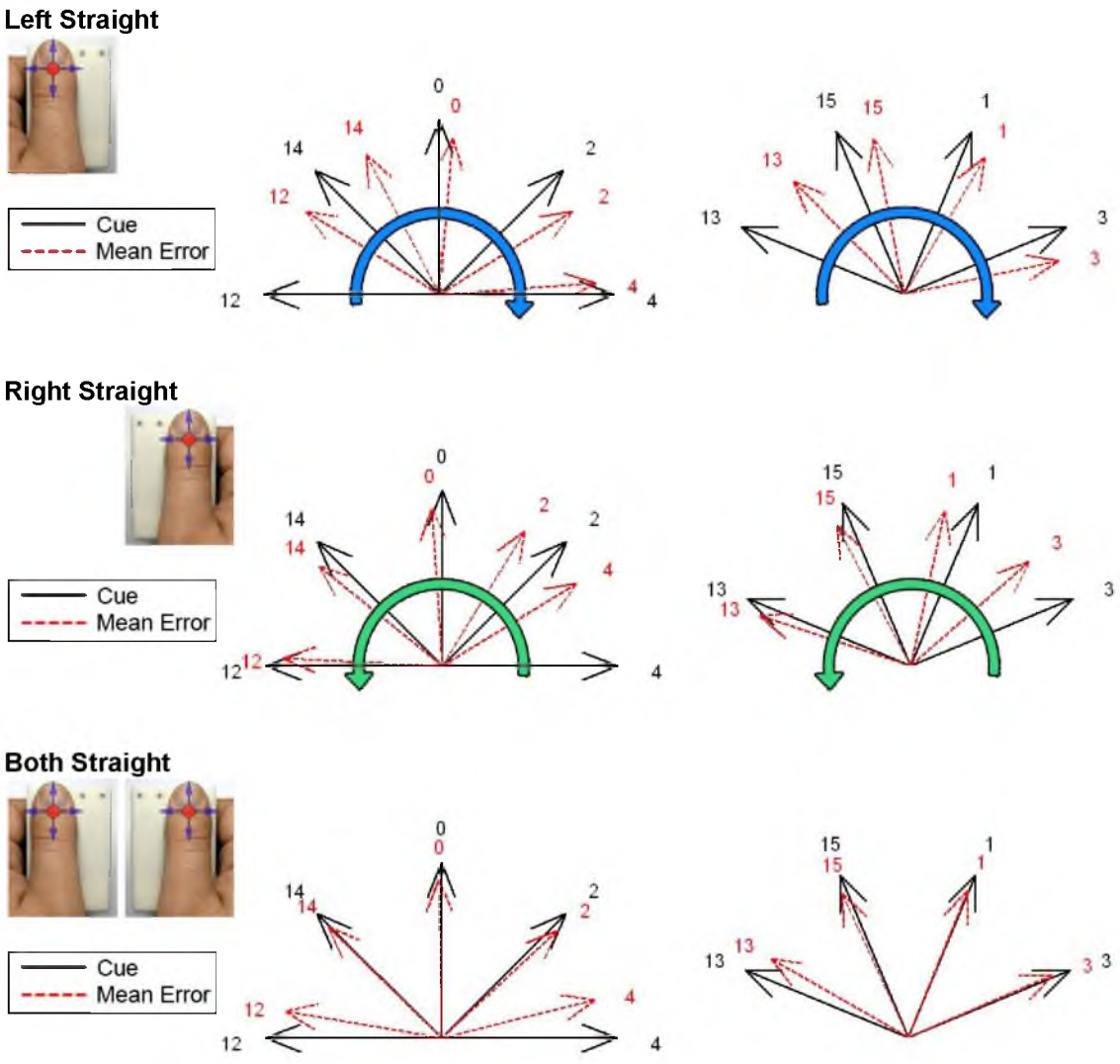

Figure 5.17 Polar plots of mean error per direction for relative identification experiment for the straight left hand, right hand and both hands conditions. The colored rotational arrow indicates a common rotational bias observed for responses in the single handed test conditions.

5.4.4 Results for Relative Identification Experiment with Angled-Thumb Orientation

5.4.4.1 Confusion Matrices

Tables 5.11 and 5.12 contain confusion matrices for the 9-direction relative identification tests with angled grip for left, right, and both thumbs. Average accuracy for the angled relative experiment does not drastically improve over straight grip configuration; however, the distribution is far more even due to lack of a strong angular rotational bias being present in the single thumb configurations.

This relative identification test for angled thumbs was analyzed with a one way ANOVA comparing the effects of handedness on accuracy for left, right, and both hands conditions. At $p < 0.05$ significance is found for handedness on accuracy [$F(2,3237) = 20.26$, $p < 0.001$]. In post hoc Tukey's HSD analysis it is found that users are significantly more accurate with the both hands than either the left hand or right hand configurations ($p < 0.001$). No significant difference was found between the left and right hand only conditions. Average accuracy and confidence intervals for the relative identification tests for all hand conditions and both straight and angled thumbs are given below in Figure 5.18.

As was done for the absolute test, one-way ANOVA is used to check for a material effect on accuracy from the user's thumb angle. Again moving from straight to angled-thumb orientation was found to provide a significant accuracy improvement [$F(1,6478) = 23.13$, $p < 0.001$]. Thus for both the absolute and relative identification tests user's thumbs should be in the angled orientation to provide the highest recognition rates.

Table 5.11 Confusion Matrices showing the pooled responses for all 12 participants for relative identification left hand (top) and right hand (bottom) angled grip

Left Hand Relative Identification Test Angle Grip

	Percieved										Acurracy	
Rendered	12	13	14	15	0	1	2	3	4	Total	On	On +/- 1
12	51	46	22	1						120	43%	81%
13	4	25	69	22						120	21%	82%
14		1	46	69	4					120	38%	97%
15			4	72	39	5				120	60%	96%
0			1	15	89	15				120	74%	99%
1				1	33	69	15	2		120	58%	98%
2					2	24	69	20	5	120	58%	94%
3							18	58	44	120	48%	100%
4							8	26	86	120	72%	93%
Total	55	72	142	180	167	113	110	106	135		52%	93%
Percent	5%	7%	13%	17%	15%	10%	10%	10%	13%		Avg. Accuracy	

Avg Absolute Error	
0.5454	Increments
12.27	Degrees

Right Hand Relative Identification Test Angle Grip

	Percieved										Acurracy	
Rendered	12	13	14	15	0	1	2	3	4	Total	On	On +/- 1
12	94	19	7							120	78%	94%
13	28	55	34	3						120	46%	98%
14	9	23	64	24						120	53%	93%
15		5	20	71	21	3				120	59%	93%
0			2	15	90	13				120	75%	98%
1				1	45	64	10			120	53%	99%
2				1	8	59	46	6		120	38%	93%
3				1		19	63	31	6	120	26%	83%
4			1				33	50	36	120	30%	72%
Total	131	102	128	116	164	158	152	87	42		51%	91%
Percent	12%	9%	12%	11%	15%	15%	14%	8%	4%		Avg. Accuracy	

Avg Absolute Error	
0.5824	Increments
13.10	Degrees

Table 5.12 Confusion Matrix showing the pooled responses for all 12 participants for relative identification both hands angled grip

Both Hands Relative Identification Test Angle Grip

	Percieved										Acurracy	
Rendered	12	13	14	15	0	1	2	3	4	Total	On	On +/- 1
12	86	31	3							120	72%	98%
13	7	60	50	3						120	50%	98%
14	2	17	69	30	2					120	58%	97%
15		1	20	83	16					120	69%	99%
0				8	100	12				120	83%	100%
1				1	16	83	17	3		120	69%	97%
2						20	78	22		120	65%	100%
3						2	35	58	25	120	48%	98%
4							17	36	67	120	56%	86%
Total	95	109	142	125	134	117	147	119	92		63%	97%
Percent	9%	10%	13%	12%	12%	11%	14%	11%	9%		Avg. Accuracy	

Avg Absolute Error	
0.3981	Increments
8.96	Degrees

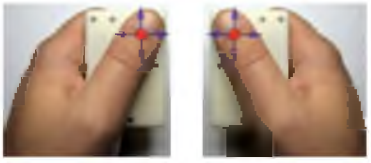

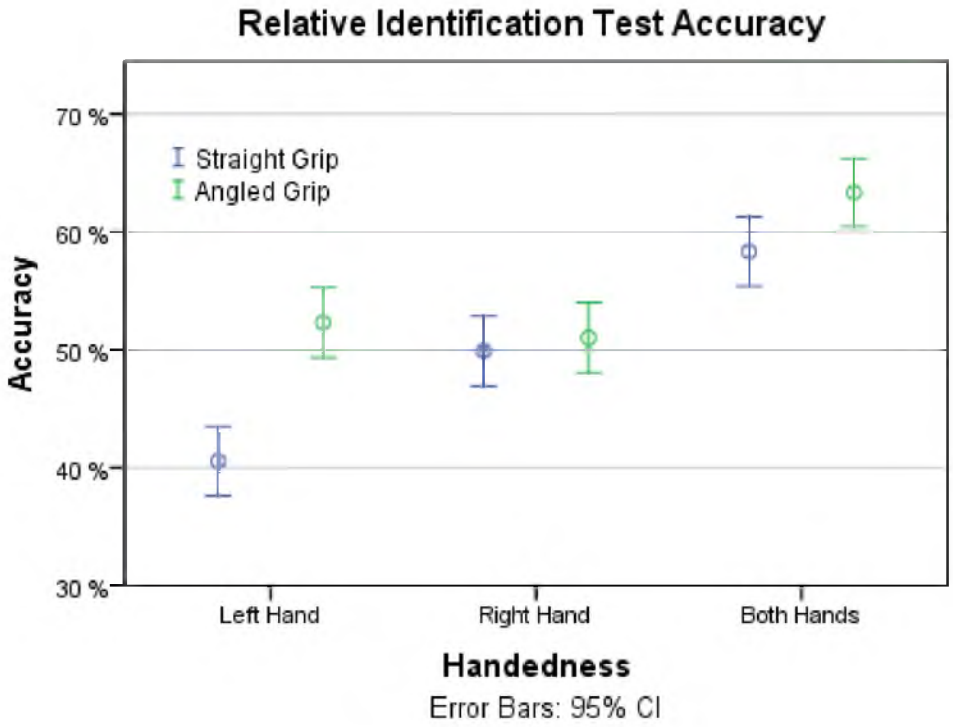

Figure 5.18 Average accuracy and confidence intervals compared between left, right, and both hand conditions and both grip orientations for the relative identification test

5.4.4.2 Accuracy and Polar Plots

The bar graph in Fig. 5.19 illustrates the corresponding directional accuracies comparing left, right and both hands on a per direction basis. The similarities in performance can be seen across directions. This experiment shows across all hands and in both grip configurations how the initial reference cue in the north direction allows for improved recognition rates of the directions adjacent. Accuracy continues to drop moving to directions further from the perceptual anchor at '0'. This holds true except at '4' and '12' which are special cases in the relative tests, as previously discussed.

The three pairs of polar plots in Fig. 5.20 show the mean signed error in responses to the left, right and both hand conditions for the relative identification test with angled

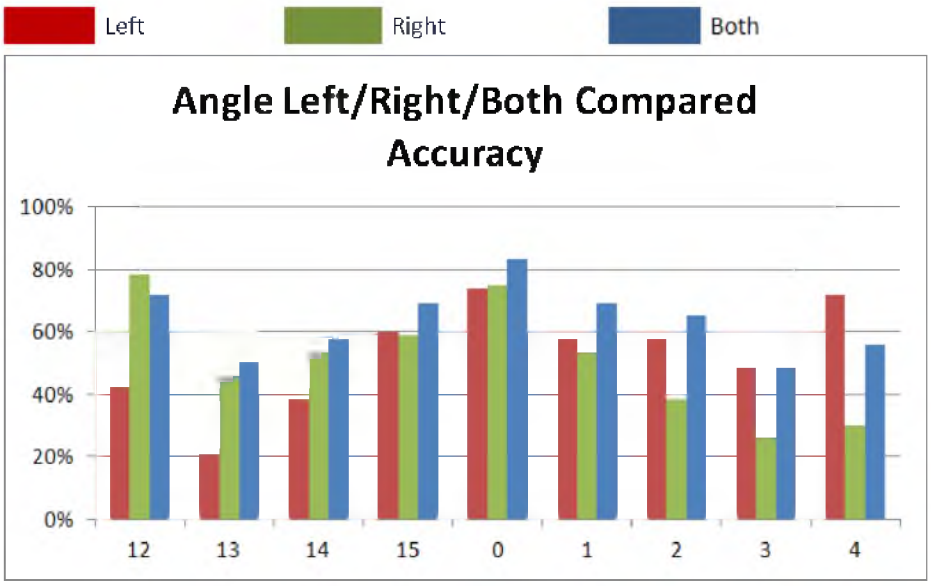

Figure 5.19 Bar graph showing the pooled accuracy levels for all 12 participants per direction comparing left, right and both hands configurations for angled grip relative identification.

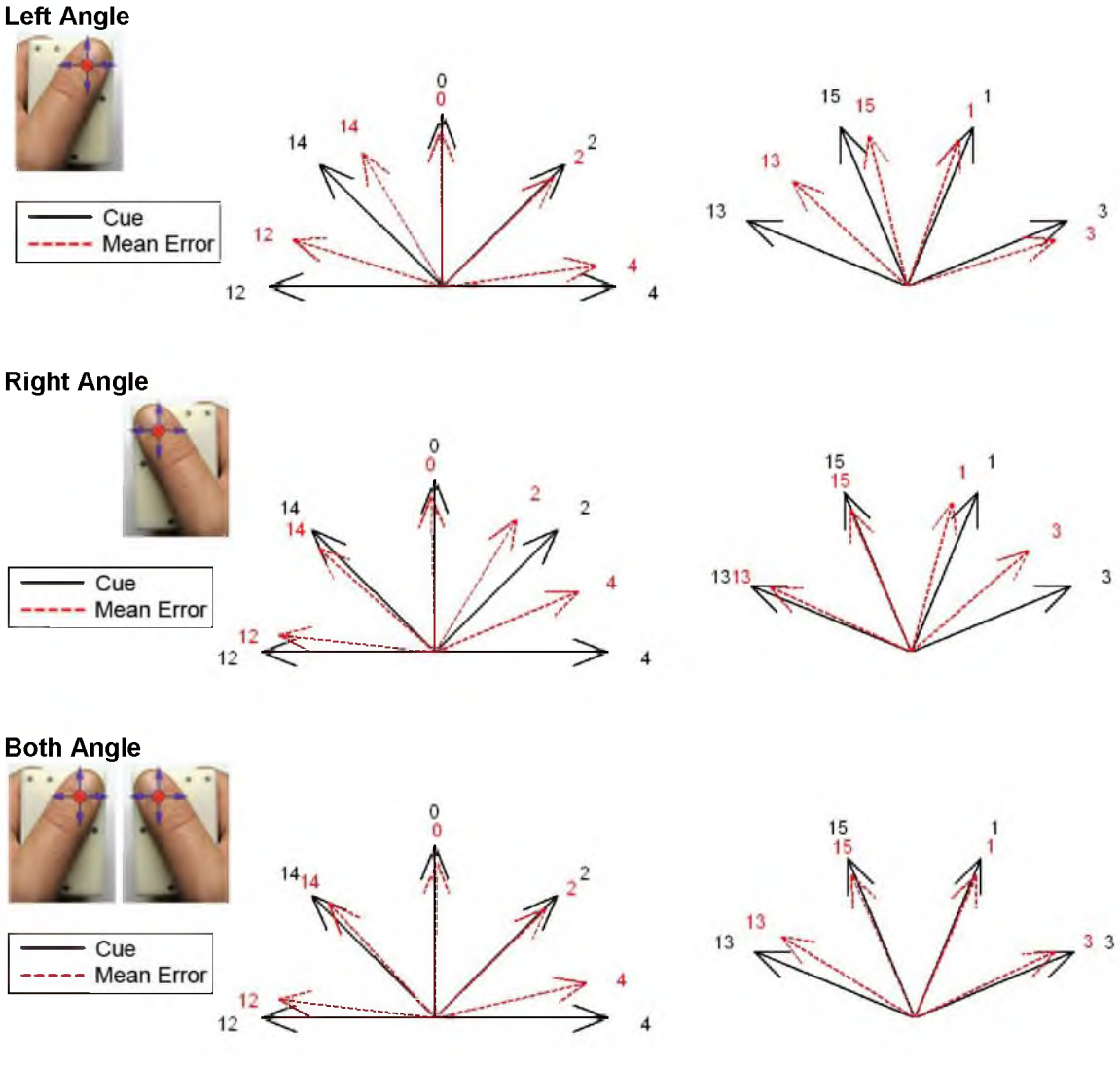

Figure 5.20 Sets of polar plots of mean signed error per direction for left, right and both hands in the relative test for angled-thumb orientations.

thumbs. Left and right plots are of the same data set, but plotted separately for clarity. Mean errors of the angled configuration are diminished from the relative test straight condition. There is no consistent CW or CCW rotation to the user's answers. Potential directions for use in a GPS assisted subtle course correction experiment are again shown to give mean directions very similar to the intended cue.

5.4.5 Performance Comparison Between Absolute Versus Relative Identification

The bar graphs shown in Figs. 5.21 through 5.26 compare the accuracy of users in the nine directions that are shared between the absolute and relative identifications tests (i.e. the lower seven directions of the absolute tests have been omitted from these comparisons). The first set of three graphs in Figs. 5.21, 5.22 and 5.23 show left, right and both hands performance with straight-thumb orientation while the second set of three display the same for angled-thumb orientation (Figs. 5.24, 5.25 and 5.26). As expected, the accuracy rates increase in the relative case, particularly in directions adjacent to the priming cue that acts as a cognitive anchor at the north (0) direction.

5.4.6 Information Transfer

Information transfer measures, in bits, the additional information provided to the user from a cue based on the user's current comprehension of the signals being sent. As such, this value is expected to grow with the user's increased training and stimulus familiarity. Values for the maximum likelihood estimate of information transfer (IT_{est}) were calculated from the confusion matrix for each configuration across both experiments. The IT_{est} value corresponds to the maximum information transfer possible when 100% accuracy is expected (i.e., perfect transfer of information). Two other terms, information

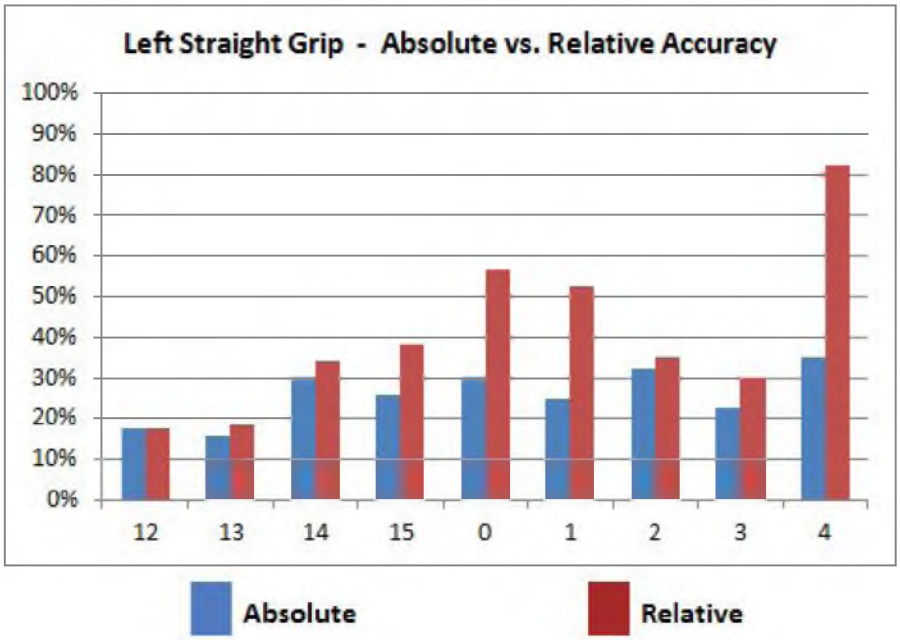

Figure 5.21 Bar graphs showing the pooled responses for all 12 participants comparing accuracy for directions shared between absolute and relative identification tests for the left thumb in straight orientation.

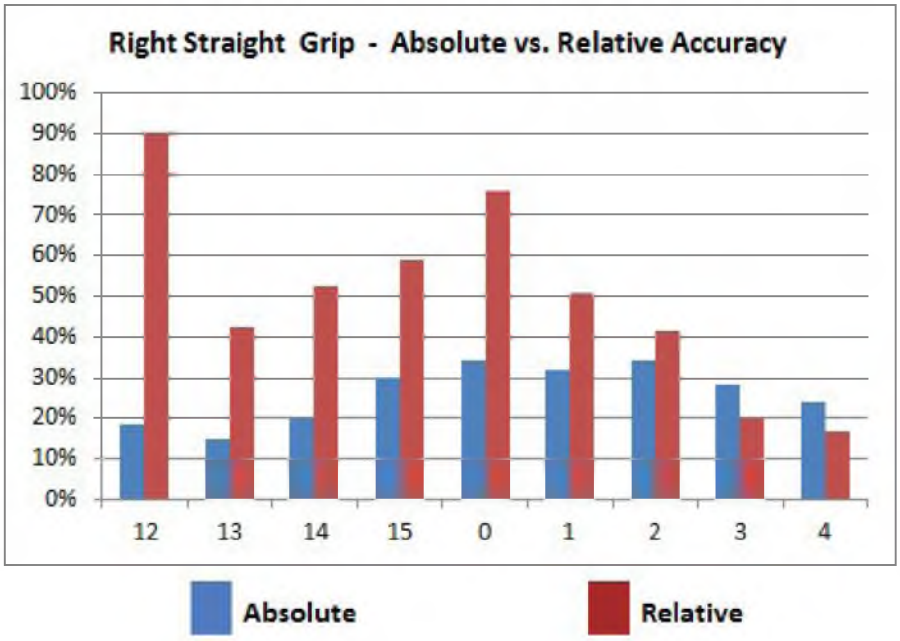

Figure 5.22 Bar graphs showing the pooled responses for all 12 participants comparing accuracy for directions shared between absolute and relative identification tests for the right thumb in a straight orientation.

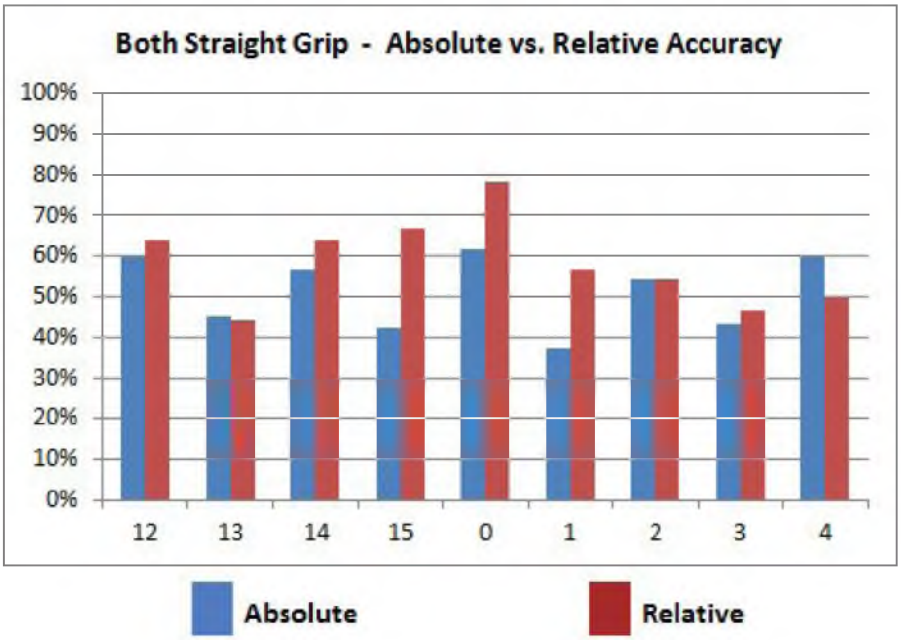

Figure 5.23 Bar graphs showing the pooled responses for all 12 participants comparing accuracy for directions shared between absolute and relative identification tests for both thumbs in straight orientation.

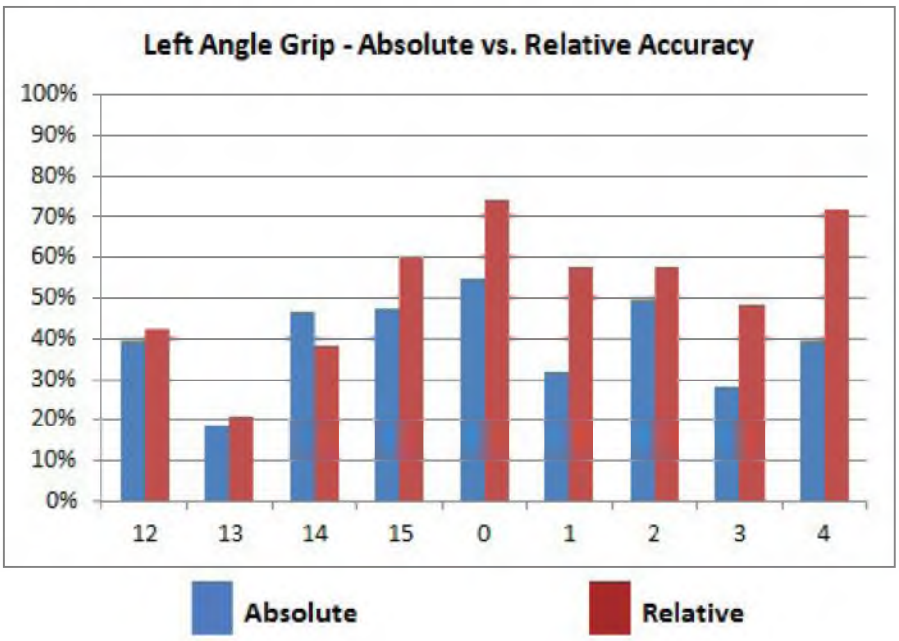

Figure 5.24 Bar graphs showing the pooled responses for all 12 participants comparing accuracy for directions shared between absolute and relative identification tests for the left thumb in an angled orientation.

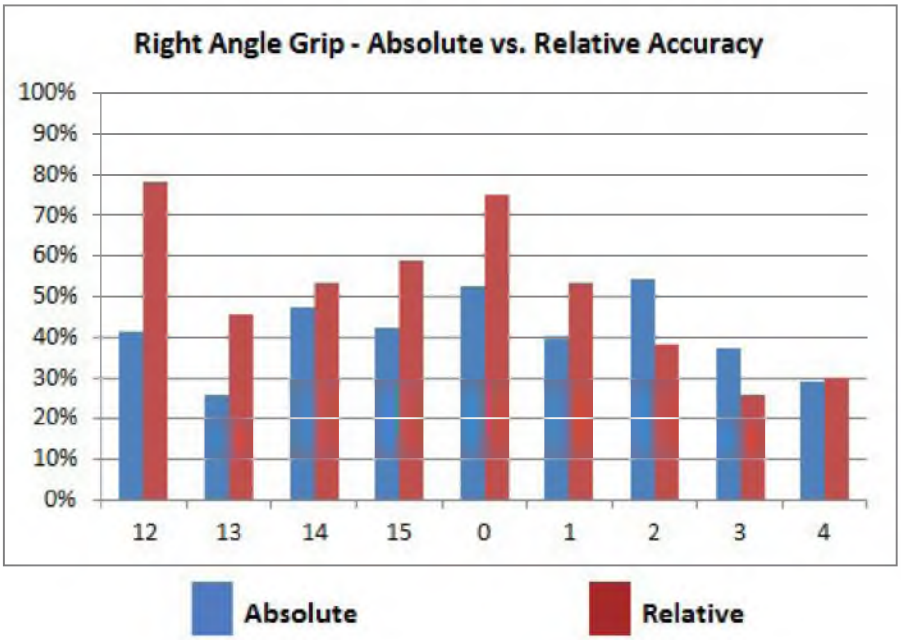

Figure 5.25 Bar graphs showing the pooled responses for all 12 participants comparing accuracy for directions shared between absolute and relative identification tests for left and right thumbs in angled orientation.

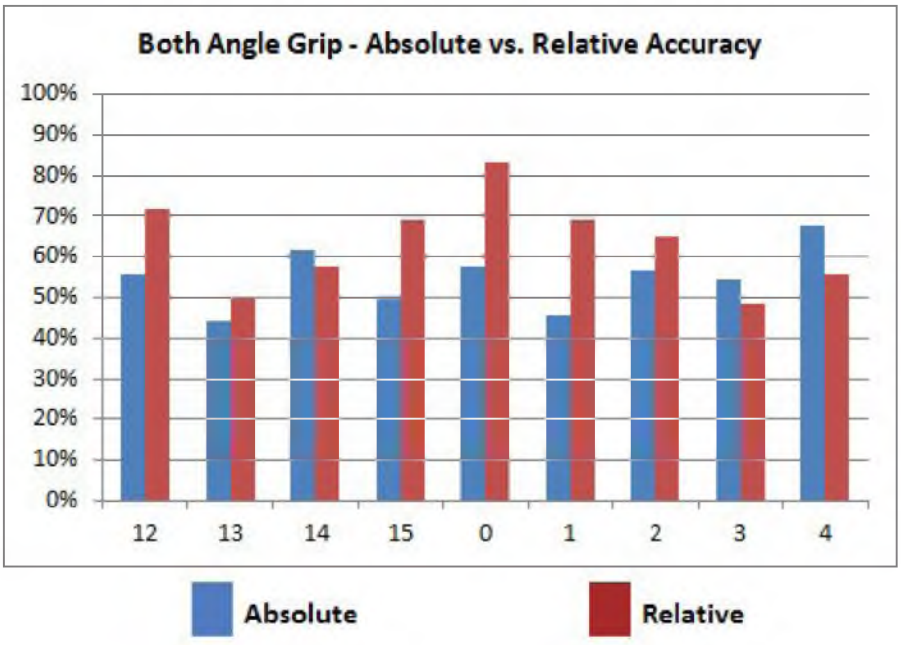

Figure 5.26 Bar graphs showing the pooled responses for all 12 participants comparing accuracy for directions shared between absolute and relative identification tests for both thumbs in angled orientation.

in stimulus (IS) and information in response (IR) are used to better understand characteristics of the user's perception of the stimulus and resulting response. The value for IS increases as the likelihood of all stimulus alternatives become equal. The information in response is an indicator that there is bias in the response. It grows to a maximum value as all responses are equally likely [29].

These values are calculated and displayed in Table 5.13 with the given equations (2), (3), and (4). S_i is stimulus, R_j the response, and P is the probability. The term n_{ij} is the number of times the stimulus matches the response in the confusion matrix. The terms n_i and n_j are the sums of the rows and columns, respectively, where stimulus matches response within the confusion matrix.

$$IS = -\sum_{i=1}^{K} P(S_i)\, log_2 P(S_i) \tag{2}$$

$$IR = -\sum_{j=1}^{K} P(R_j)\, log_2 P(R_j) \tag{3}$$

$$IT_{est} = \sum_{j=1}^{K} \sum_{i=1}^{K} \frac{n_{ij}}{n} log_2 \left(\frac{n_{ij} \cdot n}{n_i \cdot n_j} \right) \tag{4}$$

These estimates for information transfer are highest in the scenario of absolute identification with both thumbs angled which results in 2.4 bits. As two bits would correspond to four stimuli and three bits matches to eight stimuli, a value of 2.4 would suggest that direction cues should be limited to five directions if the goal is 100% accuracy.

Table 5.13 Information in stimulus (IS), information in response (IR), and information transfer estimate (IT_{est}) results for absolute and relative identification tests with both grip orientations and three handedness configurations, pooled results for all 12 participants.

	16 Direction Absolute Identification					
	Straight			Angled		
	Left	Right	Both	Left	Right	Both
Information in Stimulus	4	4	4	4	4	4
Information in Response	3.9719	3.9568	3.9579	3.9462	3.9443	3.9806
Information Transfer Test	2.0119	2.0876	2.2512	2.0906	2.1784	2.4044

	9 Direction Relative Identification					
	Straight			Angled		
	Left	Right	Both	Left	Right	Both
Information in Stimulus	3.1699	3.1699	3.1699	3.1699	3.1699	3.1699
Information in Response	3.0283	3.0514	3.1516	3.0914	3.0927	3.1532
Information Transfer Test	1.4824	1.6182	1.7125	1.7089	1.6157	1.8636

To obtain a more reliable estimate of the information transfer, an additional extended test has been completed with a single thumb receiving cues. Five users are given the 16-direction absolute identification test to the right thumb in the angled configuration. Testing conditions match those of the primary experiment but the tests are extended in length beyond the original 10 samples for each direction. In this prolonged test each of the 16 direction cues are tested with 120 repetitions across two one-hour sessions with users again responding verbally.

The information transfer estimates of this extended test are shown below in Table 5.14. The average information transfer estimate of the five users test is 2.44 bits, an improvement from the 2.18 bits average from the original test subjects with the same conditions in which only 10 repetitions are given per direction and the information transfer estimates were based on the pooled data of all 12 subjects. The 2.44 bit average

information transfer estimate of the five users in this extended test serves as a truer information transfer estimate for the angled right hand condition, and therefore one can expect slightly higher information transfer estimates than shown in Table 5.13. This means that one can likely identify more than five directions with 100% accuracy, as stated above.

5.4.7 Direction Perception Bias and Oblique Effect

Visually humans have a higher sensitivity to identifying stimuli that are aligned with the vertical or horizontal compared to those in oblique orientations (oblique angles are those which are not a right angles or a multiple of a right angle). This bias, termed the oblique effect, has also been also demonstrated in the tactile perception of spatial orientations [30].

We have tallied the count for the responses in each direction to check for indicators of biased direction response. These totals of the cardinal with ordinal directions, the even numbered directions, are compared with the remaining oblique directions (we say "remaining oblique direction" because the 45 degree "ordinal" cues are also considered to be oblique angles), odd numbered directions (see Fig. 5.4 for numbering reference).

The even numbered directions (that include the vertical, horizontal and 45 degree angled directions) have a higher proportionate number of answers given by participants in all 12 test conditions as shown in Table 5.15. While not a direct indicator of the oblique effect, these results suggest that analysis of direction response patterns is warranted.

The accuracy between these two groups was also compared to further explore this effect for absolute and relative tests, see Table 5.16 and 5.17 respectively. The group of cardinal/ordinal directions has a consistently higher accuracy than the oblique directions.

Table 5.14 Information in stimulus, information in response, and information transfer estimates for extended absolute identification test of five users with pooled average.

	Extended 16 Dir Absolute Identification					
	(6 User, 120 Cues/Direction, Right Angled Thumb)					Average
	User 1	User 2	User 3	User 4	User 5	
Information in Stimulus	4	4	4	4	4	4
Information in Response	3.921	3.922	3.964	3.957	3.954	3.943
Information Transfer Test	2.504	2.515	2.359	2.410	2.436	2.445

Table 5.15 Comparison of the proportion of answers given by all 12 users in the oblique direction versus the cardinal/ordinal directions.

	16 Direction Absolute Ident					
	Straight			Angled		
	Left	Right	Both	Left	Right	Both
Cardinal, Ordinal	55.8%	55.2%	55.8%	57.2%	55.9%	55.9%
Oblique	44.2%	44.8%	44.2%	42.8%	44.1%	44.1%

	9 Direction Relative Ident					
	Straight			Angled		
	Left	Right	Both	Left	Right	Both
Cardinal, Ordinal	51.0%	53.4%	50.8%	50.8%	51.6%	50.9%
Oblique	49.0%	46.6%	49.2%	49.2%	48.4%	49.1%

Table 5.16 Absolute identification accuracy comparisons between the cardinal/ordinal directions and oblique directions in both thumb orientations and all three handedness conditions for the pooled responses for all 12 participants.

16 Direction Absolute Identification Straight Grip

Left Hand	Mean	Std. Dev	95%	Low	High
Cardinal, Ordinal	30%	22%	3.1%	27%	33%
Oblique	24%	18%	2.5%	21%	26%

16 Direction Absolute Identification Angled Grip

Left Hand	Mean	Std. Dev	95%	Low	High
Cardinal, Ordinal	47%	22%	3.1%	44%	50%
Oblique	34%	21%	3.0%	31%	37%

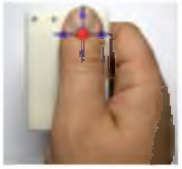

16 Direction Absolute Identification Straight Grip

Right Hand	Mean	Std. Dev	95%	Low	High
Cardinal, Ordinal	31%	25%	3.5%	28%	35%
Oblique	26%	20%	2.9%	23%	29%

16 Direction Absolute Identification Angled Grip

Right Hand	Mean	Std. Dev	95%	Low	High
Cardinal, Ordinal	47%	22%	3.2%	44%	50%
Oblique	37%	18%	2.5%	34%	39%

16 Direction Absolute Identification Straight Grip

Both Hands	Mean	Std. Dev	95%	Low	High
Cardinal, Ordinal	58%	22%	3.1%	55%	61%
Oblique	41%	19%	2.6%	38%	43%

16 Direction Absolute Identification Angled Grip

Both Hands	Mean	Std. Dev	95%	Low	High
Cardinal, Ordinal	62%	22%	3.0%	59%	65%
Oblique	50%	18%	2.5%	47%	52%

Table 5.17 Relative identification test accuracy comparisons between the cardinal/ordinal directions and remaining oblique directions in both thumb orientations and all three handedness conditions for the pooled responses for all 12 participants.

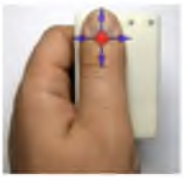

9 Direction Relative Identification Straight Grip

Left Hand	Mean	Std. Dev	95%	Low	High
Cardinal, Ordinal	45%	30%	5.6%	40%	51%
Oblique	35%	23%	4.3%	31%	39%

9 Direction Relative Identification Angled Grip

Left Hand	Mean	Std. Dev	95%	Low	High
Cardinal, Ordinal	57%	28%	5.3%	51%	62%
Oblique	47%	25%	4.7%	42%	51%

9 Direction Relative Identification Straight Grip

Right Hand	Mean	Std. Dev	95%	Low	High
Cardinal, Ordinal	55%	34%	6.4%	49%	62%
Oblique	43%	26%	5.0%	38%	48%

9 Direction Relative Identification Angled Grip

Right Hand	Mean	Std. Dev	95%	Low	High
Cardinal, Ordinal	55%	28%	5.2%	50%	60%
Oblique	46%	23%	4.3%	42%	50%

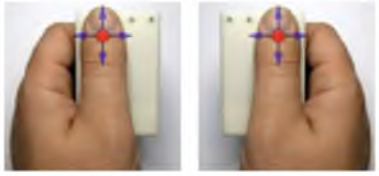

9 Direction Relative Identification Straight Grip

Both Hands	Mean	Std. Dev	95%	Low	High
Cardinal, Ordinal	62%	22%	4.2%	58%	66%
Oblique	54%	21%	4.0%	50%	58%

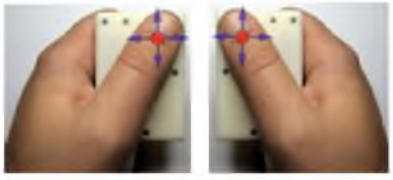

9 Direction Relative Identification Angled Grip

Both Hands	Mean	Std. Dev	95%	Low	High
Cardinal, Ordinal	67%	25%	4.7%	62%	71%
Oblique	59%	21%	3.9%	55%	63%

This cannot be completely explained by the lower number of responses in the oblique directions. Whether this effect is primarily due to thumb sensitivity and receptor arrangements within the thumb or is more based on psychophysical phenomena is a question relegated to future work.

5.4.8 d' Signal Detection Analysis

Signal detection theory concepts can be applied to these test conditions to compare the signal against the signal+noise distributions. These are described with a value d', which gives a bias-free measure of accuracy. A test in which all answers are given correctly and no false positives corresponds to a d' of 6.93. While a d' of 2.0 corresponds to getting 69% of "hits" and 69% "correct rejections." These resulting d' values are reported in Table 5.18. The d' values were calculated in each direction for each test condition and the minimum and maximum calculated d' values for each test condition and the average of these calculations for each direction is reported in Table 5.18. The d' value was also calculated on data pooled across all directions, which is shown in the last row of the tables shown in Table 5.18. As can be seen, the bias free d' values are higher for all of the relative identification conditions than for the absolute identification conditions, with the both-hand conditions again resulting in the best accuracy.

Table 5.18 d' values for all 12 test conditions showing the range of d' values across each direction calculated individually. "d' for All Combined Directions" is calculated across all directions simultaneously based on counts of "hit" and "false alarms" conditions.

	d' Signal Detection - Absolute Identification					
	Straight Configuration			Angled Configuration		
	Left	Right	Both	Left	Right	Both
Minimum Across 16 Directions	0.66	0.63	1.43	0.99	1.15	1.78
Maximum Across 16 Directions	1.61	1.81	2.34	1.89	1.98	2.42
Average d' Across 16 Directions	1.03	1.09	1.84	1.53	1.58	2.05
d' for All Combined Directions	1.04	1.11	1.81	1.52	1.56	2.04

	d' Signal Detection - Relative Identification					
	Straight Configuration			Angled Configuration		
	Left	Right	Both	Left	Right	Both
Minimum Across 9 Directions	1.04	1.11	1.62	1.13	1.22	1.78
Maximum Across 9 Directions	2.59	3.15	2.77	2.66	2.83	3.15
Average d' Across 9 Directions	1.62	1.90	2.16	2.00	1.95	2.38
d' for All Combined Directions	1.52	1.83	2.12	1.91	1.87	2.31

CHAPTER 6

CONCLUSIONS AND FUTURE WORK

6.1 Conclusions

This research presents details of an alternate design for a finger-based skin-stretch feedback device with a flat profile for the purpose of interacting with smartphones or tablets. The low-profile skin-stretch display (LPSSD) takes advantage of the on-axis stiffness and lateral compliance two orthogonal spring steel push-pull wires to provide consistent skin-stretch cues and tactor motion. This design places servos on their side to fit into the low-profile device housing. This orientation of actuation components allows for a 14.5 mm device housing height. This height was increased to 18.5 mm in the final prototype to allow additional sensors to be embedded, which is still a 58% reduction in thickness from the prior flexure-based skin-stretch display. The LPSSD has very little backlash and compliance, which plagued the previous design, while also doubling the device's motion workspace area.

The linkage design and servos used in the LPSSD have nonlinear kinematics. The LPSSD overcomes this through the application of preset manually-tuned updates to the servos to create software-corrected directional cues. These complex tactile cues allow for fine tuning of servo position at speeds high enough to correct tactor trajectories during motion. This method has been shown to deliver highly repeatable cues across a variety of users without need for adjustment, an ability not shared by the prior flexure design. This

characteristic makes the LPSDD viable for use in consumer electronics for products such as GPS, aids for visually impaired, gaming controllers, phone/computer interfaces and other handheld devices.

Results of two main user experiments have provided an initial baseline for user capabilities with 1.8 mm direction skin-stretch cues given in 16 directions. It was found that thumbs in the more ergonomic angled configuration on the tactor allow for improved direction identification abilities and that rendering to two thumbs increases perception again. A distinct rotational bias is identified that when the thumb is oriented in a straight alignment. The results of these experiments and associated user response characteristics can be used to inform future skin-stretch devices with hand orientations that promote higher accuracy and limit or take advantage of perception biases.

6.2 Contributions

Three contributions were made through this research, which relate to the fields of mechatronics and haptics perception.

1. A low-profile, low-cost, compact skin stretch tactile feedback device

   A haptic interface capable of salient and accurate skin-stretch feedback is successfully produced, based on low-cost RC grade servos. This is possible through diligence limiting compliance and backlash within linkages while also maintaining proper motion constraints to avoid undesired degrees of freedom. The consistency of skin stretch tactor motion in 16 directions, across a diverse set 10 users, suggests that the sliding tactor plate coupled with push-pull wires arrangement is capable of delivering reproducible interactions to a broad population.

2. Use of table look-up tables to correct for device nonlinearities

   It is shown that workspace nonlinearity of the low-cost actuation mechanism can be compensated for with a "waypoint" table-lookup method. This high-speed open-loop control approach is demonstrated to correct workspace distortions and permit velocity control of the skin-stretch tactor with minimal error. With expanded microcontroller capabilities this waypoint method can be further refined with improved servo control resolution and update frequency to create complex and responsive tactile cues.

3. Perceptual and cognitive data for direction perception with multiple hands that is valuable for informing portable device designs that provide directional information tactilely

   A prototype of a smartphone peripheral makes use of two low-profile skin-stretch displays to test users' abilities in detecting directional skin-stretch cues at the thumbs with an assortment of test conditions. From these results a variety of performance trends and user biases have been identified. The user accuracies of the left and right thumbs are nearly equal. Perception accuracies are significantly improved when participants received cues with both thumbs than with a single thumb. When a user's thumb is held in the angled configuration his/her direction accuracies is higher than those in the "straight" thumb configuration. Users tested with a single thumb in the straight configuration showed considerable rotation bias – answering in a direction clockwise and counterclockwise to the

rendered cue for the left and right thumbs, respectively. Additionally, providing a perceptual reference increases response accuracy, especially for direction cues closest to the reference.

6.3 Future Work

Though results of the development and testing of the completed LPSSD are promising there are many avenues for continued research.

Mobile Tasks – a variety of experiments could be run to test user abilities while walking and determine the types of cues and their ideal interval for efficient guidance.

Graphical Interface – the responsive motion of the LPSSD tactor lend itself to exploring its use supplementing audio/visual interfaces. This includes possibilities for a wider variety of complex tactile cues based on shapes, textures or timing.

Visually Impair Users – cognitive abilities for skin-stretch cues of the blind or visually impaired would determine device and control design specifications towards the production of an assistance device.

Gaming – refinement of the force sensor based controls would allow for a user input thumbstick with software tuned virtual spring. A wide range of gaming experiences would benefit from the both subtle and acute sensations.

REFERENCES

[1] S. Brewster, F. Chohan, and L. Brown, "Tactile feedback for mobile interactions," *Proc. SIGCHI Conference on Human Factors in Computing Systems - CHI '07*, p. 159, 2007.

[2] P. Laitinen and J. Maenpaa, "Enabling mobile haptic design□: piezoelectric actuator technology properties in hand held devices," *IEEE Int. Workshop Haptic Audio Visual Environments and their Applications*, vol. 9, pp. 40–43, 2006.

[3] O. Bau, I. Poupyrev, A. Israr, and C. Harrison, "TeslaTouch□: electrovibration for touch surfaces," *Proceeding UIST '10 Proc. 23nd Annu. ACM Symp. User Interface Software and Technology*, pp. 283–292, 2010.

[4] N. D. Marchuk, J. E. Colgate, and M. A. Peshkin, "Friction measurements on a large area TPaD," *2010 IEEE Haptics Symp.*, pp. 317–320, Mar. 2010.

[5] M. Salada, P. Vishton, and J. E. Colgate, "Two experiments on the perception of slip at the fingertip," *Haptic Interfaces for Virtual Environment and Teleoperator Systems, 2004. HAPTICS '04. Proc. 12th International Symp.*, pp. 146–153, 2004.

[6] J. M. Cruz-hern, "Tactile display device using distributed lateral skin stretch," *Symp. Haptic Interfaces for Virtual Environment and Teleoperator Systems, IMECE 2000 Conference*, 2000.

[7] J. Biggs and M. A. Srinivasan, "Tangential versus normal displacements of skin: relative effectiveness for producing tactile sensations," *Proc. 10th Symp. Haptic Interfaces for Virtual Environment and Teleoperator Systems. HAPTICS 2002*, pp. 121–128, 2002.

[8] K. Bark, J. Wheeler, G. Lee, J. Savall, and M. Cutkosky, "A wearable skin stretch device for haptic feedback," *World Haptics 2009 - 3rd Joint EuroHaptics Conf and Symp. Haptic Interfaces for Virtual Environment and Teleoperator Systems*, pp. 464–469, 2009.

[9] J. Wheeler, K. Bark, J. Savall, and M. Cutkosky, "Investigation of rotational skin stretch for proprioceptive feedback with application to myoelectric systems.," *IEEE Transactions Neural Systems and Rehabilitation Engineering□: A Publication of the IEEE Engineering in Medicine and Biology Society*, vol. 18, no. 1, pp. 58–66, Feb. 2010.

[10] K. Drewing, R. Zopf, M. O. Ernst, and M. Buss, "First evaluation of a novel tactile display exerting shear force via lateral displacement," *ACM Transactions Applied Perception*, vol. 2, no. 2, pp. 118–131, 2005.

[11] M. P. Vitello, M. O. Ernst, and M. Fritschi, "An instance of tactile suppression□: active exploration impairs tactile sensitivity for the direction of lateral movement," *Proceedings of EuroHaptics*, pp. 351–355, 2006.

[12] B. T. Gleeson, S. K. Horschel, and W. R. Provancher, "Communication of direction through lateral skin stretch at the fingertip," *World Haptics 2009 - 3rd Joint EuroHaptics Conf and Symp. Haptic Interfaces for Virtual Environment and Teleoperator Systems*, pp. 172–177, Mar. 2009.

[13] B. T. Gleeson, C. A. Stewart, and W. R. Provancher, "Improved tactile shear feedback: tactor design and an aperture-based restraint," *IEEE Transactions Haptics*, no. October, pp. 253–262, 2011.

[14] B. Gleeson, S. Horschel, and W. Provancher, "Design of a fingertip-mounted tactile display with tangential skin displacement feedback," *IEEE Transactions Haptics*, vol. 3, no. 4, pp. 297–301, Oct. 2010.

[15] R. L. Koslover, B. T. Gleeson, J. T. de Bever, and W. R. Provancher, "Mobile navigation using haptic, audio, and visual direction cues with a handheld test platform," *IEEE Transactions Haptics*, vol. 5, no. 1, pp. 33–38, Jan. 2012.

[16] A. Guinan, R. Koslover, and N. Caswell, "Bi-manual skin stretch feedback embedded within a game controller," *Haptics Symp. (HAPTICS), 2012 IEEE*, pp. 255–260, 2012.

[17] N. G. Tsagarakis, T. Horne, and D. G. Caldwell, "Slip aestheasis: a portable 2D slip/skin stretch display for the fingertip," *1st Joint Eurohaptics Conf and Symp. Haptic Interfaces for Virtual Environment and Teleoperator Systems*, pp. 214–219, 2005.

[18] M. Solazzi, "Design of a SMA actuated 2-DoF tactile device for displaying tangential skin displacement distal ulnar radial proximal," *Transactions Haptics (HAPTICS)*, vol. 3, no. 4, pp. 297–301, 2011.

[19] M. Solazzi, A. Frisoli, and M. Bergamasco, "Design of a novel finger haptic interface for contact and orientation display," *2010 IEEE Haptics Symp.*, pp. 129–132, Mar. 2010.

[20] K. Minamizawa and S. Fukamachi, "Gravity grabber: wearable haptic display to present virtual mass sensation," *ACM SIGGRAPH 2007*, pp. 3–6, 2007.

[21] V. Frati and D. Prattichizzo, "Using Kinect for hand tracking and rendering in wearable haptics," *2011 IEEE World Haptics Conf*, pp. 317–321, Jun. 2011.

[22] M. A. Baumann, K. E. MacLean, T. W. Hazelton, and A. McKay, "Emulating human attention-getting practices with wearable haptics," *2010 IEEE Haptics Symp.*, pp. 149–156, Mar. 2010.

[23] A. A. Stanley and K. J. Kuchenbecker, "Design of body-grounded tactile actuators for playback of human physical contact," *2011 IEEE World Haptics Conf*, pp. 563–568, Jun. 2011.

[24] Y. Wang and K. J. Kuchenbecker, "HALO□: haptic alerts for low-hanging obstacles in white cane navigation," *Haptics Symp. (HAPTICS), 2012 IEEE 2012*, pp. 527–532, 2012.

[25] B. T. Gleeson, S. K. Horschel, and W. R. Provancher, "Perception of direction for applied tangential skin displacement□: effects of speed , displacement and repetition," *IEEE Transactions Haptics - Selected for Special Issue: World Haptics Spotlight , Jul-Sept, 2010*, 2009.

[26] J. C. Craig, "Tactile pattern perception and its perturbations to problems in attending to several sites," *The Journal Acoustical Society of America*, vol. 77, no. January, pp. 238–46, 1985.

[27] D. V Keyson and a J. Houtsma, "Directional sensitivity to a tactile point stimulus moving across the fingerpad.," *Perception & Psychophysics*, vol. 57, no. 5, pp. 738–44, Jul. 1995.

[28] B. T. Gleeson and W. R. Provancher, "Mental rotation of directional tactile stimuli," *2012 IEEE Haptics Symposium (HAPTICS)*, pp. 171–176, Mar. 2012.

[29] H. Z. Tan, S. Member, C. M. Reed, and N. I. Durlach, "Optimum information transfer rates for communication through haptic and other sensory modalities," *IEEE Transactions Haptics*, vol. 3, no. 2, pp. 98–108, 2010.

[30] E. Gentaz, G. Baud-Bovy, and M. Luyat, "The haptic perception of spatial orientations.," *Experimental brain research. Experimentelle Hirnforschung. Expérimentation cérébrale*, vol. 187, no. 3, pp. 331–48, May 2008.